



HAL
open science

Design of absorbers using metamaterials

Zeinab Fneich

► **To cite this version:**

Zeinab Fneich. Design of absorbers using metamaterials. Micro and nanotechnologies/Microelectronics. Normandie Université; Université Libanaise, 2020. English. NNT : 2020NORMR095 . tel-03192631

HAL Id: tel-03192631

<https://theses.hal.science/tel-03192631>

Submitted on 8 Apr 2021

HAL is a multi-disciplinary open access archive for the deposit and dissemination of scientific research documents, whether they are published or not. The documents may come from teaching and research institutions in France or abroad, or from public or private research centers.

L'archive ouverte pluridisciplinaire **HAL**, est destinée au dépôt et à la diffusion de documents scientifiques de niveau recherche, publiés ou non, émanant des établissements d'enseignement et de recherche français ou étrangers, des laboratoires publics ou privés.

INTERNATIONAL COTUTELLE THESIS

To obtain the doctorate degree
Specialty (Applied Physics)

Prepared at the Rouen University
and the Lebanese University

Design of Absorbers Using Metamaterials

Presented by
Zeinab FNEISH

Thesis defended on (03-02-2020) before the jury composed of :		
Mr. Fabien NDAGIJIMANA	Professor in the Grenoble University	Reviewer
Mrs. Sylvie BARANOWSKI	Master of Conference /HDR Lille University	Reviewer
Mr. Ghaleb FAOUR	Research supervisor in Lebanese National Center for Scientific Research (CNRS)	Examiner
Mr. Mohammed RAMDANI	Professor at ESEO	Examiner
Mr. Moncef KADI	Instructor-Researcher /HDR ESIGELEC	Supervisor
Mr. Mohammad RAMMAL	Professor in the Lebanese University IUT Saida	Supervisor
Mr. Jalal JOMAA	Professor in the Lebanese University Branch I	Co-supervisor
Mr. Hussam AYAD	Associate Professor in the Lebanese University Branch I	Examinor

Thesis directed by

Dr. Kadi MONCEF
Prof. Mohammad Rammal

Rouen University
Lebanese University

Table of Contents

Acknowledgements	5
List of Publications	7
Abstract	8
List of Figures	9
List of Tables	14
List of Abbreviations	15
General introduction	16
1. Chapter 1: State of the Art	18
1.1 Introduction	18
1.2 Categories of Main Industrial Absorber.....	18
1.2.1 Dielectric Absorber	18
1.2.2 Structural Absorbers	19
1.2.3 Resonant Absorber.....	21
1.2.4 Magnetic Absorber.....	22
1.3 Anechoic Chamber.....	22
1.3.1 Description of its Structure	22
1.3.2 Dimension VS Operating frequencies	23
1.3.3 Anechoic Chamber Disadvantages.....	24
1.4 Metamaterial Absorber.....	24
1.4.1 Categories of Metamaterial Absorber.....	25
1.4.2 Broadening Ways	30
1.5 Conclusion.....	37
1.6 Reference.....	38
2. Chapter 2: Pyramidal Design Setup	44
2.1 Introduction	44

2.2	Plasmonic Resonance Study.....	45
2.2.1	Absorption Mechanism.....	45
2.2.2	Simulation Results.....	46
2.2.3	Conclusion.....	51
2.3	Design of Pyramidal Absorber.....	52
2.4	Parametric Analysis.....	54
2.4.1	Geometrical parameters influence.....	55
2.4.2	Material Properties Influence.....	60
2.5	Curved Altitude Enhancing Factor.....	63
2.7	Conclusion.....	66
2.8	Reference.....	67
3.	Chapter 3: Activating Metamaterial to low frequency.....	69
3.1	Introduction.....	69
3.2	Resonant Frequency Equation.....	69
3.3	Material Properties.....	70
3.3.1	Insertion of Water Substrate.....	72
3.3.2	Encapsulated Water in a FR4 Coating.....	74
3.3.3	Conclusion.....	76
3.5	Minimal Surface Geometry.....	76
3.5.1	Rough Surface Effect.....	76
3.5.1	Helicoid Model.....	81
3.6	Conclusion.....	85
3.7	Reference.....	86
4.	Chapter 4: Design of Metamaterial Broadband Absorber.....	88
4.1	Introduction.....	88
4.2	By Adding Layers.....	89
4.2.1	Simulation Setup.....	89
4.2.2	Results and Discussion.....	90
4.3	By Combining Complementary Pyramids.....	94

4.3.1 Simulation Setup.....	94
4.3.2 Results and Discussion	96
4.4 Enhanced Combined design	97
4.4.1 Simulation Setup.....	97
4.4.1 Results and discussions	97
4.5 “Heel and Heads” Structure	98
4.5.1 Simulation Setup.....	98
4.5.2 Results and Discussion	99
4.6 By Applying Helicoid Cone.....	101
4.6.1 Simulation Setup.....	101
4.6.2 Results and Discussion	102
4.7 By Stacking Multi-Band Patches	104
4.7.1 Simulation Setup.....	104
4.7.1 Results and Discussion	105
4.7 Conclusion.....	107
4.6 References	108
5. Conclusion	110
6. Appendices.....	112

Acknowledgements

First and foremost, I would like to thank *God Almighty* for giving me strength and ability to undertake this research study and complete it satisfactorily. Without God's blessings, this achievement would not have been possible.

The work of this thesis was made possible by the joint financial support of the *Lebanese University and the National Council for Scientific Research*, to whom go my grateful thanks. There are no proper words to express my deep gratitude and respect for my research supervisors, *Prof. Mohammad Rammal* and *Dr. Moncef*, whose talent and enthusiasm has inspired me to devote myself into the path of seeking truth and knowledge. I thank for their support in building up my research career. I owe my deepest respect to them. I would like to thank the two universities, *Lebanese University* and *Normandie University*, that I have spent my years in pursuing my PhD degree.

I am especially indebted to *Prof. Jalal Jomaa* for his mentorship and guidance as my PhD co-supervisor, always willing to give me time and help when required. It is through answering his harsh questions that I learned to question and defend myself, and to argue my own viewpoint and explain it to others. I thank for his training in writing, in making a presentation, and in choosing a topic. As well as to Dr. Hussam Ayad, I learned from him how to analyze a problem from the first physical principle, and to move upon a solution based on careful logical deduction, experienced mathematical derivation, and physical insights.

Many thanks also to my thesis reviewers for evaluating my work and giving their helpful suggestions and corrections.

My acknowledgments are also owed to Dr. Badia Srour who accompanied me and support me in my journey in Rouen. Without her, travelling there would be very exhausting.

My sincere thanks must also go to my dear *Lara Dbouk* and to my best friend *Fatima Mazeh*, they were always willing to give me time and help when required.

I am mostly grateful to the love I received from my family. Without the love, support and education from my father, nothing was possible. I am so grateful to my brothers Yasser, Hamza, Ali, Hussein and Hammoudi and especially my two sisters *Mariam* and *Fatima* who were always beside me, listening, helping, discussing and giving the maximum support ever possible even though the difficulties we all together went through. They have deprived herself of resting and handled tough responsibilities to dedicate more time and effort to this work to have the best ending.

Words cannot express how grateful I am to my dear husband *Ali*. I am so appreciative for his constant love, understanding, encouraging, and patience. His continuous support helped me to complete this research work. My companion on my life, we dreamed together, we planned together, and today we are reaping the fruits of our patience.

أولا وأخيرا كل الشكر لملاكي النائم... اهديك علمي وعملي. لولا دعواتك يا امي ما كان لطريقي ان يكون باليسر والتوفيق معبدا.
انت من زرع في نفسي روح الإرادة والطموح ليثمر الان علما احسبه نافعا. لك الدور الأساسي والفضل الجزيل علي طيلة عمري. الى روحك
الطاهرة كل حبي و شوقي..

List of Publications

International Conferences:

- [1] Fneish, Z., et al. "Small-Size Metamaterial in Low Frequency Region Using Minimal Surfaces". 2019 *1st International Conference of Pure and Engineering Sciences (icpes) 2020*. (Accepted)
- [2] Fneish, Z., et al. "Ultra Broadband Curved Pyramidal Absorber Metamaterial in the UHF/SHF Region". *2019 7th Mediterranean Congress of Telecommunications (CMT)*. IEEE, 2019. (Accepted and Published)
- [3] Fneish, Z., et al. "Design of a miniaturized dual wide band and tri band artificial magnetic conductor in LTE regions." *2017 Sensors Networks Smart and Emerging Technologies (SENSET)*. IEEE, 2017. (Accepted and Published)
- [4] Fneish, Z., et al. "Behavior of different structures to design AMC for Europe LTE bands." *2016 IEEE Middle East Conference on Antennas and Propagation (MECAP)*. IEEE, 2016. (Accepted and Published)

National Conferences (accepted):

- [1] Fneish, Z., et al. "Design of an Octave Bandwidth Metamaterial Absorber". 2018 *Lebanese Association for the Advancement of Science (LAAS)*.
- [2] Fneish, Z., et al. "Miniaturized Dual Wide Band AMC for LTE Applications". 2017 *Lebanese Association for the Advancement of Science (LAAS)*.

Articles (Submitted):

- [1] Fneish, Z., et al. " Curved Pyramidal Metamaterial Absorber: From Theory to an Ultra-Broadband Application in the [0.3 - 30] GHz Frequency Band".

Abstract

In this thesis, we aim to design a broadband absorber that can effectively operate at low frequencies. To achieve such an aim, we take advantage of the properties of the metamaterial to reach a stage in which the former is capable of replacing the present bulky anechoic chamber. After studying the state of the art of metamaterial absorber, we choose the pyramidal design to be the basis of our research view of its suitable properties for our application. We perform a complete parametric study to adjust its geometrical parameters and material properties to obtain the best absorption response. Besides, we enhance its relative absorptive bandwidth by making a novel curved altitude design. The latter two modifications lead to an increase in the Relative Absorptive Bandwidth (RAB) from 63.3% in the literature to 73.4% with an absorption level greater than 80%. In addition, we discuss the requirements needed to reach a low-frequency band absorber that can be summarized by the necessary high relative permittivity material dielectric substrate and the need for bigger dimensions. After applying these requirements, we succeeded to shift the frequency to UHF bands. We achieved a miniaturized unit cells by applying minimal surface geometry as a novel way in miniaturizing absorber. Moreover, to widen the broadband absorption of the conventional pyramidal absorber, we present different new absorber prototypes. We cite the prototype with a total thickness of 12.7 cm, consisting of 35 curved resonant layers where numerical simulations show an enhanced design with an absorption band from 0.3 GHz to 30 GHz. Concerning the second proposed prototype, the latter is dedicated to combining complementary bands for different pyramidal structures dimensions in one unit cell. After introducing many enhancement factors and taking into account optimization, this prototype reached a well-combined band with a relative absorptive bandwidth of 128.69%. These prototypes are tested using the numerical simulator High-Frequency Structure Simulator (HFSS). All calculations were performed on an HPC of 24 cores with a system memory of 192 GB RAM. For the reliability of the results, discrete frequency analysis mode was adjusted with numerous data points to reach simulation results with a very high level of precision.

List of Figures

Figure 1.1: Illustration of Pyramidal Dielectric Absorber.....	19
Figure 1.2: Illustration of Taped Loading Absorber and Matching Layer Absorber.	20
Figure 1.3: Illustration of Destructive Interference Phenomenon.	21
Figure 1.4: Photo took in a Semi Anechoic Chamber.	23
Figure 1.5: Unit Cell of a Plasmonic Metamaterials Absorber of square patches type of periodicity $P = 17.5$ mm, the thickness of the substrate is $h_s = 0.3$ mm, $g = 1$ mm, and the length of the metallic patch $W = 15.2$ mm.....	26
Figure 1-6: Absorption response obtained by Simulation of a Square Metamaterials Absorber with Ansys HFSS and CST Microwave Studio [42].....	27
Figure 1.7: Photograph of the periodic BST array [57]......	28
Figure 1.8: Reflection and absorption spectra for an absorber with BST cube array with period $P_x = P_y = 9$ mm and side length $a_x = a_y = a_z = 1.8$ mm on a 0.2 mm-thick dielectric layer and a metal substrate [57]......	29
Figure 1.9: Absorption spectra as a function of frequency for incidence angle ranging from 0° to 75° [57].	29
Figure 1.10: Schematic of metal/dielectric/metal resonator grouped in the same ground plane with different dimensions (a) MultiCross design (b) different rectangular patches [42].....	31
Figure 1.11: Simulation showing the absorption of the metamaterials absorbent consisting of: (a) the MultiCross design (b) design of several rectangular patches juxtaposed with Ansys HFSS [42].	32
Figure 1.12: Design and fabrication of a microwave ultra-broadband MA. (a) Three-dimensional illustration of the simulated MA, (b) schematic of an MA unit cell, and (c) photograph of the fabricated sample. The optimized dimensions of a unit are $W_t = 5$ mm, $W_l = 5$ mm, $P = 11$ mm, $t_m = 0.05$ mm, $t_d = 0.2$ mm, and $T = 5$ mm [58].	33
Figure 1.13: Simulated and Experimental absorption performance of the MA in Fig. 1.12.	34

Figure 1.14: Simulated angular absorption of the MA in Fig 1.11 for TE configuration. The incident angle is varied from 0 degrees to 60 degrees [58]. 34

Figure 1.15: Photograph of the random BST cubes sample deposited on the copper plate [57]. 35

Figure 1.16: Experimental absorption spectrum for the random structure in figure 1.15 [57].... 35

Figure 1.17: Comparison of the Absorption of the MultiCross / Magnetic Absorber Stack and the Magnetic Absorber alone [42]. 36

Figure 2.1: Representation of the Reflection and the Transmission of a wave at the interface of two medium. 46

Figure 2.2: Sectional view of the square patch absorber. 46

Figure 2.3: 3D Model of a unit cell of square patches simulated by HFSS..... 47

Figure 2.4: Simulated absorption response of the square patch of **Fig. 2.2**..... 49

Figure 2.5: (a) Magnitude of electrical field at 4.05 GHz (b) Magnitude of magnetic field at 4.05 GHz. 49

Figure 2.6: Reflection coefficient of the simulated patch square of **Fig. 2.2**. 50

Figure 2.7: Design of an ultra-broadband PMA, (a) 3-D illustration of the simulation MA, (b) Side view of the PMA unit cell..... 52

Figure 2.8: Absorption response simulated of the optimized pyramidal structure with dimensions of: $W_{\min}=2.975$ mm, $W_{\max}=6.3$ mm, $P=6.65$ mm, $t_m=35\mu\text{m}$, $t_d=140\mu\text{m}$ 53

Figure 2.9: Simulated Electric and Magnetic Magnitude distributions at three resonance frequencies. 54

Figure 2.10: Absorption coefficient with respect to frequency for four spacing ranging from 6.65 mm to 8.05 mm. 55

Figure 2.11: Diagram showing the static spacing between upper layers imposed geometrically. 56

Figure 2.12: Absorption coefficient with respect of frequency for basic length W ranging from 6.3 mm to 7.7 mm. 56

Figure 2.13: Absorption coefficient with respect of frequency with different number of resonator layers ranging as 12, 15, 17 and 20 layers. 58

Figure 2.14: Absorption response corresponding different dielectric thickness for: (a) The first basic layer then (b) the tenth layer and (c) the fifth layer. 59

Figure 2.15: Absorption coefficient as a function of frequency Absorption under influence of dielectric loss tangent varying from 0.02 to 0.08..... 60

Figure 2.16: Absorption coefficient as a function of frequency Absorption under influence of relative permittivity varying from 4.4 to 15..... 61

Figure 2.17: Absorption coefficient as a function of frequency under influence of dielectric thickness for different relative permittivity value: (a) 4.4 (b) 15 and (c) 20..... 62

Figure 2.18: Absorption coefficient as a function of frequency under influence of metal conductivity ranging from 5×10^5 S/m to 5.8×10^7 S/m. 63

Figure 2.19 : Different shape altitude designs of a Pyramidal structure: (a) Sawtooth Altitude (b) Linear Altitude (c) Curved Altitude. 64

Figure 2.20: Absorption response from numerical simulations for different altitude shape designs in the PA: (a) Sawtooth Altitude (b) Linear Altitude (c) Curved Altitude..... 65

Figure 3.1: Debye model of water properties: (a) Relative permittivity frequency dependence (b) Dielectric loss frequency dependence..... 72

Figure 3.2: Patch design with water substrate. 73

Figure 3.3: Absorption response of the patch design shown in **Fig. 3.2**. 73

Figure 3.4: Patch design with water substrate encapsulated in FR4 box..... 75

Figure 3.5: Absorption response of the patch design shown in **Fig. 3.4**. 75

Figure 3.6: Droplet drops on the water surface creating the first roughness form modeled. 77

Figure 3.7: The first roughness form modeled in HFSS..... 77

Figure 3.8: Absorption response of the Droplet Water surface. 78

Figure 3.9: Regular patch with same dimension length of the model in **Fig. 3.7**..... 78

Figure 3.10: Absorption response of the regular patch..... 79

Figure 3.11: Three different RMS Height values applied to a random rough surface in a patch absorber..... 80

Figure 3.12: Absorption response of different roughness with different RMS Height. 80

Figure 3.13: Different Mobius resonator shape for different applications [12-14].	81
Figure 3.14: The helicoid surface shape.	82
Figure 3.15: Resonator patch absorber with metallic Helicoid Model.	83
Figure 3.16: Circular Patch Design.	83
Figure 3.17: Absorption response of the circular patch design.	84
Figure 3.18: Absorption response of helicoid model.	84
Figure 4.1: Enhanced Pyramid Design Absorbers. (a) Structure of the basic pyramid optimized in UHF Band. (b) Structure of the Pyramid Absorber after adding 15 layers, the basic layer is 72 mm of length and the smaller patch at the top is 11.7mm.	89
Figure 4.2: Absorption response of the enhanced pyramidal design of Fig. 4.3(a) in the UHF band.	91
Figure 4.3: Absorption response of the EP design of Fig. 4.3(b) in the UHF/SHF band after adding 15 layers. (a) Phase I of absorption. (b) Phase II of absorption.	92
Figure 4.4: Simulated Electric and Magnetic magnitude distributions at some frequencies at phase I of absorption [0.3 -1.92 GHz].	93
Figure 4.5: Simulated Electric magnitude distributions at some frequencies at Phase II of absorption [1.92 - 30 GHz].	93
Figure 4.6: Structure of the combined structure operating in complementary bands.	95
Figure 4.7: The operating absorption band of structures composing the unit cell with geometrical dimensions: $W_{1max}=72$ mm; $W_{1min}=33$ mm; $W_{2max}=31.5$ mm; $W_{2min}= 14.7$ mm.	95
Figure 4.8: Absorption response of the first combined design presented in Fig. 4.6 .	96
Figure 4.9: Enhanced Model of the combined structure, considering these geometrical dimensions for structure 3: $W_{3max} =50.22$ mm; $W_{3min} = 21.06$ mm.	97
Figure 4.10: Absorption response of the enhanced combined design presented in Fig. 4.6 .	98
Figure 4.11: “Heal and Heads” structure.	99
Figure 4.12: Absorption response of the simulated “Heel and Heads” structure of Fig 4.11 .	100
Figure 4.13: Absorption response of the inverted pyramid.	100

Figure 4.14: Helicoid cone design: **(a)** metallic helicoid cone **(b)** metallic helicoid cone covered by FR4 substrate (Altitude = 4.5 cm, Radius = 1.2 cm) 101

Figure 4.15: Absorption response of the helicoid cone structure. 102

Figure 4.16: Magnitude of Electrical and Magnetic Field distribution on the helicoid structure for different frequencies. 103

Figure 4.17: (a) Multi-band absorber design (b) stacked multi-band absorber design. 104

Figure 4.18: Current Density Distribution in the quad-band absorber at the four-absorber frequencies. 105

Figure 4.19: Absorption response of the quad-band absorber. 106

Figure 4.20: Absorption response of the stacked multi-band absorber. 106

List of Tables

Table 1-1: Heights of APM (Pyramidal Foam Absorber) depending on the operative frequencies with the value of Reflectivity performance attained at normal incidence.	24
Table 2-1: The values of different parameter of our simulated unit cell:	47
Table 2-2: Relative Absorption Bandwidth for different altitude form obtained by simulation .	64
Table 3-1: Practical Properties of high relative permittivity dielectric substrate.	71

List of Abbreviations

RCS:	Radial Cross Section
EM:	Electromagnetic Wave
EMC:	Electromagnetic Compatibility
APM:	Pyramidal Absorber
UHF:	Ultra-High Frequency
SHF:	Super High Frequency
TL:	Transmission Line
MPA:	Metamaterial Perfect Absorber
MA:	Metamaterial Absorber
BST:	$Ba_{1-x}Sr_xTiO_3$
TE:	Transverse Electric
TM:	Transverse Magnetic
RAB:	Relative Absorption Bandwidth
HFSS:	High Frequency Structure Simulator
RMS:	Root Mean Square
HPC:	High Performance Cluster
PA:	Pyramidal Absorber
PMA:	Pyramidal Metamaterial Absorber
MA:	Metamaterial Absorber

General introduction

Recently, almost all telecommunication systems that include television broadcasting, mobile phone (3G/4G/LTE/5G) frequencies and Wi-Fi applications are in the lower microwave region ranging from 0.3 to 30 GHz. It is experiencing unprecedented development not only in indoor communication but also in monitoring security systems as well. Nowadays, active and passive components are integrated into various systems, which are developed to be more and more compact and robust. Together with high performance in terms of absorption level, relative frequency bandwidth, insensitivity to polarization and angle of incidence, thin and flexible perfect absorbers are welcome and are even requested in these systems.

The current absorbers in research started during the Second World War. They were created both in USA and Germany. The first applications of absorbers were limited to the signature of the planes and the submarine periscopes while trying to not increase their mass. Today, their use has diversified to other applications including Electromagnetic Compatibility (EMC), reduction of interference between bands of frequencies in telecommunications systems, sensors and thermo photovoltaic systems. Moreover, an absorber is essentially used in test chambers of the electromagnetic property called “Anechoic Chambers”. The latter is a shielded room covered with absorber materials on all walls, ceiling, and floor to prevent any reflection.

The lining materials of current anechoic chambers are designed to absorb in the microwave region view the numerous application cited before (0.3 GHz-30 GHz). Despite its high performance in terms of the absorption coefficient, bandwidth, and its insensitivity to polarization and angle of incidence, anechoic chambers are expensive to acquire, and it is difficult to achieve good echo-free conditions at low frequencies. It also suffers from its immensity and its fragility on the surface. Despite of the evolution that has occurred in electromagnetic engineering in which metamaterial science contributes, the anechoic chamber remains the unique solution presented for low broad frequency band absorber.

Metamaterial research is recent; they are periodic arrangements of artificial microstructures that exhibit singular properties not found with natural materials. The improvement brought by this

type of material compared to different conventional categories lies in the reduction of the thickness for the structure to pass under the quarter-wavelength of the lowest wavelength of the desired band [1]. Herein, some efforts and works have been devoted to this area aiming to design a low-frequency Metamaterial Absorber **MA** with small-size unit cell [2-3]. In spite of the validity of these approaches, there is still a lack of sufficient progress to the design and fabrication of high-performance low-frequency broadband **MA** resulting from the sensitive perfect absorption conditions.

To add novelty in this research area, we propose in this work the design of a low-frequency broadband MA. For that, we take the challenge to benefit from metamaterials to design a broadband absorber that can effectively operate in low frequencies trying to discover the potential of metamaterial to test the feasibility of the latter in replacing the present anechoic chamber.

In the first chapter, we discuss the state of the art with some key points concerning the techniques of different existing absorbers. We will focus on the contribution of MA in literature. The history, the theory, and the characterization of the metamaterial perfect absorbers (**MPA**) and the engineered way to obtain the broadest band is addressed in this chapter. From this bibliography, we will select a metamaterial structure based on its properties to be suitable as a basic unit in our study.

In the second chapter, we cover a detailed study about the selected structure from chapter one. Looking toward studying the effect of its geometrical and material properties parameters, a parametric study is done. That was useful to do the necessary optimizations in order to reach the best absorption response. In this section, we enhance this structure and improve its absorption response by a new geometrical modification.

Through the third chapter, we study all the requirements needed to achieve a low-frequency response. Besides, we will apply these requirements to design and investigate small-size MA.

In the last chapter, we present different novel structures based on pyramidal absorber that give an ultra-broadband absorption. We investigate its response and show the Relative Absorptive Bandwidth (**RAB**) reached by these structures.

1. Chapter 1: State of the Art

1.1 Introduction

The motivation for studying absorbers comes mainly from their efficient use in potential applications. These applications include emitters, sensors, spatial light modulators, IR camouflage, anechoic chambers and wireless communication.

Absorbers in the mentioned applications are presented through different classical and commercial categories: dielectric, structural, resonant, magnetic and metamaterial. Each category is developed by different scientific researches but nowadays researches focus on the metamaterial category view its miniaturization capacity.

Anechoic chambers is considered as a developed dielectric absorber, and now it is considered as a principal way to achieve a broadband response at low frequency in spite of its fragility, humidity sensibility and bulkiness as addressed in this chapter. We will start by presenting the characterization of the different conventional and commercial absorber material. We highlight the properties of the latter operating in narrow and broad band of absorption to draw a conclusion concerning its pros compared to the commercial absorbers found in literature.

1.2 Categories of Main Industrial Absorber

In this section, we sum up the main absorber categories presented historically.

1.2.1 Dielectric Absorber

This type of absorber is basic. These are foams, polymers or honeycomb structures loaded with carbon or metal particles (iron, aluminum, copper)... These materials are realized to have the highest dielectric loss constant thus transforms into heat the maximum of the incident wave. The impedance of this type of material is not strongly adapted to the impedance of the free space. Thus, they can present a strong reflection at their interface. These materials can be found in industry. Recent research on dielectric absorbers is focusing more on conductive polymer materials [1]. They have the particularity of having a low relative permittivity and a very strong

dielectric loss. The manufacture of this type of material is quite complex where it is usually deposited on textile to have a certain strength.

1.2.2 Structural Absorbers

It is known that a wave is reflected at the interface of the material proportionally to the impedance of the latter. From this observation, three categories of absorbers (pyramidal, progressively loaded and impedance matching layers) were developed to improve the diffusion of the wave in a dielectric absorbing layer. For good attenuation over a wide band, this type of material requires large thickness with a significant weight. We mainly focused on the pyramidal absorber structure that is used in the anechoic chamber.

1.2.2.1 Pyramidal Absorbers

The pyramidal absorbers are typically thick materials with regularly spaced structures of pyramidal or conical shape disposed perpendicularly to the surface [4]. The pyramidal absorbers have been developed in such a way that the interface has a gradual transition from the impedance of air to that of the absorber. The height and periodicity of the pyramids tend to be in the order of the wavelength. These absorbers provide very good performance. The disadvantage of pyramidal absorbers is their thickness and tendency to be fragile. This category is applied to manufacture anechoic chambers (**Fig. 1.1**).

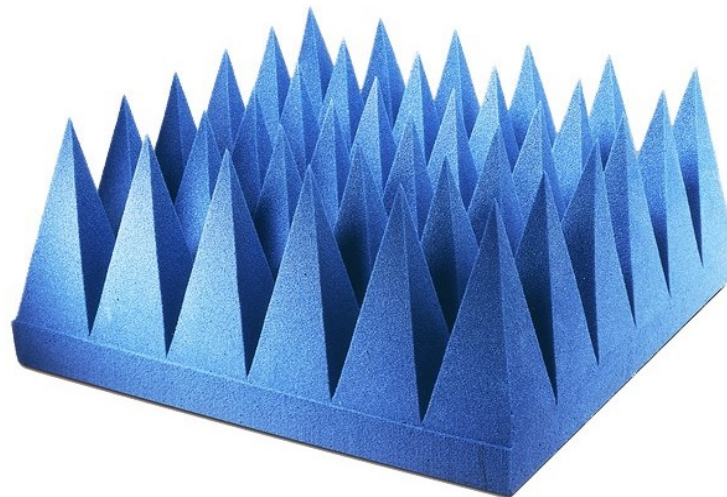


Figure 1.1: Illustration of Pyramidal Dielectric Absorber.

1.2.2.2 Taped Loaded Absorber

This type of material is generally composed of a plate of a low loss material associated with a plate of a material with high losses. The advantage of these materials is that they are thinner than pyramidal absorbers but less efficient [1] (**Fig. 1.2**).

1.2.2.3 Matching Layer Absorber

Matching Layer Absorber attempts to reduce the thickness required for progressively loaded materials. This type of absorber provides an absorption transition layer between the incident wave and the absorbent materials. The transition layer has an impedance value between the impedances of the two media. The idea is to have an impedance transition between different environments. This matching occurs when the thickness of the matching layer is a quarter of the wavelength of the incident wave with:

$$Z1 = \sqrt{Z0 \times Z3} \quad (1.1)$$

Impedance matching then occurs only at the desired frequency. Therefore, this type of absorber is narrow band [1] and very thick at low frequency (**Fig. 1.2**).

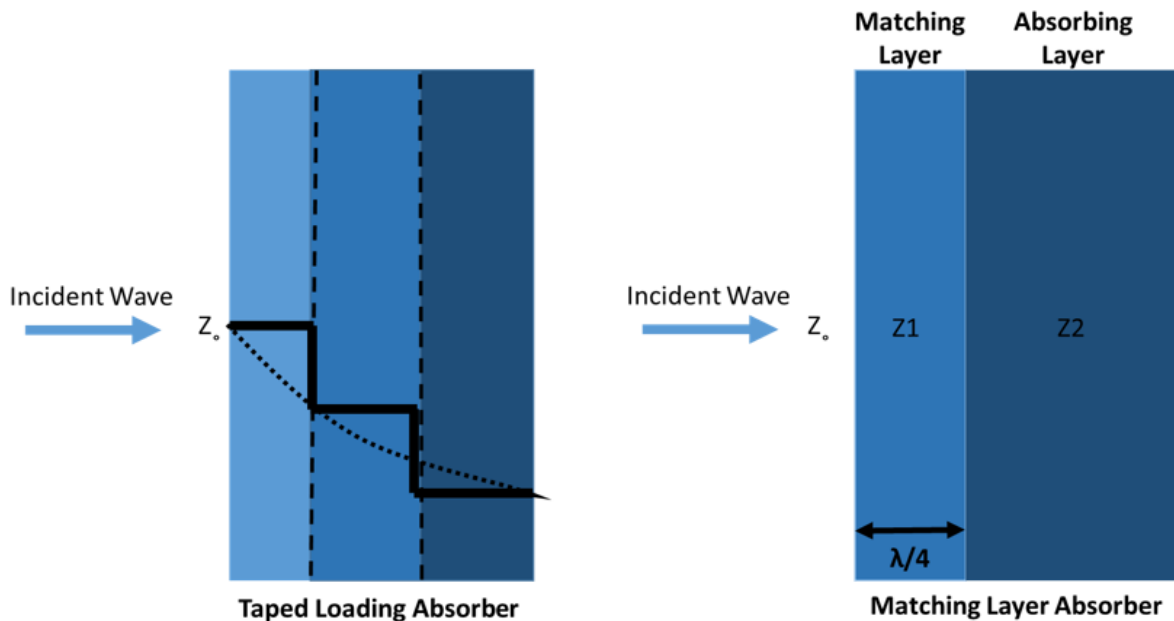


Figure 1.2: Illustration of Taped Loading Absorber and Matching Layer Absorber.

1.2.3 Resonant Absorber

They are called also tuned absorber. They include the Dällenbach layer [5], Salisbury [6] and Jaumann [7] layers. In this class of materials, the impedance is not necessarily adapted between the medium of the incident wave and the absorbing one. These materials are thin and do not absorb all the energy to which they are subjected. They operate through the destructive interference of the reflected waves. The mechanism employed uses reflection and transmission at the first interface. The reflected wave undergoes 180° phase shift. The transmitted wave travels through the absorbing medium to the metal plane that reflects it. This second reflection also undergoes a phase shift of 180° in absorbing medium before the propagation of waves towards the medium of the incident wave. If the optical distance traveled by the transmitted wave is a multiple of half wavelengths then the two reflected waves will be out of phase at the interface, which will cause destructive interference. If the amplitude of two reflected waves is equal then the total reflected intensity is zero (see **Fig. 1.3**). For that, this kind of absorber requires a considerable thickness essentially in lowest frequency regions when the wavelength is dimensional.

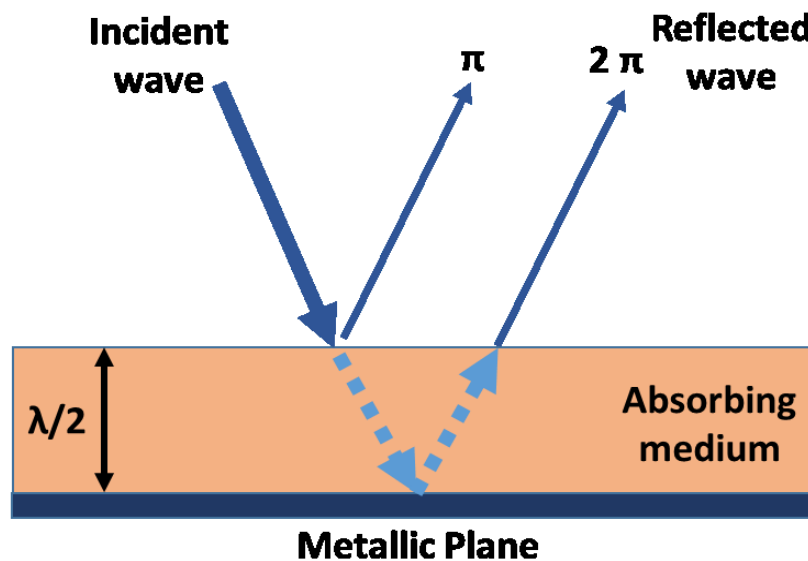


Figure 1.3: Illustration of Destructive Interference Phenomenon.

1.2.4 Magnetic Absorber

These materials are based on the use of iron or ferrite particles. An important advantage of magnetic absorbers is the fact that, despite their small thickness, they offer very good reflection attenuation characteristics in low frequencies starting from 30 MHz. The biggest disadvantage, however, is the relatively high price and the heaviness as well as the limitation of frequencies up to 1 GHz. Magnetic absorbers should be considered in all the cases where pyramid absorbers cannot be used due to limited space.

1.3 Anechoic Chamber

Current Anechoic Chamber present high-performance broadband electromagnetic absorbers spread along all surfaces by periodic units. Such an absorber belongs to the dielectric structural absorber category explained before. Each unit consists of a single block of polyurethane foam, pyramidal-shaped with a carbon-based aqueous solution. They are suitable for broadband applications and are used to line semi-anechoic and fully anechoic chambers for antenna measurements, Radar Cross Section, compact ranges, telecom, Electromagnetic Compatibility (EMC), and military applications.

1.3.1 Description of its Structure

The lining materials of anechoic chambers are made from two distinctly different types of materials although both types are commonly met in different areas of the same chamber:

- Closed-cell polyurethane or polystyrene foam molded into a steep pyramidal shape and “dosed” with carbon then painted with a fire-resistant paint. The principle of this type of absorber is to mimic free space by “progressive impedance”; i.e., absorbing the radio or microwave by internal reflection through a resistive structure that has a progressively larger shape during which the wave energy is being converted into heat.

- Ferrite tiles which are made as thick pieces with a central fixing hole. They are made from sintered iron/nickel material, which is ground to a precise shape so that large wall sections can be precisely assembled. Ferrite linings operate well at lower frequencies where the wavelength is too long for pyramidal absorbers to work effectively.

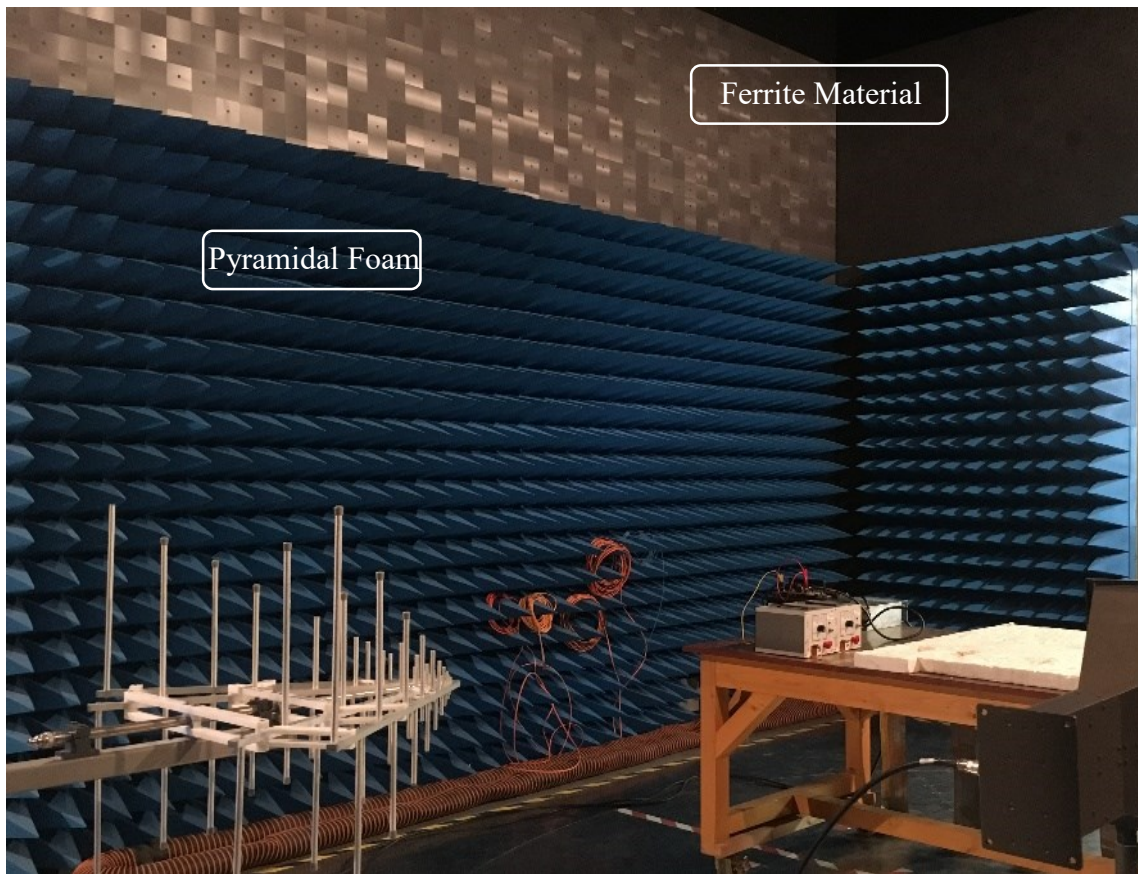


Figure 1.4: Photo took in a Semi Anechoic Chamber.

1.3.2 Dimension VS Operating frequencies

Pyramid absorbers are available in many sizes. The required dimensions depend mainly on the wavelength of the lowest usable frequency specified for the anechoic chamber. These dimensions differ slightly between companies. However, we present in **Table 1.1** the relation between frequencies and the height of a required pyramid as presented by one of the most sophisticated companies [8].

By referring to **Table 1.1**, to reach good absorption performance at low frequency, the height of APM must be higher than 1 meter of altitude, which is considered as a bulky structure in a test chamber.

Table 1-1: Heights of APM (Pyramidal Foam Absorber) depending on the operative frequencies with the value of Reflectivity performance attained at normal incidence [8].

GUARANTEED REFLECTIVITY PERFORMANCES (dB) OF APM ABSORBERS (normal incidence)													
TYPE	Total overall height		80 MHz	200 MHz	300 MHz	500 MHz	1 GHz	2 GHz	4 GHz	8 GHz	12 GHz	18 GHz	40 GHz
	mm	in											
APM 3	28	1.1							-12	-13	-13	-17	-22
APM 5	55	2.2						-20	-21	-25	-31	-35	-38
APM 9	89	3.5					-15	-21	-29	-36	-40	-43	-40
APM 12	115	4.5					-19	-20	-33	-40	-40	-50	-40
APM 20	210	8.3				-14	-25	-36	-45	-46	-52	-52	-40
APM 30	305	12				-25	-36	-40	-48	-52	-52	-52	-40
APM 45	455	18				-27	-41	-42	-50	-52	-52	-52	-40
APM 55	550	21.6			-26	-36	-44	-45	-50	-52	-52	-52	-40
APM 66	660	26	-6	-21	-27	-38	-45	-47	-52	-52	-52	-52	-40
APM 85	850	33.5	-10	-24	-28	-42	-49	-52	-52	-52	-52	-52	-40
APM 100	1000	39.4	-13	-26	-33	-43	-52	-52	-52	-52	-52	-52	-40
APM 115	1150	43.7	-15	-28	-38	-43	-52	-52	-52	-52	-52	-52	-40

1.3.3 Anechoic Chamber Disadvantages

The Polyurethane foam material of pyramids is sensitive to atmospheric humidity, fragile and support a limited incident wave power view its highly flammable properties [8]. An anechoic chamber is until now the unique solution for measurement application in spite of all these entire disadvantages because it can insure an absorption bandwidth more than one decade from 0.3 GHz. Trying to resolve such a problem, the next section introduces our proposed way to find a new type of absorber in broadband operation with miniaturized dimensions using “Metamaterial”.

1.4 Metamaterial Absorber

Metamaterial is introduced as an effective medium where the designer can control the electromagnetic properties by engineering the geometry that exhibits unnatural material with singular properties. Such kinds of materials are usually made of assemblies of dielectric and metallic elements at scales that are much smaller than the wavelength and exhibit singular dispersion properties such as negative permittivity (ϵ_{eff}) and permeability (μ_{eff}) [9-11].

Thanks to these properties, the metamaterial can be used to manipulate electromagnetic waves by absorbing, filtering, enhancing or bending waves. As a consequence, extensive potential applications are foreseen as microwave and optical filters, high sensitivity detectors, low profile directive antennas, right- and left-handed phase shifters, invisible cloaks, ultra-thin total absorbers and so on [12-23]. Particularly, the branch of metamaterial perfect absorber (MPA) has garnered interest because it can achieve unity absorptivity of electromagnetic waves at scales that are much smaller than the wavelength. Since the first experimental demonstration of MPA in 2008 by N. I. Landy et al. [24], a large number of efforts [25-31] have been made on Metamaterial absorbers to achieve multi-band absorption, broadband absorption, polarization-insensitive absorption, and wide incident angle absorption. Normally, metamaterials can be realized through several kinds of structures such as photonic crystal structures [32-35], Transmission line (TL) based structures [36-39], resonant structures [24], and full dielectric materials [40]. MPA belongs to the resonant structure, so it operates in narrow band.

In the coming section, we present the different ways of absorption achieved by metamaterials in a narrow band. After that, we present the ways applied to broaden the band of absorption.

1.4.1 Categories of Metamaterial Absorber

In literature, almost metamaterial absorber is presented based on the resonant category by different principles. We address in this section the main principles of metamaterial absorber and we will cite its efficiency view its absorption level, incident angle sensitivity, polarization sensitivity based on an overview of some models in the literature.

1.4.1.1 Plasmonic Resonance

It is the simplest design presented in the literature. It is considered as the basic element for a resonant absorber. Throughout the development of the MPA, the plasmonic resonant based MPAs have grown rapidly during the last decade because they can possess broadband behaviors and other useful properties for real applications. Most of the MPAs are composed of three layers: (i) periodically metallic structured patterns, (ii) dielectric layer and (iii) continuous metallic plate [40].

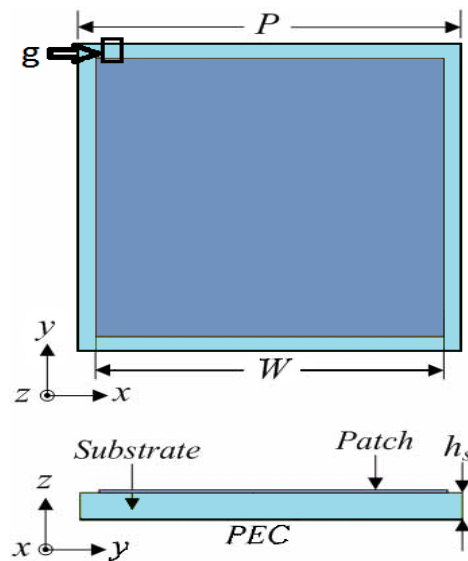


Figure 1.5: Unit Cell of a Plasmonic Metamaterials Absorber of square patches type of periodicity $P = 17.5$ mm, the thickness of the substrate is $h_s = 0.3$ mm, $g = 1$ mm, and the length of the metallic patch $W = 15.2$ mm.

The periodically arranged metallic layers should be carefully designed to provide a certain resonance at the targeted frequency. Fulfilling the impedance matching condition to the free space is achieved by varying the dimensions of the resonators which can have various shapes such as ring, cross, patch, circular, snowflake and so on. Under this impedance matching condition so that reflectivity on the device vanishes and all the incidence EM waves should be coupled to the device.

The second dielectric layer plays a basic role by trapping the incident electromagnetic wave EM wave. At the resonant frequency of the absorber, the EM waves are bouncing back and forth inside the resonator so that the EM energy is dissipated efficiently.

In other words, the generic metal-dielectric-metal structure plays a role in the resonant cavity with a lifetime in the cavity related to the frequency selectivity of the resonance through the quality factor. The primary role of the third metallic layer is to stop any transmission of the impinging wave. Besides, we will see in the following chapters devoted to plasmonic-type structures that the metallic regions facing the structured top metal layers support backside local currents flowing in the opposite direction to the top ones.

To sum up, when an EM wave is impinging on such a tri-layered medium, the fact that the transmission is zero and the reflection vanishes at the resonance means that all the EM energy is absorbed justifying the term of PMA. More details about this operating principle will be discussed in the next chapter.

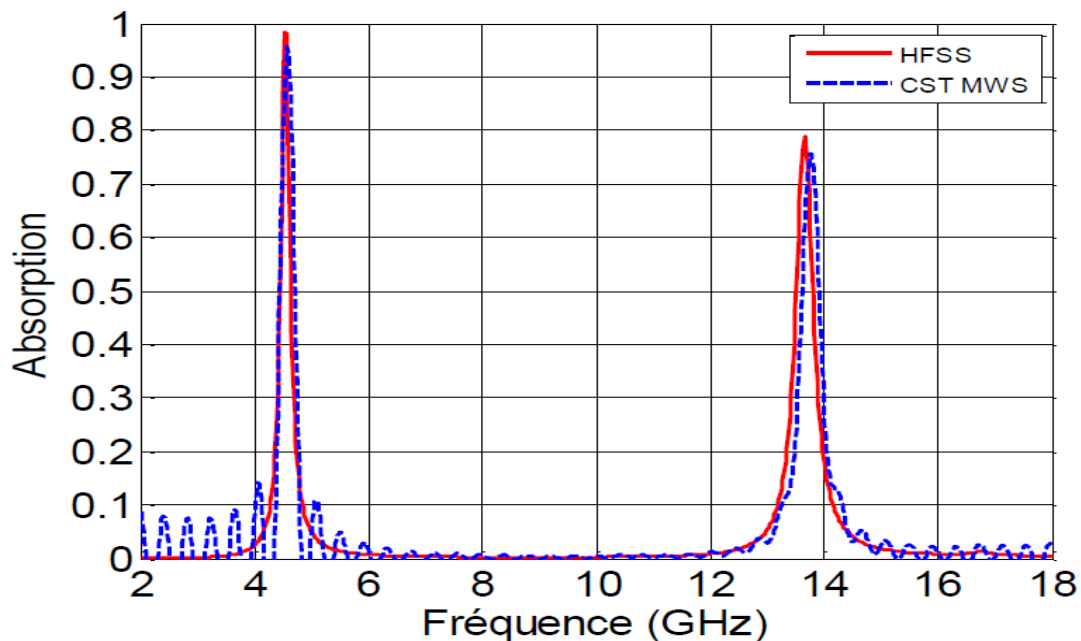


Figure 1-6: Absorption response obtained by Simulation of a Square Metamaterials Absorber with Ansys HFSS and CST Microwave Studio [42].

After simulation using Ansys HFSS [42], we can see that the modification of the incidence around the axis has several effects. We observe the resurgence of some dark modes and degradation of the performances with the increase of the angle.

1.4.1.2 Mie Resonance Based

Ferroelectric materials, such as BaTiO₃(BTO), Pb(Zr,Ti)O₃ (PZT) and LiNbO₃ (LNO) have attracted much interest owing of their applications in many domains including high-density capacitors, filters, oscillators, resonators and tunable microwave devices [43-46].

Among these ferroelectric materials, BTO-based films with Sr doping, namely $Ba_{1-x}Sr_xTiO_3$ (BST) are the essential components for wide spectrum applications, especially for electric field response components and devices such as phase shifter [46-47], varactors [49], antenna [50], accelerator [51], cloaking [52], and so on because of its high dielectric constant, reasonable dielectric loss, high tunability, and large breakdown strength [53-56].

Thanks to high permittivity, BST particles, normally cubes with a sub-wavelength scale, shown in **Fig. 1.7**, can support strong resonances based on Mie scattering theory [45]. Based on the principle of surface impedance matching of ferroelectric cubes, ferroelectric $BaSrTiO_3$ (BST) cubes were arrayed onto a metal ground plane to get a near unit absorption at Mie resonance frequency (refer to **Fig. 1.8**).

This periodic array of dielectric cubes exhibits a magnetic and electric activity that cancels the reflectivity by impedance matching whereas a backside metal plane stops the transmitted wave.

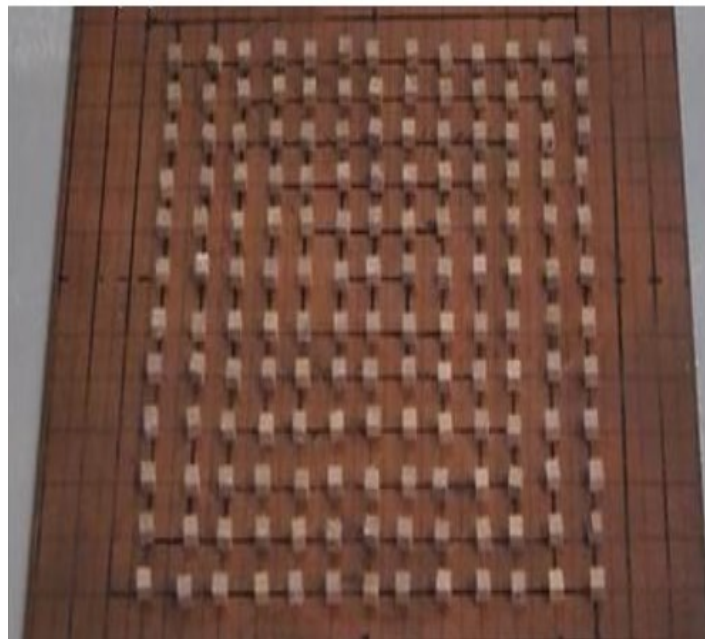


Figure 1.7: Photograph of the periodic BST array [57].

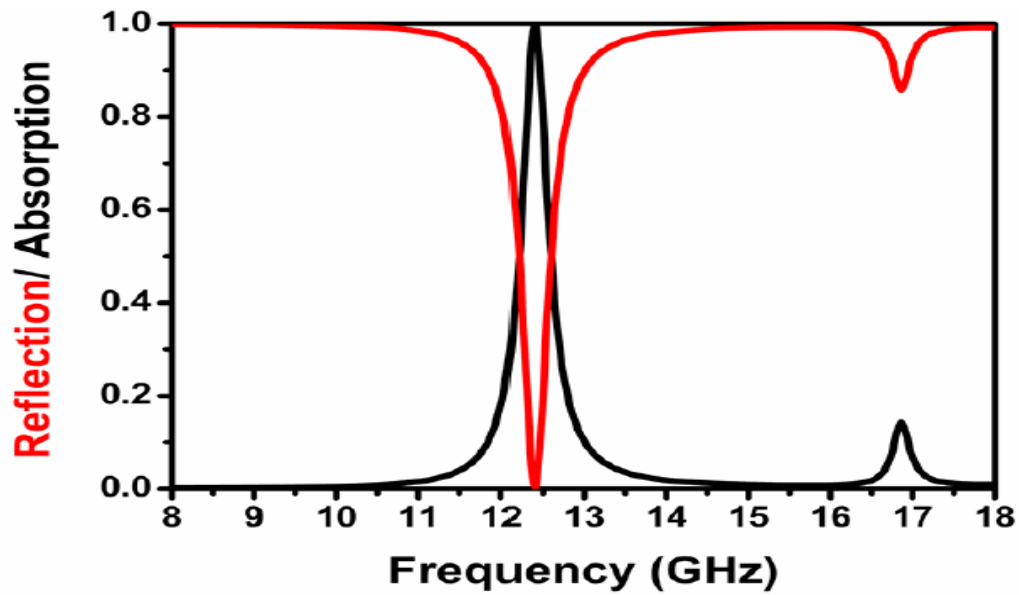


Figure 1.8: Reflection and absorption spectra for an absorber with BST cube array with period $P_x = P_y = 9$ mm and side length $a_x = a_y = a_z = 1.8$ mm on a 0.2 mm-thick dielectric layer and a metal substrate [57].

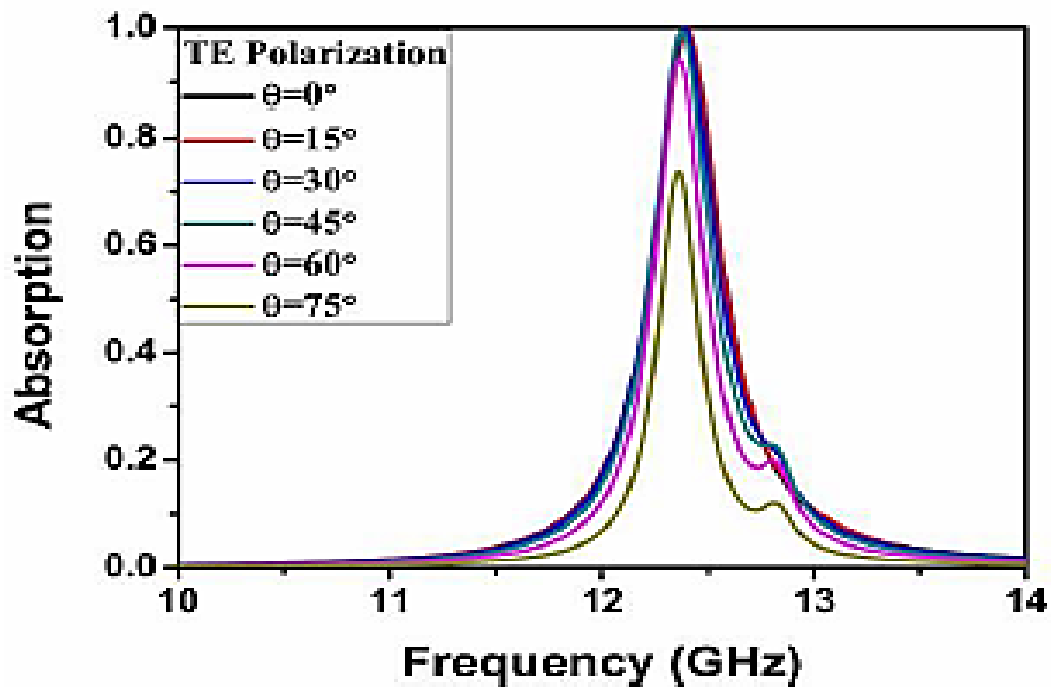


Figure 1.9: Absorption spectra as a function of frequency for incidence angle ranging from 0° to 75° [57].

The 2D BST absorber could keep a high absorption above 90% even if the incident wave is up to 60° with respect to the absorber surface (see **Fig. 1.9**). Moreover, thanks to the symmetric shape of the individual BST cube and the same period along with two orthogonal directions, *TE* and *TM* polarizations show the same response.

1.4.2 Broadening Ways

Referring to these cited absorption principles, we notice that the main principle of metamaterial is based on resonant structure. Indeed, the simultaneously electric and magnetic resonance will result in a narrow absorption bandwidth, which may limit its application in practice. In this section, we propose the main methods applied in the literature to obtain broadband metamaterial absorber.

It is worth mentioning that the parameter of real broadband response is the relative absorbing bandwidth (RAB) expressed by:

$$RAB = \frac{\Delta f}{f_c} \quad (1.2)$$

$$\Delta f = f_L - f_U \quad (1.3)$$

$$f_c = \frac{f_u + f_l}{2} \quad (1.4)$$

Where f_U and f_L are the upper and lower limits of the absorptive frequency range respectively.

1.4.2.1 Juxtaposition

This broadening way consists of adding metallic resonator patches in the same ground plane with different dimensions. Each resonator is realized employing three layers of the plasmonic design cited before. All the patches are centered in each sub-cell.

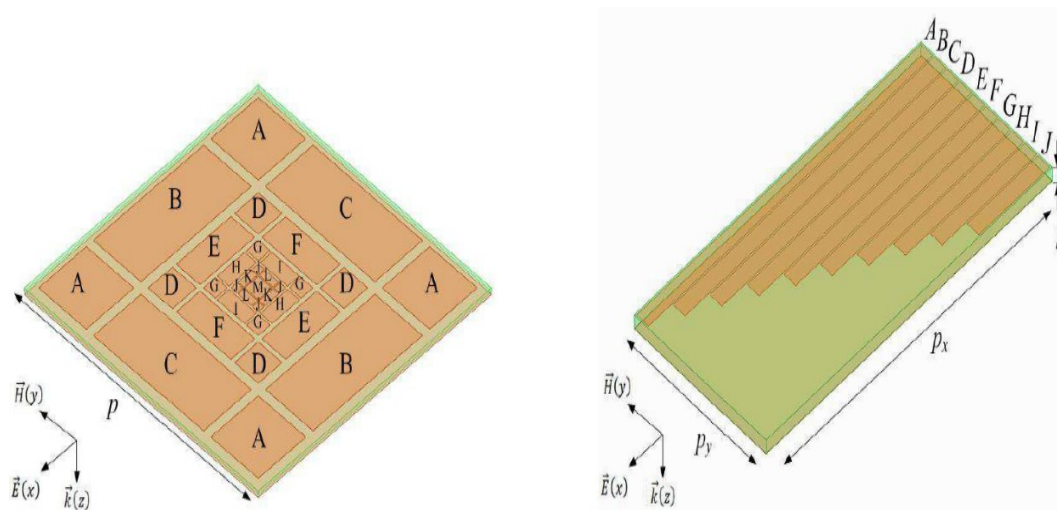
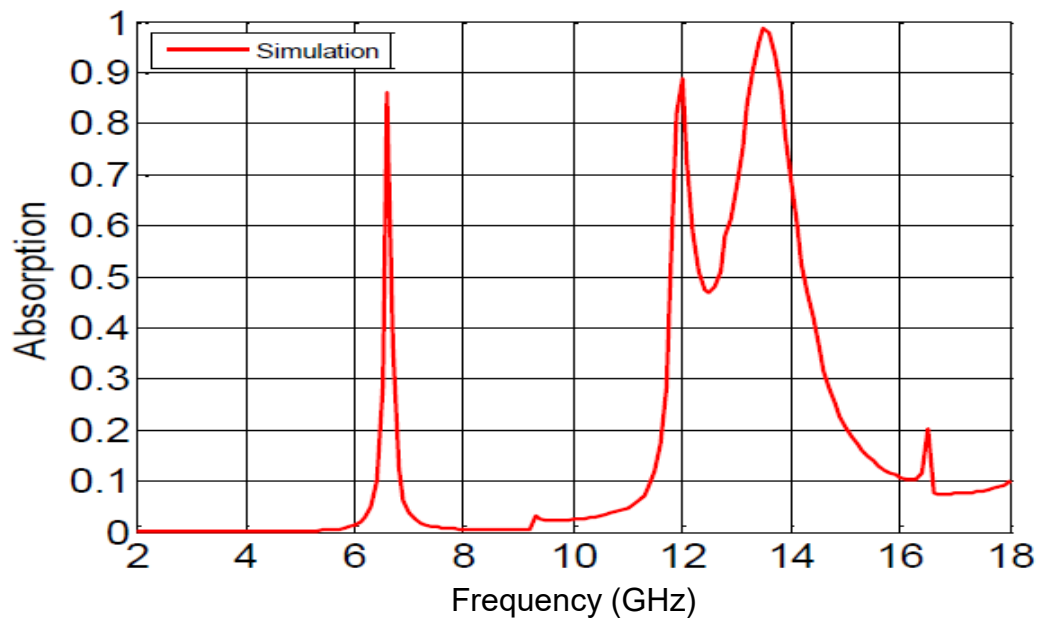
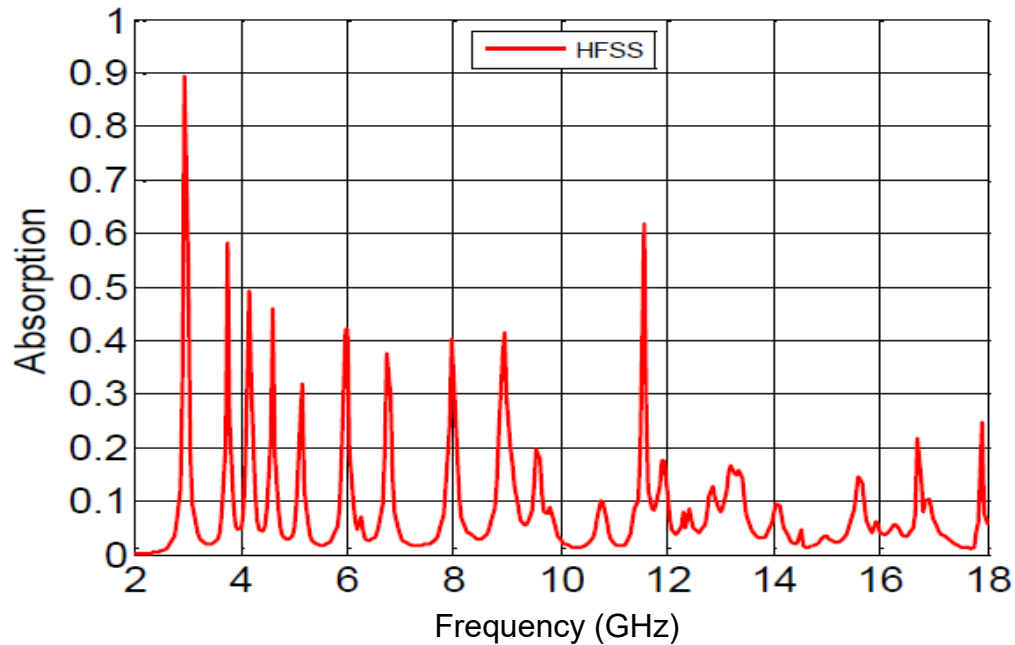


Figure 1.10: Schematic of metal/dielectric/metal resonator grouped in the same ground plane with different dimensions (a) MultiCross design (b) different rectangular patches [42].

Each patch contributes to this structure thanks to their different sizes, and they resonate at different frequencies. There is a progressive frequency of resonance according to the decrease of the patch size (see **Fig. 1.10**).



(a)



(b)

Figure 1.11: Simulation showing the absorption of the metamaterials absorbent consisting of: (a) the MultiCross design (b) design of several rectangular patches juxtaposed with Ansys HFSS [42].

The results obtained in **Fig. 1.11** show different peaks of resonance obtained by each patch but with degradation in the absorption level. The loss of absorption in each patch is caused by the distance increased between patches of the same size. Such distance results some reflections therefore the absorption level of sizable patches is under 50 %. This structure is quite simple and is developed for operation under a single polarization angle of the incident wave [42].

1.4.2.2 Stacked Layers

S. He et al. have proposed a stacked structure shaped like a pyramid which can totally absorb waves in the microwave regime [58]. Since the size of the metal-dielectric unit layers is gradually increased along the transverse direction (refer to **Fig. 1.12**) so that a pyramidal shape is achieved, this type of structure is generally called pyramidal absorber.

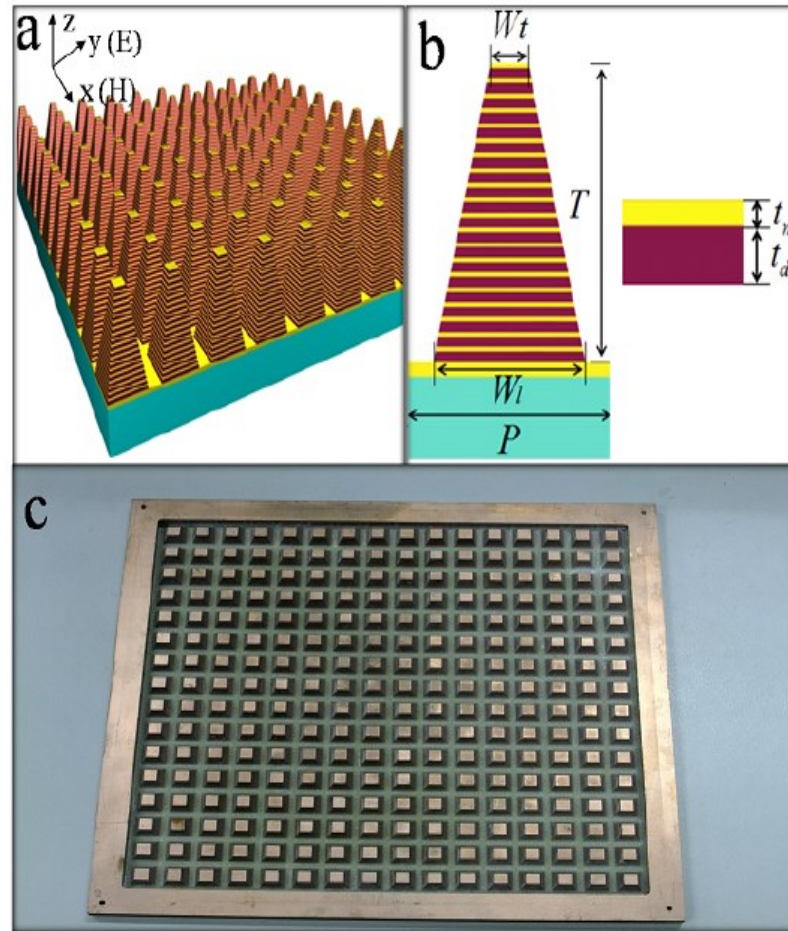


Figure 1.12: Design and fabrication of a microwave ultra-broadband MA. (a) Three-dimensional illustration of the simulated MA, (b) schematic of an MA unit cell, and (c) photograph of the fabricated sample. The optimized dimensions of a unit are $W_t = 5$ mm, $W_l = 5$ mm, $P = 11$ mm, $t_m = 0.05$ mm, $t_d = 0.2$ mm, and $T = 5$ mm [58].

In the pyramidal absorber, each unit layer corresponds to a certain resonant frequency and an ultra-wideband absorption can be achieved by superposition of multiple resonances with small frequency intervals. The absorption in this type of absorber is independent of polarization due to the symmetry of the designed MA. Even, its absorption is robust for non-normal incidence (**Fig. 1.13**) [58].

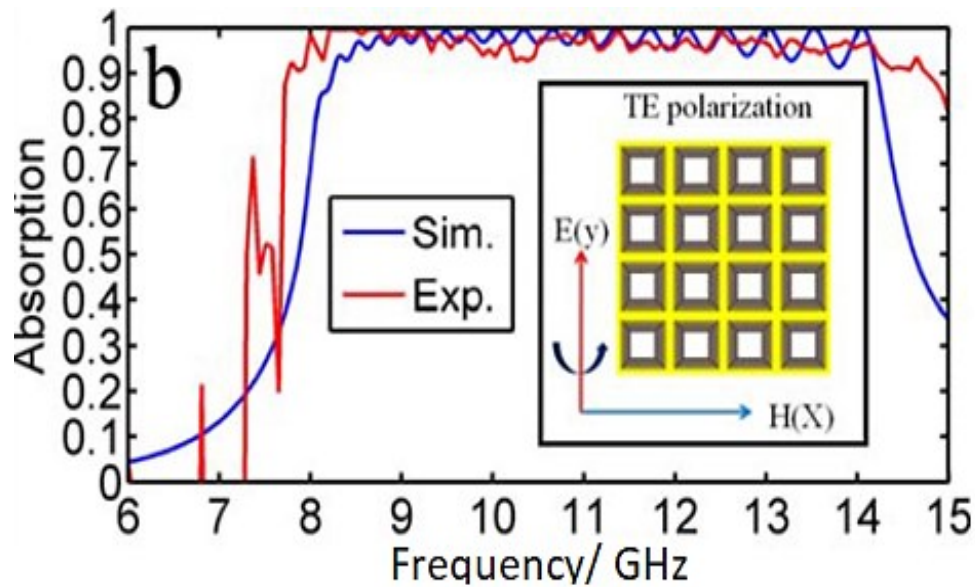


Figure 1.13: Simulated and Experimental absorption performance of the MA in Fig. 1.12.

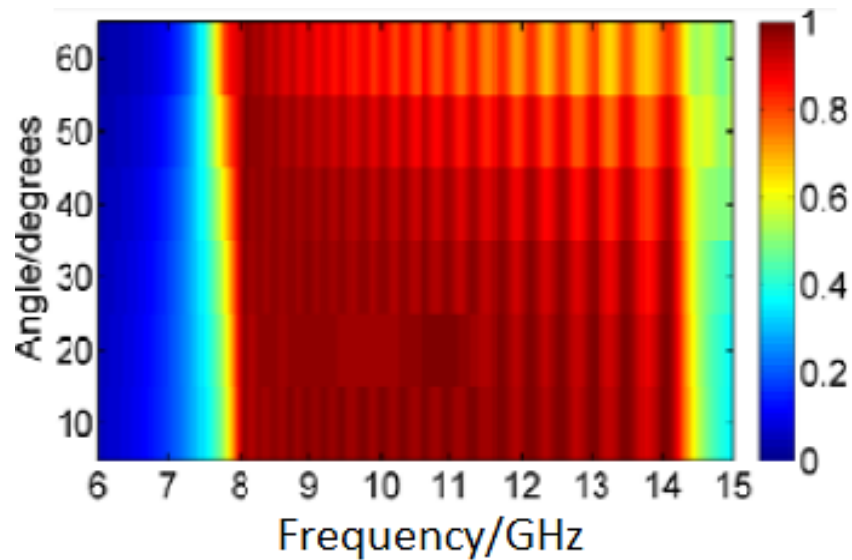


Figure 1.14: Simulated angular absorption of the MA in Fig 1.11 for TE configuration. The incident angle is varied from 0 degrees to 60 degrees [58].

1.4.2.3 Random Distribution

We focused on a recent way of broadening the absorption window of metamaterial-based absorbers by extending magnetic resonance modes in disordered metamaterials. Barium Strontium Titanate (BST) cubes resonating at centimeter wavelength was used in a random array of identical

size cubes (see **Fig. 1.15**). This arrangement was proved that it could lead to a broadening in the absorption bandwidth concerning the response obtained by periodic arrangement. Such a response is affected by different parameters such as filling factor of cubes, polarization and oblique incidence were studied both numerically and experimentally in reference [57].



Figure 1.15: Photograph of the random BST cubes sample deposited on the copper plate [57].

Disordered metamaterial absorbers proved that they could exhibit 4 times enhancement of their half-maximum bandwidth when compared to the periodic one (see **Fig 1.16**). Such enhancement in the bandwidth was explained by the coupling of the magnetic dipole when the resonators are nearby.

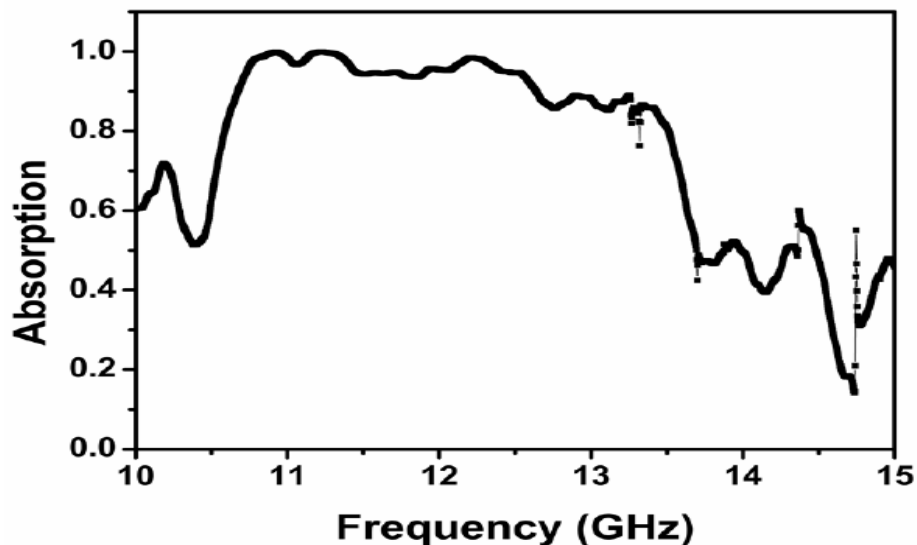


Figure 1.16: Experimental absorption spectrum for the random structure in figure 1.15 [57].

1.4.2.4 Metamaterial with Magnetic Element

Magnetic absorbers have good absorption performance over wide bands and are generally very small in front of the wavelength. As cited before in section 1.2.4, their main problem is that they are very dense because they are heavily loaded with ferrous materials. The thickness and the charge rate of these materials are very influential in their operating frequency. Therefore, absorber metamaterial was introduced in [42] with magnetic absorber to widen the operating frequency and shifting it to lower frequencies.

Different plasmonic models were tested in combining with a magnetic material in reference [42]. It is realized that it is better to place the metamaterials absorbent under the magnetic absorber for optimal results. In **Fig. 1.17**, the impact of this combining idea is shown by comparing the absorption response of the magnetic material alone (dotted curve) with the combined structure (magnetic stacked in the MultiCross plasmonic design). It shows that the target of shifting frequencies was attained but with a degradation in high frequency. Naturally, such an idea suffers from the sensitivity in the angle of incidence and polarization due to its sensitivity with the plasmonic structure.

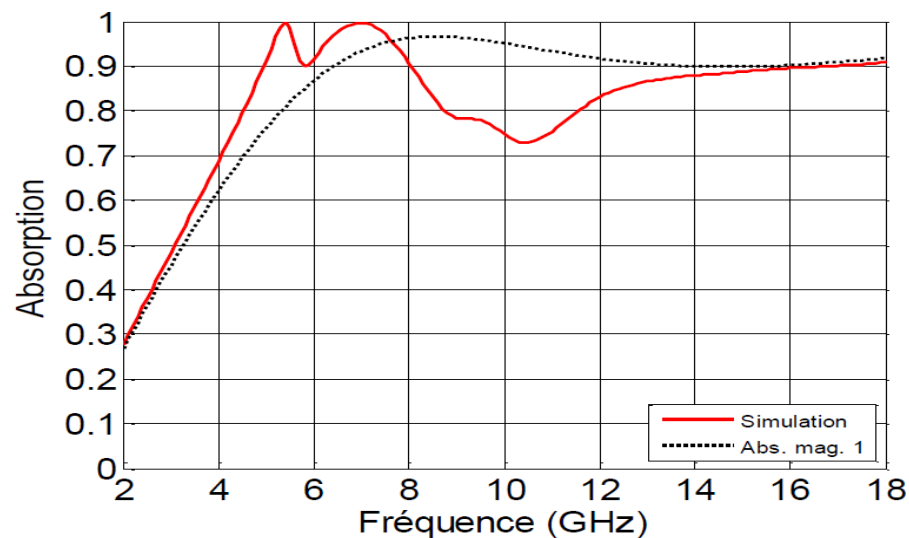


Figure 1.17: Comparison of the Absorption of the MultiCross / Magnetic Absorber Stack and the Magnetic Absorber alone [42].

1.5 Conclusion

In this chapter, we presented a full overview of most categories of absorbers presented in the industry (dielectric, structural, dielectric, resonant, and magnetic). We highlighted the disadvantages of each category. We found that the most sophisticated category is the Pyramidal dielectric presented now by important companies to manipulate anechoic chambers. Such a category suffers from its fragility, humidity sensitivity, its high cost even its bulkiness especially when the operating frequency been below 1 GHz. Starting from what is discussed, the need for a new category of absorbers arises seeking a good absorption response in better conditions.

In this context, we presented the benefits of metamaterial absorber in reaching unit absorption with lightweight and reduced thickness with respect to the wavelength in its both type: plasmonic and Mie resonance-based. The metamaterial creates perfect absorbers by electromagnetic resonance causes resulting in absorption in a narrow bandwidth which may limit its application in practice.

Thence, we present the ways proposed in the literature to designs a broadband absorber metamaterial-based. We found that the design that can offer insensitivity from wave polarization and angle of incidence even can reach an Ultra-Wideband with low cost is the “Stacked Pyramidal Design”. Essaying to reach our objective, this model is selected to be the basis of our research study. Therefore, in the following chapter, we present the absorption mechanism of the stacked design and we study all parameters affecting its absorption response to guide the designing of an innovative metamaterial absorbers stacked-resonators based.

1.6 Reference

- [1] Sellier, Alexandre. *Absorbants à métamatériaux: étude théorique et expérimentale*. Diss. Université Paris Sud-Paris XI, 2014.
- [2] Yoo, Y. J., et al. "Flexible and elastic metamaterial absorber for low frequency, based on small-size unit cell." *Applied physics letters* 105.4 (2014): 041902.
- [3] Bui, Son Tung, et al. "Small-size metamaterial perfect absorber operating at low frequency." *Advances in Natural Sciences: Nanoscience and Nanotechnology* 5.4 (2014): 045008.
- [4] Tanner, Howard A. "Fibrous microwave absorber." U.S. Patent No. 2,977,591. 28 Mar. 1961.
- [5] Dallenbach, W., and W. Kleinstaubler. "Reflection and absorption of decimeter-waves by plane dielectric layers." *Hochfreq. u Elektroak* 51 (1938): 152-156.
- [6] Salisbury, W. W. "US Patent, Absorbent body for electromagnetic waves." (1952).
- [7] Naishadham, Krishna, and Prasad K. Kadaba. "Measurement of the microwave conductivity of a polymeric material with potential applications in absorbers and shielding." *IEEE Transactions on Microwave Theory and Techniques* 39.7 (1991): 1158-1164.
- [8] <https://www.siepel.com/>
- [9] Pendry, John B., et al. "Magnetism from conductors and enhanced nonlinear phenomena." *IEEE transactions on microwave theory and techniques* 47.11 (1999): 2075-2084.
- [10] Smith, D. R., et al. "Determination of effective permittivity and permeability of metamaterials from reflection and transmission coefficients." *Physical Review B* 65.19 (2002): 195104.
- [11] Shelby, Richard A., David R. Smith, and Seldon Schultz. "Experimental verification of a negative index of refraction." *science* 292.5514 (2001): 77-79.
- [12] Capolino, Filippo. *Applications of metamaterials*. CRC press, 2009.

- [13] Rudykh, Stephan, and Mary C. Boyce. "Transforming wave propagation in layered media via instability-induced interfacial wrinkling." *Physical review letters* 112.3 (2014): 034301.
- [14] Pendry, John Brian. "Negative refraction makes a perfect lens." *Physical review letters* 85.18 (2000): 3966.
- [15] Vora, Ankit, et al. "Exchanging ohmic losses in metamaterial absorbers with useful optical absorption for photovoltaics." *Scientific reports* 4 (2014): 4901.
- [16] Enoch, Stefan, et al. "A metamaterial for directive emission." *Physical Review Letters* 89.21 (2002): 213902.
- [17] Emerson, W. "Electromagnetic wave absorbers and anechoic chambers through the years." *IEEE Transactions on Antennas and Propagation* 21.4 (1973): 484-490.
- [18] Alù, Andrea, and Nader Engheta. "Achieving transparency with plasmonic and metamaterial coatings." *Physical Review E* 72.1 (2005): 016623.
- [19] Pendry, John B., David Schurig, and David R. Smith. "Controlling electromagnetic fields." *science* 312.5781 (2006): 1780-1782.
- [20] Schurig, David, et al. "Metamaterial electromagnetic cloak at microwave frequencies." *Science* 314.5801 (2006): 977-980.
- [21] Alu, Andrea, and Nader Engheta. "Plasmonic materials in transparency and cloaking problems: mechanism, robustness, and physical insights." *Optics Express* 15.6 (2007): 3318-3332.
- [22] Caloz, Christophe, and Francisco P. Casares-Miranda. "Active metamaterial structures and antennas." *MELECON 2006-2006 IEEE Mediterranean Electrotechnical Conference*. IEEE, 2006
- [23] Grbic, Anthony, and George V. Eleftheriades. "A backward-wave antenna based on negative refractive index LC networks." *IEEE Antennas and Propagation Society International Symposium (IEEE Cat. No. 02CH37313)*. Vol. 4. IEEE, 2002.

- [24] Landy, N. I., et al. "Perfect metamaterial absorber." *Physical review letters* 100.20 (2008): 207402.
- [25] Shen, Xiaopeng, et al. "Triple-band terahertz metamaterial absorber: Design, experiment, and physical interpretation." *Applied Physics Letters* 101.15 (2012): 154102.
- [26] Ding, Fei, et al. "Ultra-broadband microwave metamaterial absorber." *Applied physics letters* 100.10 (2012): 103506.
- [27] Sun, Jingbo, et al. "An extremely broad band metamaterial absorber based on destructive interference." *Optics Express* 19.22 (2011): 21155-21162.
- [28] Zhu, Bo, et al. "Switchable metamaterial reflector/absorber for different polarized electromagnetic waves." *Applied Physics Letters* 97.5 (2010): 051906.
- [29] Cheng, Hua, et al. "A polarization insensitive and wide-angle dual-band nearly perfect absorber in the infrared regime." *Journal of Optics* 14.8 (2012): 085102.
- [30] Wei, Xingzhan, et al. "Artificial metal with effective plasma frequency in near-infrared region." *Optics express* 18.4 (2010): 3370-3378.
- [31] Munday, Jeremy N., and Harry A. Atwater. "Large integrated absorption enhancement in plasmonic solar cells by combining metallic gratings and antireflection coatings." *Nano letters* 11.6 (2010): 2195-2201.
- [32] Seo, Byoung-Joon, et al. "Isotropic left handed material at optical frequency with dielectric spheres embedded in negative permittivity medium." *Applied physics letters* 88.16 (2006): 161122.
- [33] Rennings, A., C. Caloz, and I. Wolff. "A novel clustered dielectric cubes metamaterial (CDC-MTM)." *2006 IEEE Antennas and Propagation Society International Symposium*. IEEE, 2006.
- [34] Shumpert, John D., William J. Chappell, and Linda PB Katchi. "Parallel-plate mode reduction in conductor-backed slots using electromagnetic bandgap substrates." *IEEE Transactions on Microwave Theory and Techniques* 47.11 (1999): 2099-2104.

- [35] Pendry, J. B., L. Martin-Moreno, and F. J. Garcia-Vidal. "Mimicking surface plasmons with structured surfaces." *science* 305.5685 (2004): 847-848.
- [36] Caloz, Chirtophe, and Tatsuo Itoh. "Transmission line approach of left-handed (LH) materials and microstrip implementation of an artificial LH transmission line." *IEEE Transactions on Antennas and propagation* 52.5 (2004): 1159-1166.
- [37] Eleftheriades, George V., Ashwin K. Iyer, and Peter C. Kremer. "Planar negative refractive index media using periodically LC loaded transmission lines." *IEEE transactions on Microwave Theory and Techniques* 50.12 (2002): 2702-2712.
- [38] Grbic, Anthony, and George V. Eleftheriades. "Periodic analysis of a 2-D negative refractive index transmission line structure." *IEEE Transactions on Antennas and Propagation* 51.10 (2003): 2604-2611.
- [39] Caloz, Christophe. "Dual composite right/left-handed (D-CRLH) transmission line metamaterial." *IEEE microwave and wireless components letters* 16.11 (2006): 585-587.
- [40] Vandembem, Cédric, and Jean Pol Vigneron. "Mie resonances of dielectric spheres in face-centered cubic photonic crystals." *JOSA A* 22.6 (2005): 1042-1047.
- [41] Watts, Claire M., Xianliang Liu, and Willie J. Padilla. "Metamaterial electromagnetic wave absorbers." *Advanced materials* 24.23 (2012): OP98-OP120.
- [42] Sellier, Alexandre. *Absorbants à métamatériaux: étude théorique et expérimentale*. Diss. Université Paris Sud-Paris XI, 2014.
- [43] Bao, P., et al. "Barium strontium titanate thin film varactors for room-temperature microwave device applications." *Journal of Physics D: Applied Physics* 41.6 (2008): 063001.
- [44] Cole, M. W., et al. "The influence of Mg doping on the materials properties of Ba_{1-x}Sr_xTiO₃ thin films for tunable device applications." *Thin Solid Films* 374.1 (2000): 34-41.
- [45] Cole, M. W., P. C. Joshi, and M. H. Ervin. "La doped Ba_{1-x}Sr_xTiO₃ thin films for tunable device applications." *Journal of Applied Physics* 89.11 (2001): 6336-6340.

- [46] Tagantsev, A. K., et al. "Ferroelectric materials for microwave tunable applications." *Journal of electroceramics* 11.1-2 (2003): 5-66.
- [47] Kuylenstierna, Dan, et al. "Composite right/left handed transmission line phase shifter using ferroelectric varactors." *IEEE Microwave and Wireless Components Letters* 16.4 (2006): 167-169.
- [48] Vélú, G., et al. "A 310/spl deg//3.6-dB K-band phaseshifter using paraelectric BST thin films." *IEEE microwave and wireless components letters* 16.2 (2006): 87-89.
- [49] Burgnies, Ludovic, et al. "A TRL-like calibration for tunable interdigitated BST varactors." *IEEE Transactions on Instrumentation and Measurement* 57.6 (2008): 1127-1132.
- [50] Pan, K. C., et al. "Frequency tuning of CPW bowtie antenna by ferroelectric BST thin film varactors." *Proceedings of the 2011 IEEE National Aerospace and Electronics Conference (NAECON)*. IEEE, 2011.
- [51] Kanareykin, Alexei, et al. "Observation of an Anomalous Tuning Range of a Doped BST Ferroelectric Material Developed for Accelerator Applications." *Conf. Proc.* Vol. 100523. No. IPAC-2010-THPEB051. 2010.
- [52] Gaillot, Davy P., Charles Croënne, and Didier Lippens. "An all-dielectric route for terahertz cloaking." *Optics express* 16.6 (2008): 3986-3992.
- [53] Kim, S. S., et al. "Ferroelectric Properties of (Bi, Sm) $4\text{Ti}_3\text{O}_{12}$ (BST) Thin Films Fabricated by a Metalorganic Solution Deposition Method." *Journal of electroceramics* 13.1-3 (2004): 83-88.
- [54] Jiang, Yongdong, et al. "BST and other ferroelectric thin films by CCVD and their properties and applications." *Ferroelectrics: Material Aspects* 3 (2011): 30.
- [55] Lepetit, T., E. Akmansoy, and J-P. Ganne. "Experimental measurement of negative index in an all-dielectric metamaterial." *Applied Physics Letters* 95.12 (2009): 121101.
- [56] Houzet, Gregory, et al. "Dispersion and loss of ferroelectric $\text{Ba}_{0.5}\text{Sr}_{0.5}\text{TiO}_3$ thin films up to 110 GHz." *Applied Physics Letters* 93.5 (2008): 053507.

[57] Hao, Jianping. *Broad band electromagnetic perfect metamaterial absorbers*. Diss. Lille 1, 2016.

[58] Ding, Fei, et al. "Ultra-broadband microwave metamaterial absorber." *Applied physics letters* 100.10 (2012): 103506.

2. Chapter 2: Pyramidal Design Setup

2.1 Introduction

In many systems, high performance in terms of the absorption coefficient, large bandwidth, insensitivity to incident wave polarization and angle of incidence are welcome and are even requested. In this context, we aimed to design an ultra-broadband metamaterial absorber by stacking multiple resonators with varying dimensions in a transverse direction forming a Pyramidal Absorber (PA). Stacking multilayered metamaterial structures is considered as a promising candidate for designing such design with all these specifications. It presents an effective method to extend the absorption band making the MA units resonate at several neighboring frequencies [1, 3].

This principle was first demonstrated in the microwave range [4]. Jingbo Sun et al. proposed an extremely broadband metamaterial absorber based on the destructive interference mechanism exhibited in a multilayered SRRs stack [5-6]. After that, S. He et al. have proposed a stacked structure shaped as a pyramid [7]. Besides the microwave broadband absorber, an infrared ultra-broadband absorber that can also be regarded as a pyramid structure, namely sawtooth structure was presented by Y. Cui [8]. Following these proposed design absorbers, many articles based on pyramid broadband absorbers in the microwave, THz, infrared and visible regions have been published [9-13].

View the great specification of the pyramidal design, this chapter is dedicated to describe in detail the operation of such design. The first section will explain the absorption mechanism that occurred by the square patch, which is the basic unit of the pyramidal absorber. After that, we will identify the role of different parameters affecting the absorption response by a parametric study. The last section will give an added factor that provide an excellent enhancement on the absorption response and put a new degree of freedom that optimize well the absorption response of this elegant design.

2.2 Plasmonic Resonance Study

As mentioned above, the basic unit of the pyramidal design is the square patches. For that in this section, we present more details about the absorption mechanism of this basic unit. The electric and magnetic resonance occurred and the impedance of the patch at resonance will be shown. This study is based on simulation results collected using Ansoft High Frequency Structure Simulator (HFSS).

2.2.1 Absorption Mechanism

The basic operating principle of this type of designs is to successfully trap the incident wave in the metamaterial. For that, it is necessary to adapt the impedance of the metamaterial with the characteristic impedance of the free space in order to limit the reflection at the air/metamaterial interface. The incident wave once begins involved in the structure of the metamaterial is attenuated to avoid reflection.

Knowing that the characteristic impedance of a material is:

$$Z_c = \sqrt{\frac{\mu_r}{\epsilon_r}} \times Z_0 \quad (2.1)$$

Therefore, to achieve the impedance matching, the permittivity and / or permeability of the metamaterial absorbent must be modified in order to perform a function giving:

$$\sqrt{\frac{\mu_r}{\epsilon_r}} = 1 \quad (2.2)$$

The transmission (T) and reflection (R) coefficients being related to the impedance by:

$$T = \frac{2\sqrt{Z_1 \times Z_2}}{Z_1 + Z_2} \quad (2.3)$$

$$R = \frac{Z_2 - Z_1}{Z_1 + Z_2} \quad (2.4)$$

Where Z_1 is the impedance of the medium of the incident wave and Z_2 is the impedance of the medium of the absorbing material (fig. 2.1).

Once transmitted within the structure of the metamaterial absorber, the energy of the incident wave is retained by a cavity effect formed by the space between the pattern and the ground plane. The reflections inside the cavity and the losses of the dielectric, even if they are low, strongly dampen the energy of incident wave due to the resonance effect.

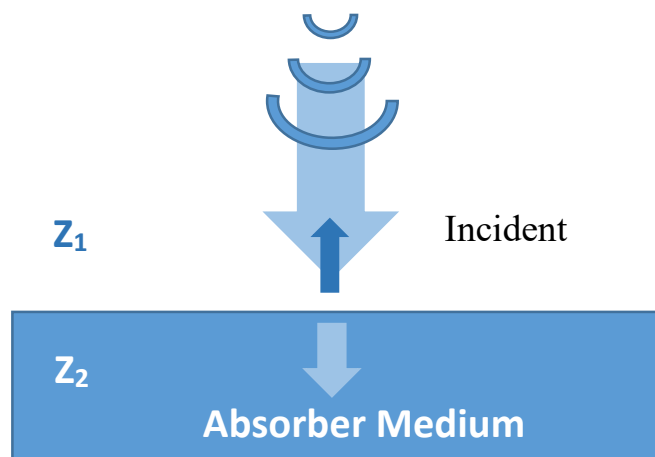


Figure 2.1: Representation of the Reflection and the Transmission of a wave at the interface of two medium.

2.2.2 Simulation Results

Figure 2.2 and 2.3 show the 3D model of the unit cell structure of a metamaterial absorber with square patches and its sectional view respectively.

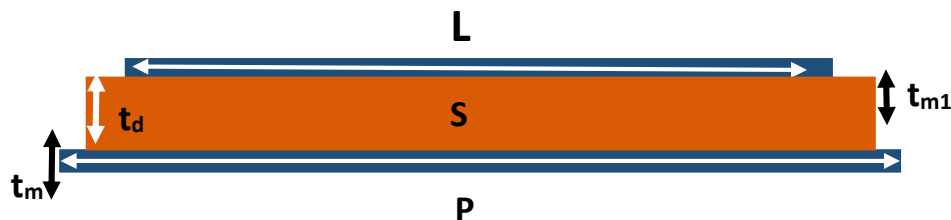


Figure 2.2: Sectional view of the square patch absorber.

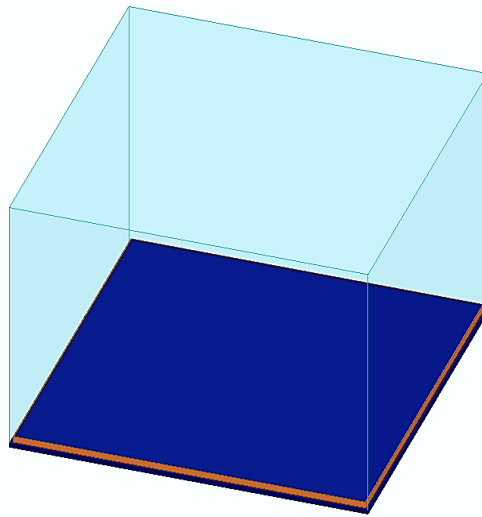


Figure 2.3: 3D Model of a unit cell of square patches simulated by HFSS.

Table 2-1: The values of different parameter of our simulated unit cell:

Thickness of the dielectric substrate (t_d)	0.03 mm
Thickness of the metallic ground plan (t_m)	0.5mm
Thickness of the upper metallization layer (t_{m1})	0.017 mm
Length of the periodic cell (P)	17.5 mm
Length of the metallization layer (L)	15.2 mm
Length of the dielectric substrate (S)	17.2 mm

The substrate used in this unit cell is FR4 epoxy. The ground plane is made from copper where its thickness is unimportant. It must only be thick enough to reflect the incident wave.

In the simulation, periodic boundary conditions are assigned along the x and y -direction. An incident wave port is launched along the z -direction with E field polarized along the y -direction.

The transmittance $T(\omega)$ and reflectance $R(\omega)$ are obtained from the frequency-dependent S -parameters $S_{11}(\omega)$ and $S_{21}(\omega)$. Then, the absorption $A(\omega)$ can be calculated as:

$$A(\omega) = 1 - T(\omega) - R(\omega) \quad (2.5)$$

Where $T(\omega) = |S_{21}(\omega)|^2$ and $R(\omega) = |S_{11}(\omega)|^2$. Since the ground is metallic, $S_{21}(\omega)$ is considered zero. The reference impedance taken in our consideration theoretically and by simulation is $Z_0 = 50 \Omega$. Therefore:

$$Absorption = 1 - |S_{11}|^2 \quad (2.6)$$

By simulation, we obtain the absorption curve shown in **Fig. 2.4**. There is an absorption peak of around 4.05 GHz. At this resonant frequency, the metamaterial absorber has an absorption of 99.8 % for a thickness of approximately $\lambda/250$.

For this absorption peak, we plotted the electrical and magnetic fields presented in **Fig. 2.5**. From these results, we can observe the formation of the electromagnetic mode. A concentration of energy in the substrate under the patch at the absorptive frequency is observed. Therefore, the structure behaves like a cavity formed by the patch and the ground plane.

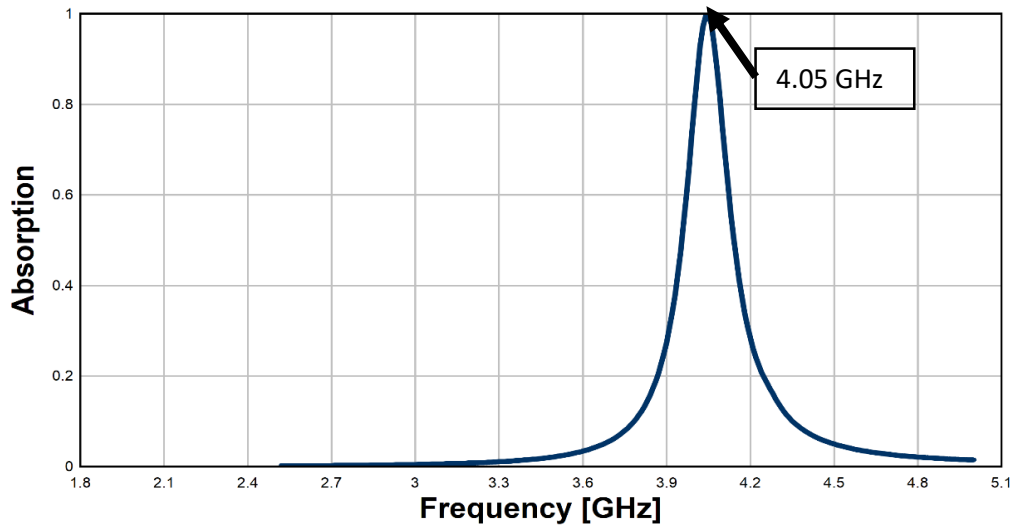


Figure 2.4: Simulated absorption response of the square patch of Fig. 2.2.

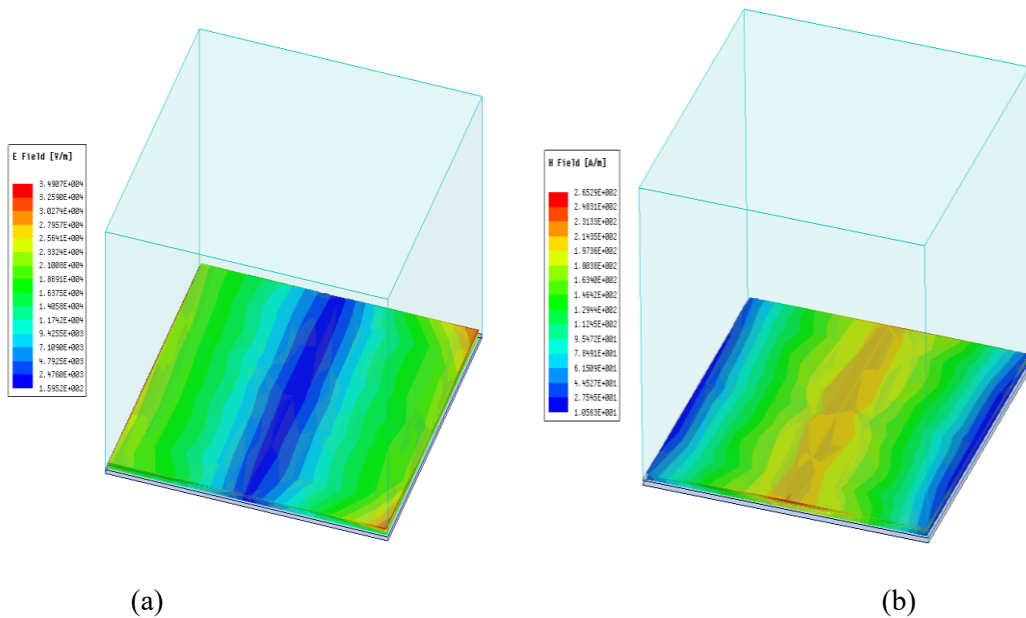


Figure 2.5: (a) Magnitude of electrical field at 4.05 GHz (b) Magnitude of magnetic field at 4.05 GHz.

It is possible to extract the reduced characteristic impedance of the structure by the relation that D. Smith gives for inhomogeneous materials [14]:

$$Z = \frac{z_c}{z_0} = \sqrt{\frac{\mu_r}{\epsilon_r}} = \sqrt{\frac{(1 + S_{11})^2 - (S_{21})^2}{(1 - S_{11})^2 - (S_{21})^2}} \quad (2.7)$$

Thus, we neglect the value of the transmission coefficient S_{21} and we can deduce that:

$$Z_c = \sqrt{\frac{(1 + S_{11})^2}{(1 - S_{11})^2}} \times Z_0 \quad (2.8)$$

The characteristic impedance (Z_c) of the material is analyzed based on the reflection coefficient $S(1, 1)$ plotted in **Fig. 2.6**. It is observed that at resonances, the real part of the $S(1, 1)$ tends to zero, then referring to the eq.2.8 the characteristic impedance of the material is matched with impedance of medium at resonance. While the imaginary part of $S(1, 1)$ tends to zero then basing on eq.2.8 the characteristics impedance of the absorbing medium is purely resistive at resonance. The metamaterial thus obtains a negligible reflection coefficient at resonance. Then, the energy is trapped to be absorbed into the structure.

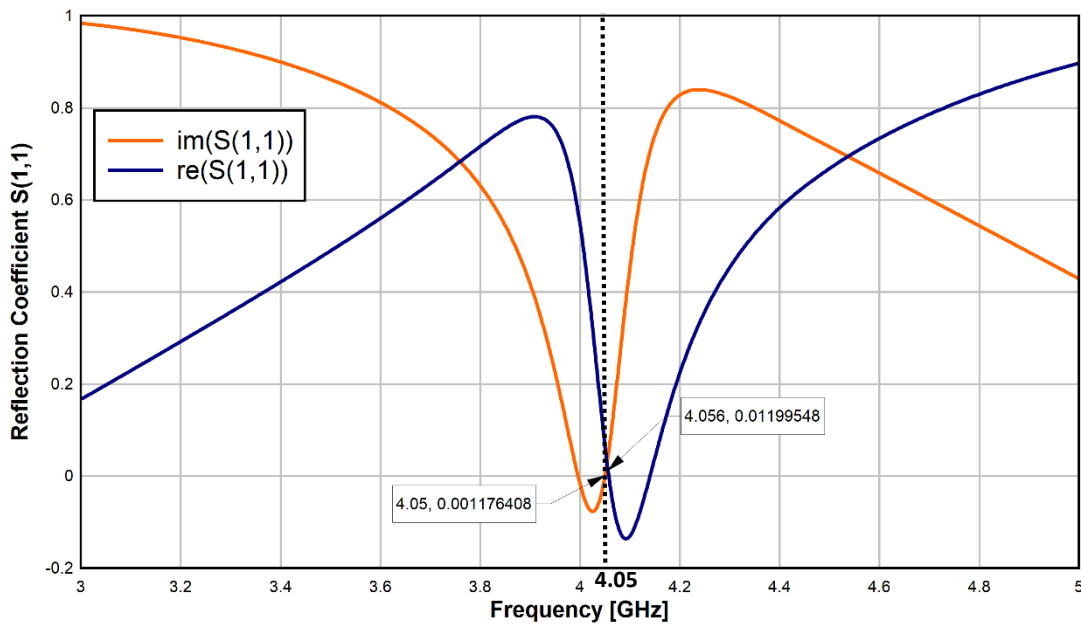


Figure 2.6: Reflection Coefficient of the simulated patch square of **Fig. 2.2**.

The imaginary part of the characteristic impedance, also called reactance, gives information on the inductance and the capacity of the material. We can write the impedance as follows:

$$Z_c = R + jX \quad (2.9)$$

With R is the resistance and X is the reactance that can be defined as follows:

$$X = X_L - X_C = \omega L - \frac{1}{\omega C} \quad (2.10)$$

Where X_L is the inductive reactance (in Ω) and X_C is the capacitive reactance (in Ω). Therefore, when X is equal to 0, we are in the case of a purely resistive impedance.

2.2.3 Conclusion

After this set of simulations, we discovered deeply the potential that these new-engineered materials can have. We can conclude that the absorption achieved by the structure does not come directly from the losses of the substrate because its thickness and tangent losses are too low.

The absorption of a dielectric is estimated by the Beer-Lambert law with:

$$Absorption = -\log(T) = -\log\left(\frac{P}{P_0}\right) \quad (2.11)$$

$$P = P_0 \cdot e^{-\alpha h} \quad (2.12)$$

P_0 is the incident power, P is the recovered power after having crossed the material, and h is the thickness of the substrate. Here α is the absorption coefficient of the material:

$$\alpha = \frac{4\pi k}{\lambda} \quad (2.13)$$

With k is the linear extinction coefficient expressed by the imaginary part of the complex refractive index of the substrate.

For the studied design, the absorption resulting from the losses in the substrate is very low, less than 1%. Therefore, this absorption phenomenon of the simulated patch is not caused by the substrate. This is a purely resonant phenomenon resulting in a narrow operating band.

2.3 Design of Pyramidal Absorber

After studying the basis of absorption theoretically and by simulation now, we are concerned about the PA Structure in details. Such design provides broadband of absorption with insensitivity to incident wave polarization due to its symmetrical geometry. It consists of a periodic array of pyramids with a quadrangular cross shape and a homogeneous metal ground in the bottom, the latter blocking any transmission of the incidence wave ($S_{21} = 0$). The reflection coefficient (S_{11}) is minimized by properly structuring the square patches discussed above.

The thickness of the metallization layer and the dielectric layers in each patch layer are optimized to be; $t_m = 35 \mu\text{m}$, $t_d = 140 \mu\text{m}$ respectively. The metal is copper with the electric conductivity of $\sigma = 5.8 \times 10^7 \text{ S/m}$. FR4 is also used for the dielectric substrate. Here, 20 resonator layers are chosen.

In the simulation, the periodic boundary conditions are assigned along the x and y -directions. A wave port is launched along the z -direction with E field polarized along the y -direction.

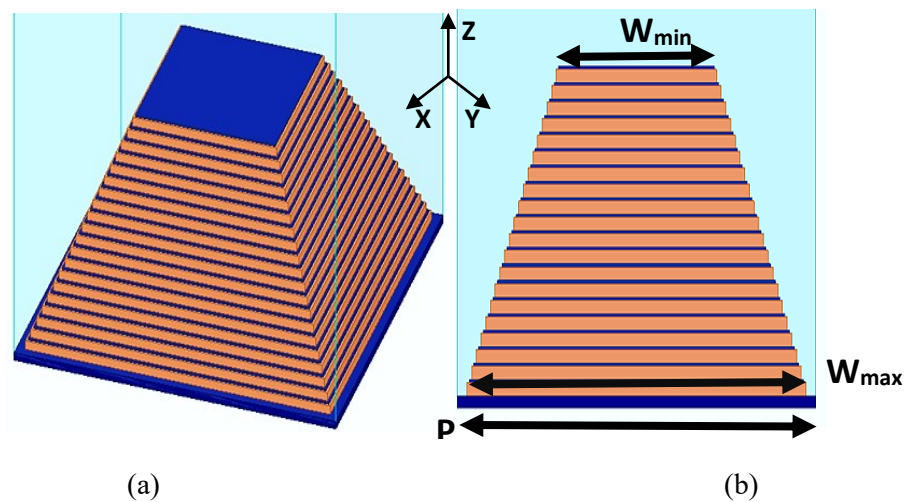


Figure 2.7: Design of an ultra-broadband PMA, (a) 3-D illustration of the simulation MA, (b) Side view of the PMA unit cell.

The absorption coefficients as a function of frequency from 10 GHz to 28 GHz are shown in **Fig. 2.8**. There are 20 absorption peaks with absorption approximately above 80%, corresponding to the number of dielectric patches between two neighboring metal interfaces. As cited before, relative fractional bandwidth is used to describe the absorption performance of such PMA. It is equals to 63.3 % for the designed PMA shown in **Fig.2.7**, which thus exhibits good absorption performance with a level of absorption higher than 80%.

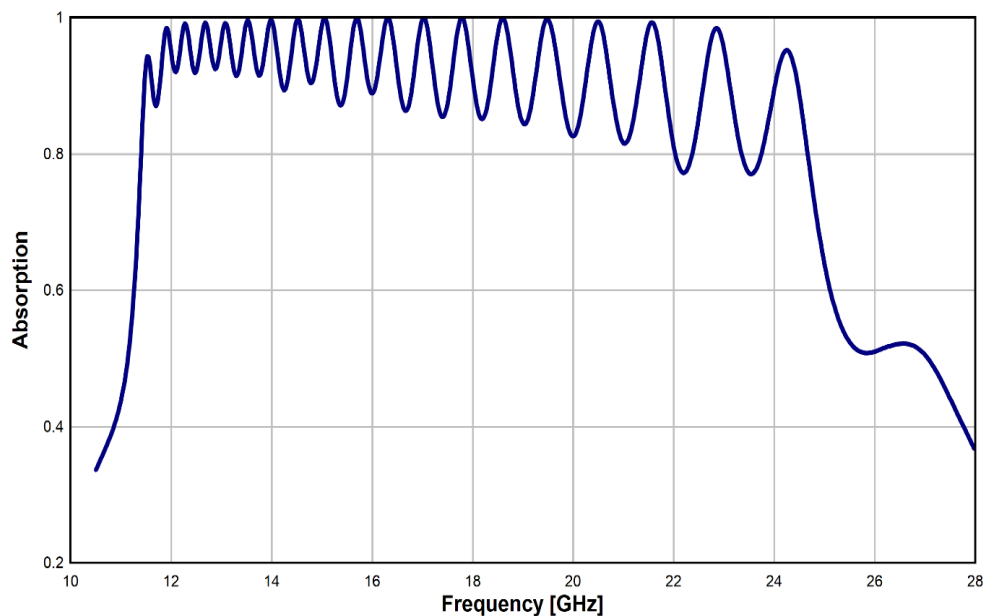


Figure 2.8: Absorption response simulated of the optimized pyramidal structure with dimensions of: $W_{\min}=2.975$ mm, $W_{\max}=6.3$ mm, $P=6.65$ mm, $t_m=35\mu\text{m}$, $t_d=140\mu\text{m}$.

To provide matching between the study of the simple patch discussed above with the origin of absorption of this PMA structure, electric and magnetic field distribution are plotted at three frequencies (11.5, 17 and 20.45 GHz) as shown in **Fig.2.9**.

Two adjacent metal layers spaced with a dielectric layer can localize the electric and magnetic field at special frequencies as shown in **Fig. 2.9**. Such resonances lead to zero-reflection and thus unit absorption is obtained by impedance matching to the free space. At lower frequencies, the electromagnetic field is localized at the bottom pyramid layers. As the frequency is increased, the electromagnetic field is localized in the top pyramid layers. As the pyramids

absorbers gradually decrease in width from the bottom to the top, they resonate at different frequencies. Since the resonance frequencies of neighboring resonators are overlapping to each other, this results in an ultra-broadband absorption.

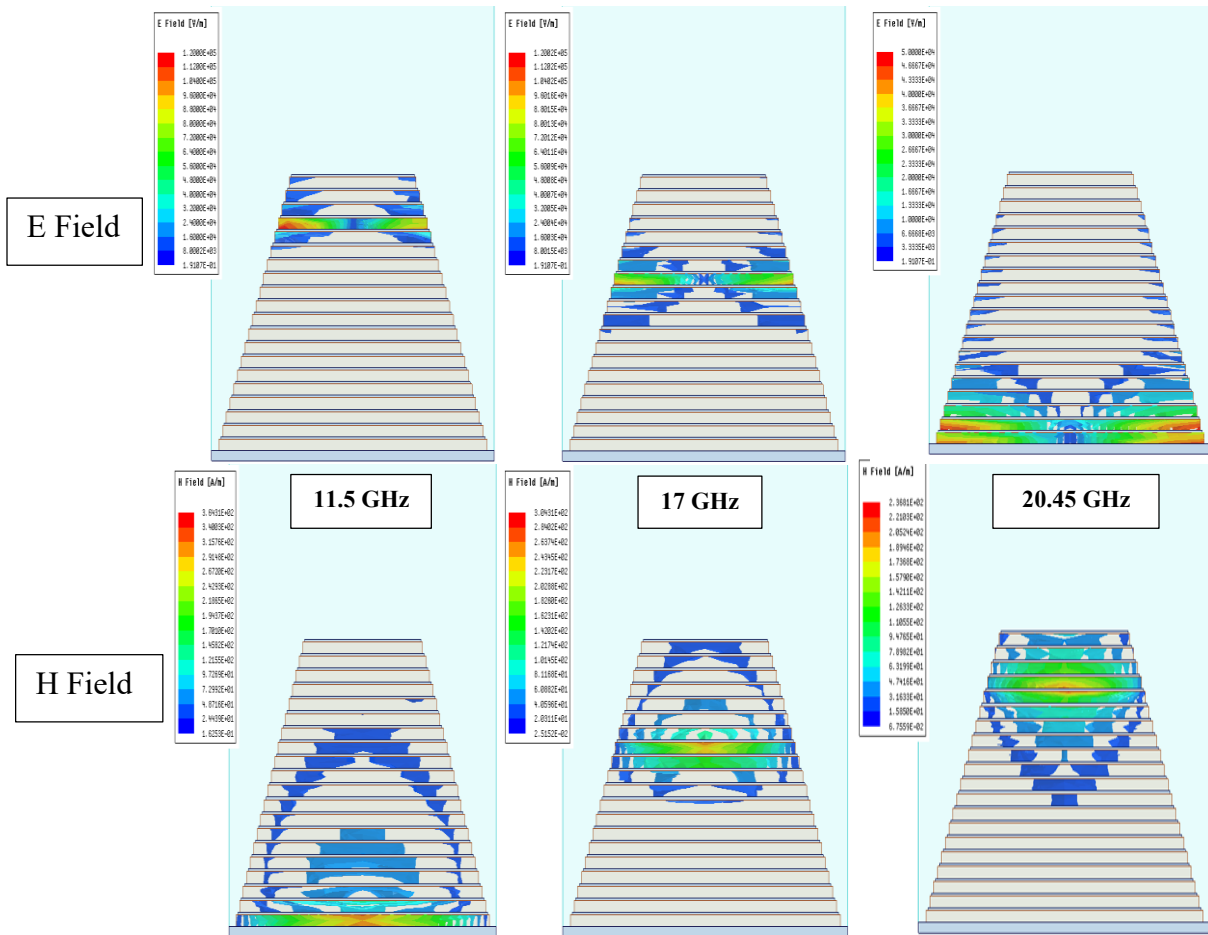


Figure 2.9: Simulated Electric and Magnetic Magnitude distributions at three resonance frequencies.

2.4 Parametric Analysis

In order to optimize the PMA structure well, we orient our study to examine the influence of the geometrical parameters such as periodicity, transverse dimensions of the resonators and number of layers. In addition, the material properties, particularly the imaginary part of the dielectric layer, which governs the dielectric absorption, and the conductivity of metal films will be considered.

2.4.1 Geometrical parameters influence

Fig. 2.10 shows the absorption coefficient as a function of frequency for four spacing ranging from 6.65 mm to 8.05 mm. Just to notice that in this simulation we kept the other parameters constant as used above by only varying the spacing P . From the former figure, it can be noted that there is an optimized spacing here where $P = 6.65$ mm, and that period has more influence at higher frequencies.

This result can be explained by the necessity to keep the higher patch that is responsible for the high frequency absorption close to each other because the geometrical periodicity imposes statically dimensional spacing between these upper layers which makes it more sensitive from larger periodicity (refer to **Fig. 2.11**).

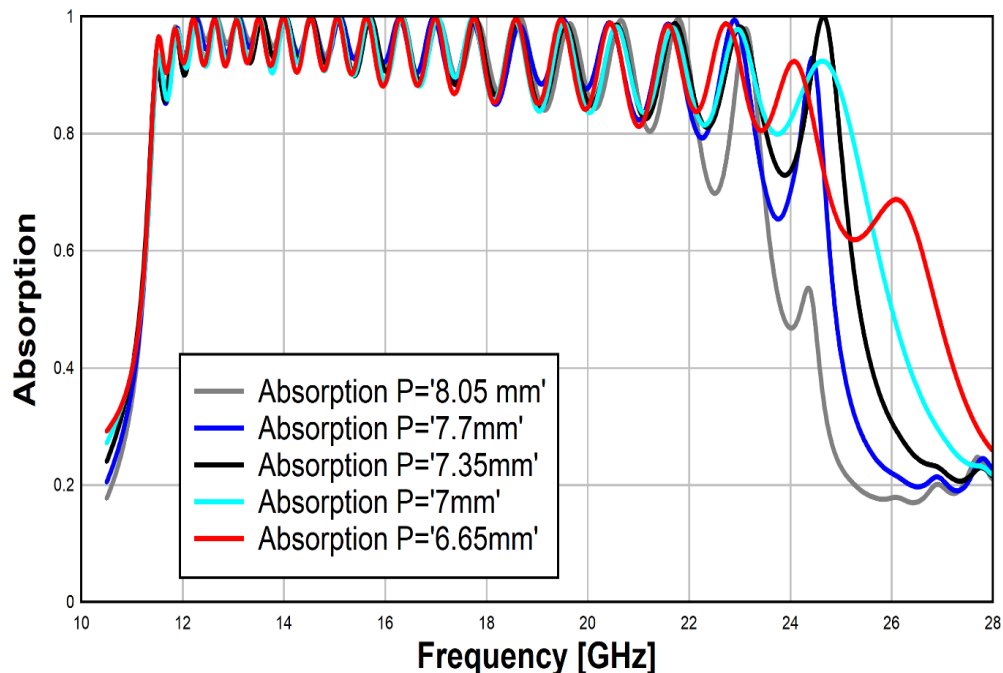


Figure 2.10: Absorption coefficient with respect to frequency for four spacing ranging from 6.65 mm to 8.05 mm.

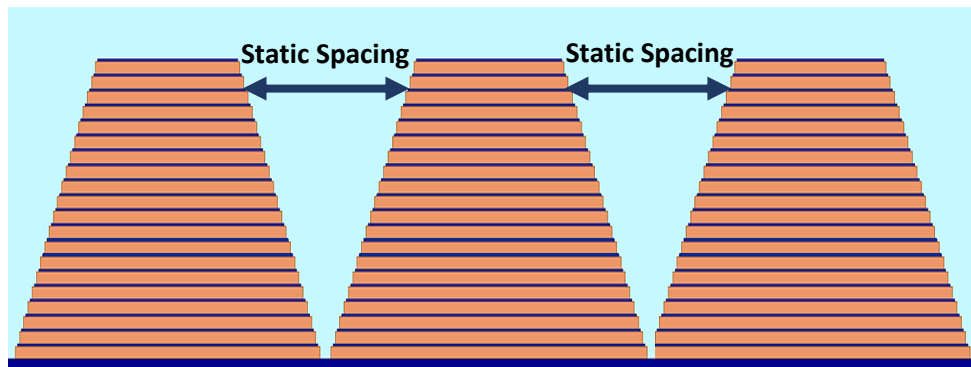


Figure 2.11: Diagram showing the static spacing between upper layers imposed geometrically.

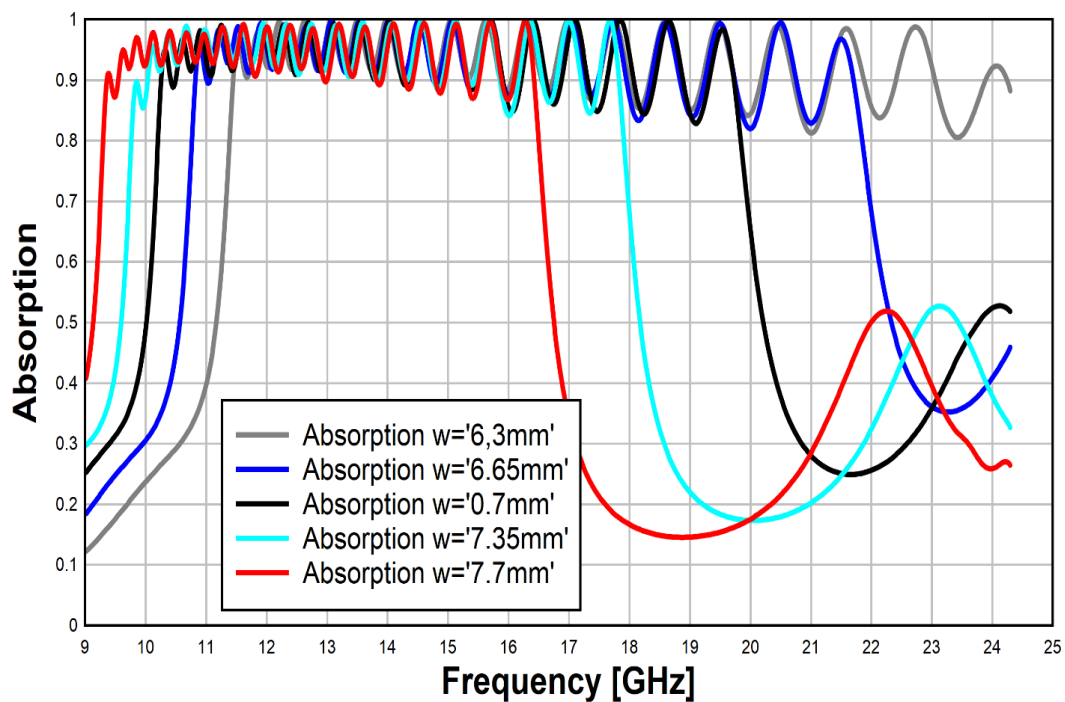


Figure 2.12: Absorption coefficient with respect of frequency for basic length W ranging from 6.3 mm to 7.7 mm.

Fig. 2.12 shows the absorption spectra when the transverse dimension W was changed from 6.3 mm to 7.7 mm by a step of 0.35 mm by keeping $P = 6.65$ mm.

As an interpretation of **Fig. 2.12**, it can be concluded that the transverse dimensions govern the operating frequency with Fabry Perot type resonance.

For example, when $W=7.7$ mm:

$$f_r = \frac{c}{2W\sqrt{\epsilon_r}} = 9.28 \text{ GHz} \quad (2.14)$$

Which is approximately the first resonance frequency in **Fig. 2.12** (red line). It is also found that when the transverse bottom dimension increases, the bandwidth window shifts towards lower frequency. It can be seen that as W is reduced, RAB is increased. However, W cannot be too small; otherwise the width of neighboring metal patches in a unit will vary too abruptly. Consequently, the frequency difference between their supported resonant modes becomes too large and pronounced oscillation forms will appear in the absorption spectra. As a conclusion, the transverse dimension of resonator patches impacts dramatically the resonant frequencies and their variations have to be sufficiently gradual to avoid a multi-peak absorption spectrum rather than a low ripple broadband absorption window.

Fig. 2.13 shows the absorption spectrum when the number of resonator layers is varied. In this simulation, the bottom length is $W=6.3$ mm and the difference length between two adjacent layers was kept constant as $87.5 \mu\text{m}$. The number of layers varies from 12 to 20. One can see that, as the number of layer increases, the absorption window broadens gradually with significant improvement in the bandwidth for a large number of resonators such as $N=20$.

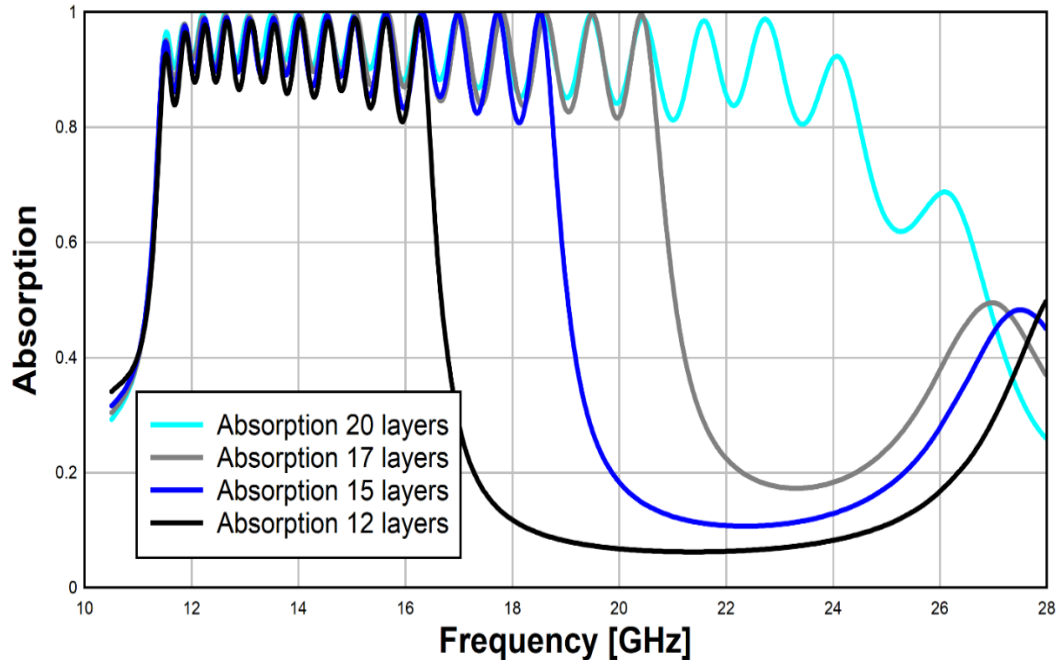
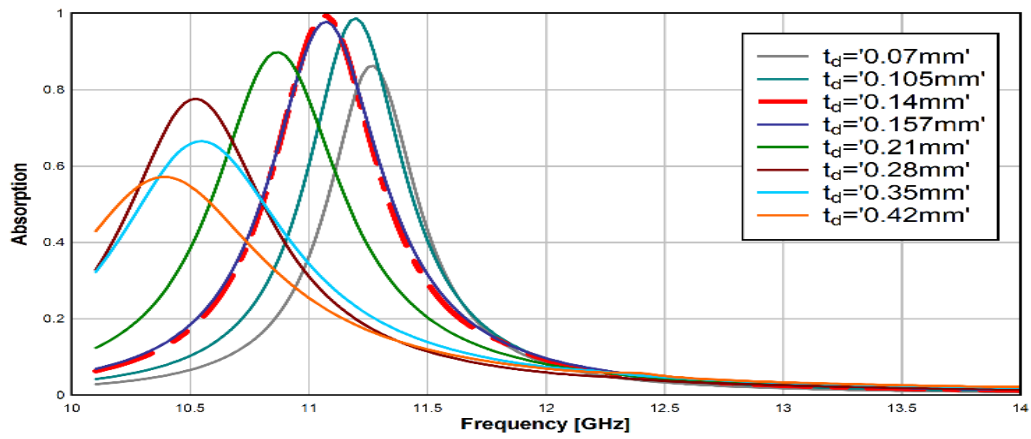


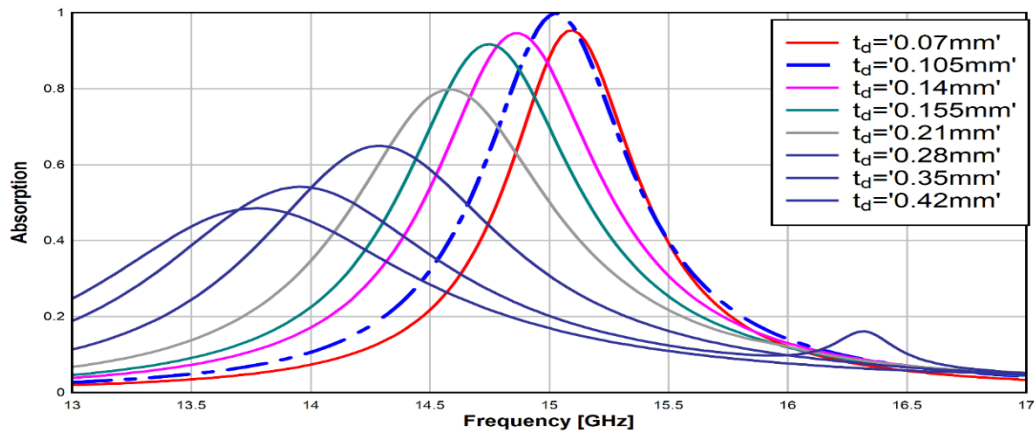
Figure 2.13: Absorption coefficient with respect of frequency with different number of resonator layers ranging as 12, 15, 17 and 20 layers.

In **Fig. 2.8**, we remark that the absorption level of the 20 peaks of resonance is different, and it decreases at a higher frequency. For that, in the study shown in **Fig. 2.14**, we try to improve the absorption level by presenting the study relating each resonant layer dimension to a specific substrate thickness. For that, different layers were taken from the pyramidal structure to be studied alone. **Fig. 2.14** shows the absorption response of the first basic layer alone then the tenth layer and the fifth layer corresponding to different dielectric thickness.

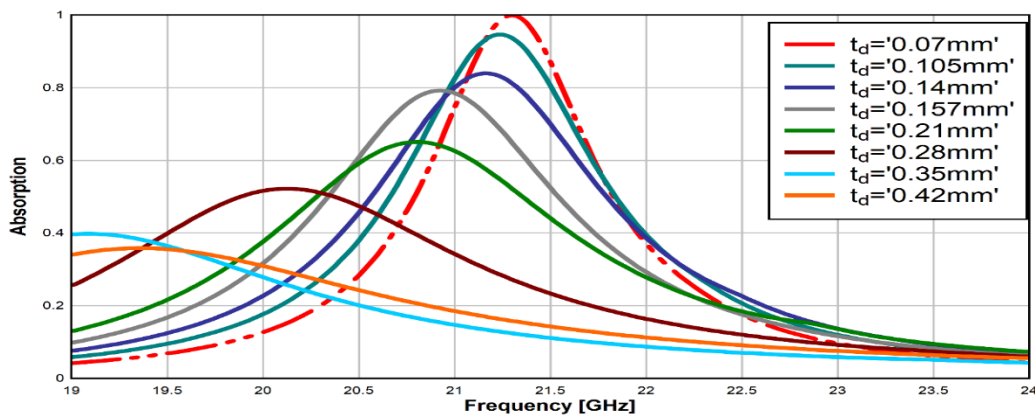
Fig. 2.14 shows that there is a relation between the patch dimensions and the dielectric thickness. The best absorption level for the first patch has occurred when the substrate thickness is 0.14 mm. On the other hand, for the tenth patch, the best absorption level has occurred when the thickness of the substrate is 0.105 mm. We remark that the higher frequency absorption needs thicker dielectric substrate. Therefore, to design a pyramidal design with best response we must study well this relation.



(a)



(b)



(c)

Figure 2.14: Absorption response corresponding different dielectric thickness for: (a) The first basic layer then (b) the tenth layer and (c) the fifth layer.

2.4.2 Material Properties Influence

In this part of the study, we consider a single patch absorber to study the material properties and its effect on the resonance absorption operation without taking into account any geometrical effect. This step comes to facilitate the study. Knowing that the material properties conditions for best absorption to a simple path are the same in the pyramidal structure.

Fig. 2.15 shows the absorption spectrum by varying the loss tangent of the dielectric layer from 0.02 to 0.08. It is found that the introduction of higher losses broadens each elementary peak accompanied with a decreasing in the level of absorption. Such result proves that the absorption mechanism is not related to the loss in the substrate that agrees with the theoretical study of the resonant patch addressed above.

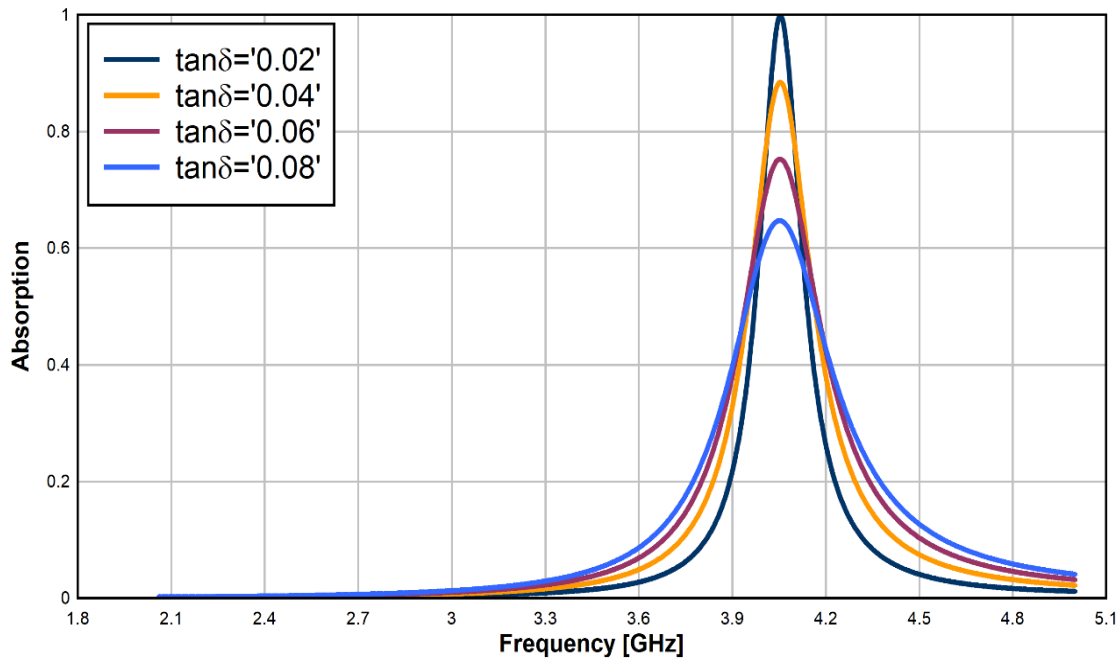


Figure 2.15: Absorption coefficient as a function of frequency Absorption under influence of dielectric loss tangent varying from 0.02 to 0.08.

Now, four values of relative permittivity ranging from 4.4 to 15 mm are considered. From this figure, it can be noted that there is a shifting in the absorptive frequency when the value of relative permittivity increase that is compatible with the equation (2.13).

We can observe from the **Fig. 2.16** a decreasing in the absorption level with increasing of the relative permittivity value. **Fig. 2.17** shows the cause of such decreasing where it studies the absorption coefficient under the influence of different dielectric thickness for a constant relative permittivity. It shows that it is necessary to adapt the value of the relative permittivity with a specific value of a dielectric thickness to obtain the best absorption. Moreover, it is noticed that higher relative permittivity needs thicker substrate to obtain the unit absorption at resonance.

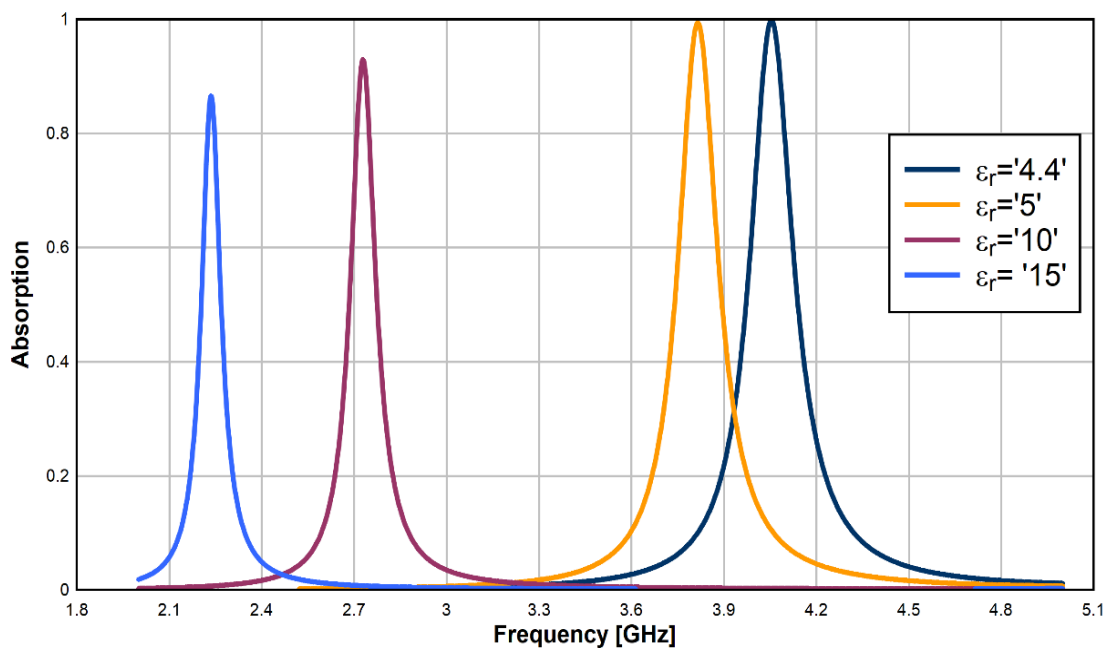


Figure 2.16: Absorption coefficient as a function of frequency Absorption under influence of relative permittivity varying from 4.4 to 15.

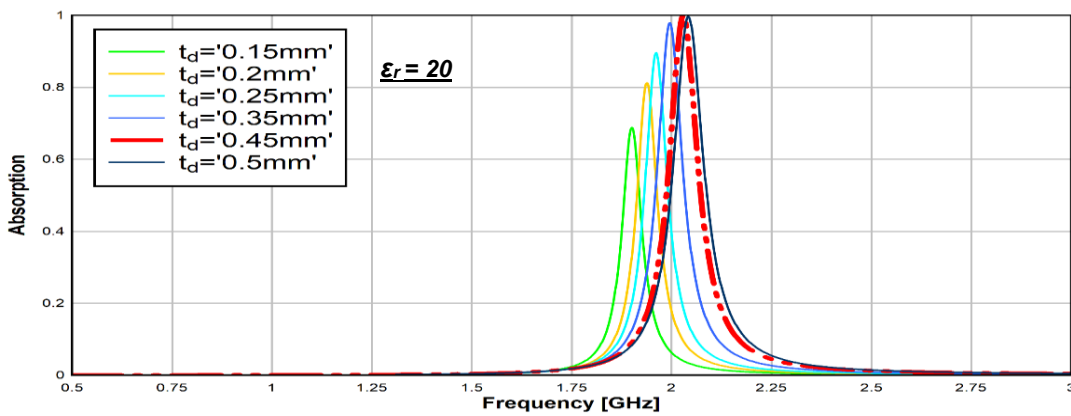
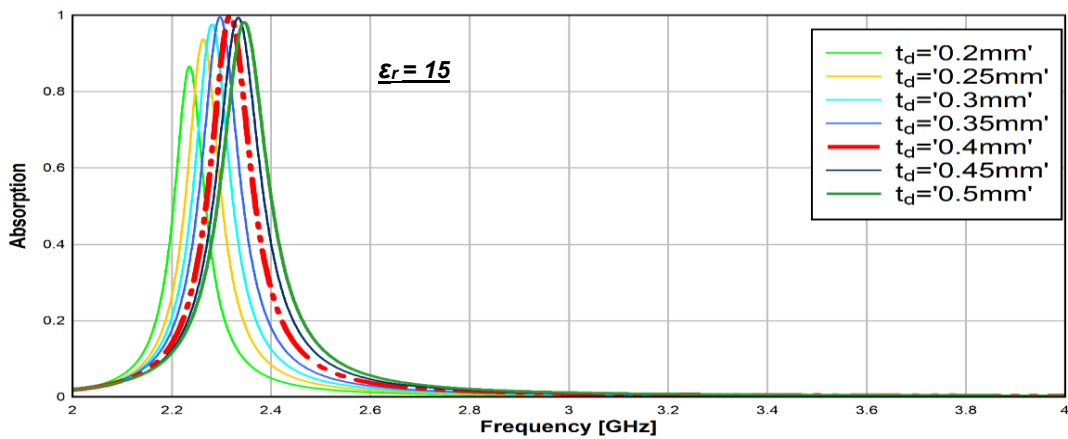
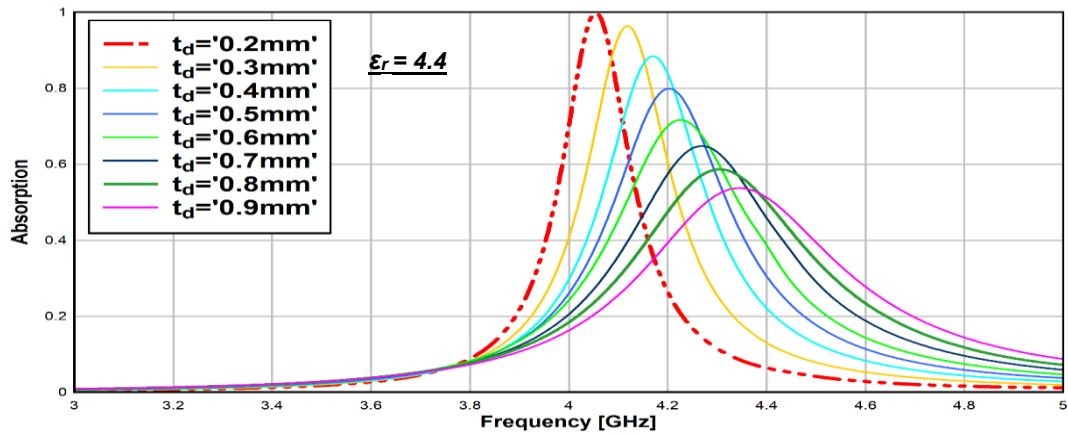


Figure 2.17: Absorption coefficient as a function of frequency under influence of dielectric thickness for different relative permittivity value: (a) 4.4 (b) 15 and (c) 20.

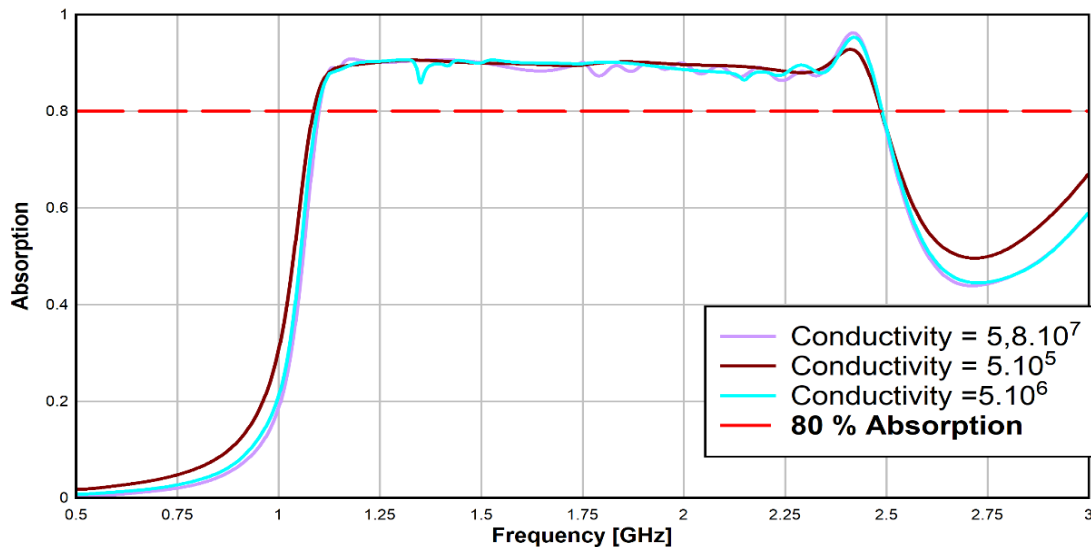


Figure 2.18: Absorption coefficient as a function of frequency under influence of metal conductivity ranging from 5×10^5 S/m to 5.8×10^7 S/m.

Fig. 2.18 shows the absorption spectrum of a pyramidal structure varying the conductivity of metal from 5.10^5 S/m to $5, 8.10^7$ S/m, the latter value corresponding to the conductivity of a metal film as copper. There are similar effects with those observed by varying the dielectric losses with improved absorption qualities associated with the decrease of conductivity.

2.5 Curved Altitude Enhancing Factor

This section includes the numerical simulations that show an enhancement in the Relative Absorptive Bandwidth (RAB) by applying curved altitude on the pyramidal structure. This factor adds a new degree of freedom that can improve well any pyramidal structure. The unit cell of the pyramidal structure taken above in **Fig. 2.7** is considered as criterion for evaluation of the effect of applying a curved altitude to the pyramidal structure.

Figure 2.19 shows three different form of altitude applied on the same structure parameters. We take the sawtooth altitude (**Fig. 2.19 (a)**), the linear altitude (**Fig. 2.19(b)**) and the curved altitude (**Fig.2.19(c)**). The curved design is drawn based on a 3-point arc and optimized well to give the best result. For different altitude shape designs, the frequency dependent absorption response is displayed in **Figure 2.20**.

Table 2-2: Relative Absorption Bandwidth for different altitude form obtained by simulation

	RAB with Absorption level above 80%	RAB with Absorption level above 90%
Sawtooth Altitude	63.3%	25.9%
Linear Altitude	46.3%	33.3%
Curved Altitude	73.4%	71.82%

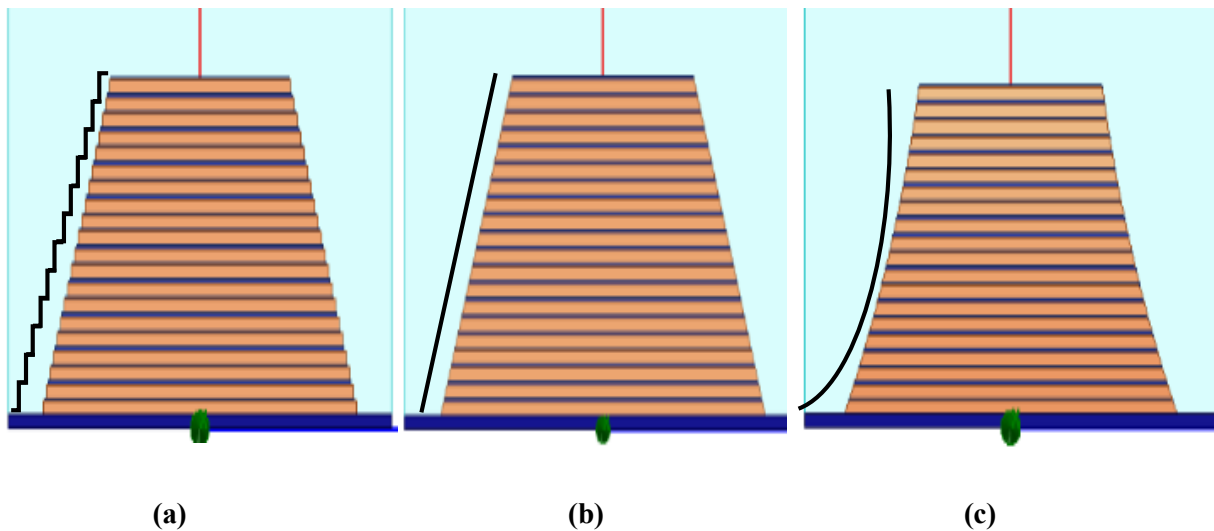


Figure 2.19 :Different shape altitude designs of a Pyramidal structure: **(a)** Sawtooth Altitude **(b)** Linear Altitude **(c)** Curved Altitude.

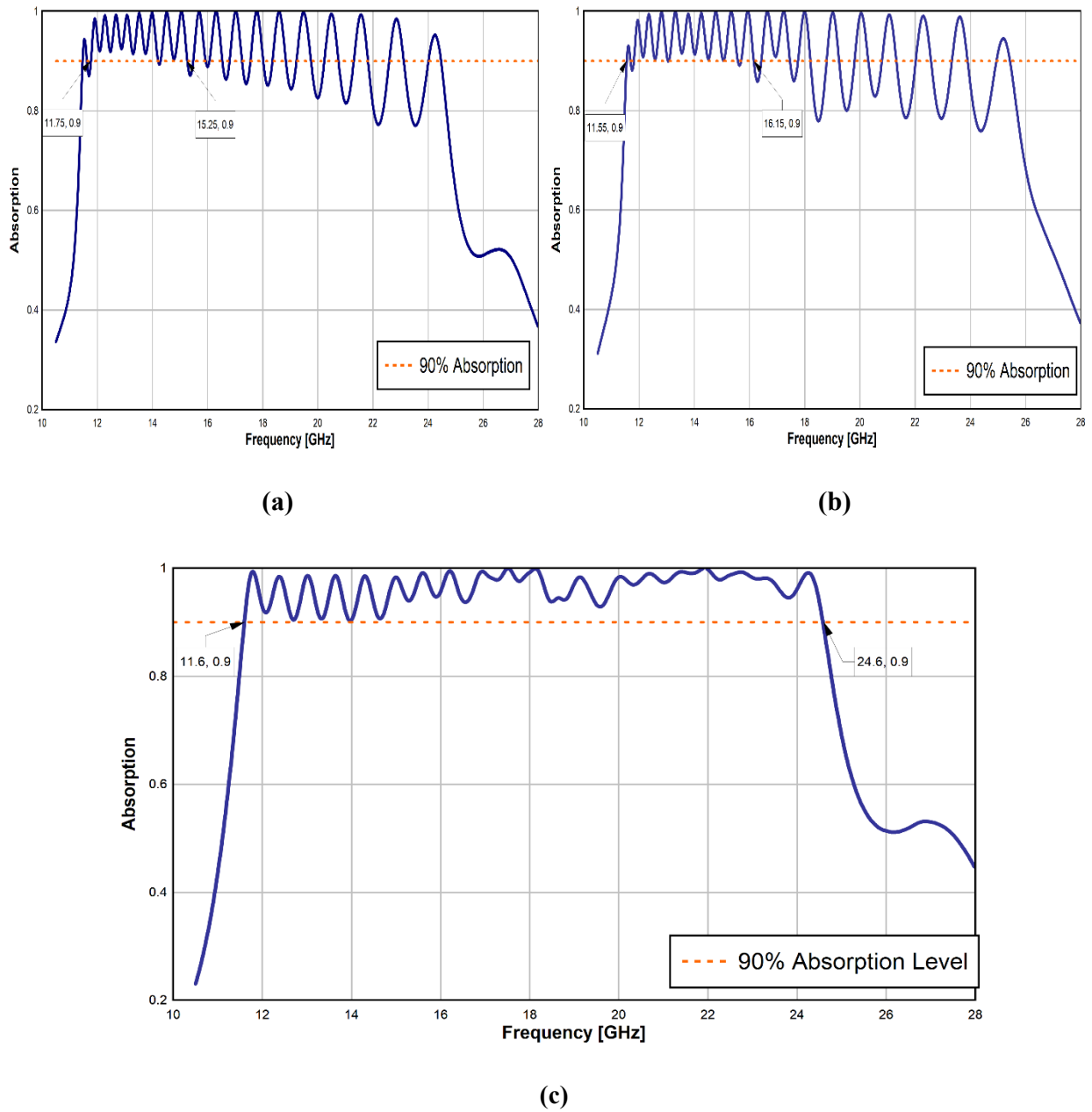


Figure 2.20: Absorption response from numerical simulations for different altitude shape designs in the PA: **(a)** Sawtooth Altitude **(b)** Linear Altitude **(c)** Curved Altitude.

The simulation results show that the level of absorption in linear and sawtooth altitude is below than 90% at a higher frequency. It can cover a broad band of absorption but with an oscillator level of absorption (**Figure 2.20** (a) and (b)). Applying curved altitude, the peaks of

resonance became nearer and smoother combined. Therefore, the curved Pyramidal absorber achieves a 71.82 % RAB with absorption level above 90%, which is much larger than that obtained from other altitude forms as shown clearly in **Table 2.2**. This result puts a new degree of freedom in optimizing parameters in such design.

2.7 Conclusion

In summary, we numerically demonstrated the absorption basics of the pyramidal absorber coming from resonant patches, and we proved theoretically and by simulation that the absorption mechanism does not need lossy material. Then, we demonstrated that 20 metal-dielectric layers staked in periodic arrays and shaped as quadrangular frustum pyramids can realize ultra-broadband PMA with a fractional bandwidth equals to 73.4% with an absorption level greater than 90% by available cheap material. This value is not reached by the same design in reference [4] which was the principle of our design.

After properly designing the multilayered structure, the geometrical and material parameters' influences were assessed to optimize the absorption quality. This study was helpful for a better understanding of the parameter effect to find the tools to enhance more and optimize this structure. Finally, a novel idea that permits successive resonant frequencies to be combined properly to have a broadest optimized response is presented by applying curved altitude. This puts a new degree of freedom in optimizing such structure.

2.8 Reference

- [1] Ye, Yu Qian, Yi Jin, and Sailing He. "Omnidirectional, polarization-insensitive and broadband thin absorber in the terahertz regime." *JOSA B* 27.3 (2010): 498-504.
- [2] Liu, Xianliang, et al. "Infrared spatial and frequency selective metamaterial with near-unity absorbance." *Physical review letters* 104.20 (2010): 207403.
- [3] Liu, Na, et al. "Infrared perfect absorber and its application as plasmonic sensor." *Nano letters* 10.7 (2010): 2342-2348.
- [4] Ding, Fei, et al. "Ultra-broadband microwave metamaterial absorber." *Applied physics letters* 100.10 (2012): 103506.
- [5] Sun, Jingbo, et al. "An extremely broad band metamaterial absorber based on destructive interference." *Optics Express* 19.22 (2011): 21155-21162.
- [6] Xiong, Han, et al. "An ultrathin and broadband metamaterial absorber using multi-layer structures." *Journal of Applied Physics* 114.6 (2013): 064109.
- [7] Cui, Yanxia, et al. "Ultrabroadband light absorption by a sawtooth anisotropic metamaterial slab." *Nano letters* 12.3 (2012): 1443-1447.
- [8] Lobet, Michaël, et al. "Plasmon hybridization in pyramidal metamaterials: a route towards ultra-broadband absorption." *Optics express* 22.10 (2014): 12678-12690.
- [9] Lobet, Michaël, et al. "Plasmon hybridization in pyramidal metamaterials: a route towards ultra-broadband absorption." *Optics express* 22.10 (2014): 12678-12690.
- [10] Liang, Qiuqun, et al. "Numerical study of the meta-nanopyramid array as efficient solar energy absorber." *Optical Materials Express* 3.8 (2013): 1187-1196.
- [11] Liang, Qiuqun, et al. "Metamaterial-based two dimensional plasmonic subwavelength structures offer the broadest waveband light harvesting." *Advanced Optical Materials* 1.1 (2013): 43-49.
- [12] Zhu, Jianfei, et al. "Ultra-broadband terahertz metamaterial absorber." *Applied Physics Letters* 105.2 (2014): 021102.
- [13] Zhou, Jing, et al. "Experiment and theory of the broadband absorption by a tapered hyperbolic metamaterial array." *ACS photonics* 1.7 (2014): 618-624.

[14] Smith, D. R., et al. "Electromagnetic parameter retrieval from inhomogeneous metamaterials." *Physical review E* 71.3 (2005): 036617.

3. Chapter 3: Activating Metamaterial to low frequency

3.1 Introduction

Metamaterial Perfect Absorber has been numerously investigated and presented for different frequency regions such as GHz frequencies [1-3] and THz frequencies [4-6]. Nowadays, the application of perfect absorption in telecommunications (UHF bands) is one of the prior concerns for practical purposes used for television broadcasting, cell phones, and satellite communication including GPS, personal radio services including Wi-Fi and Bluetooth, walkie-talkies, cordless phones, and numerous other applications.

Unfortunately, conventional absorbers would be too thick in these bands (around 8.5 cm) and magnetically loaded absorber are too heavy. Added to the massive weight, the big size of the presented metamaterial absorber is an obstacle when operating at radio frequencies. Most recent MPAs have the ratio of lattice constant over wavelength ranging from one third to a fifth, which is difficult to integrate into real radio devices [4-7]. Therefore, miniature size is an essential requirement in the telecommunications area.

In this chapter, we study all the requirements needed to achieve a low-frequency response. Besides, we apply these requirements to design and investigate small-size metamaterial absorbers.

3.2 Resonant Frequency Equation

As cited in previous chapters, MA belong to the resonant branch of metamaterial science. For that, it is necessary to begin our study based on the resonant equation that relates the value of resonant frequency with the influencing factors for a simple patch design. This equation is expressed as:

$$f_r = \frac{c}{2w\sqrt{\epsilon_r}} \quad (3.1)$$

Where w represents the length of a square patch and ϵ_r represents the relative permittivity of the substrate.

So referring to this equation, the value of resonant operating frequency is related to material substrate properties and on the dimension of the patch. Shifting of absorption operating frequency in the lower band requires a high value of relative permittivity and an increasing in the dimensions. For example, if we use FR4 as a substrate, we need a dimension of 143 mm to get an absorption response at 0.5 GHz.

Thus, to avoid the increasing dimension of the absorptive design we directed our research in two ways. As a first task, we looked up for a substrate material having high relative permittivity value with a low cost. Such material must be studied as a causal material looking forward to its characteristics with our targeted ultra-broadband of frequency. In this context, we benefit from the parametric analysis presented in the last chapter to select the best material properties needed. Besides, we need to find a way to exploit areas in small geographical locations. In this context, we use an innovative mathematical branch: “Minimal Surface Structure” that locally minimizes its area. Minimal surfaces are the surfaces of the smallest area spanned by a given boundary.

3.3 Material Properties

Basing on our parametric study in Chapter 2, we select the required characteristics for our application that gives the best absorption level at resonance. We are interested in finding a cheap substrate having relative permittivity greater than 60 and dielectric loss tangent greater than 0.01. We found some materials with high relative permittivity values (refer to **Table 3.1**). Besides, to select the best dielectric material we categorized them by their experimental practical properties concerning cost, mass density, and their breakdown voltage. The breakdown voltage of a dielectric is the minimum voltage that causes a portion of an insulator to become electrically conductive. It is proportionally related to the maximum incident wave power that can be absorbed before the damage of the substrate.

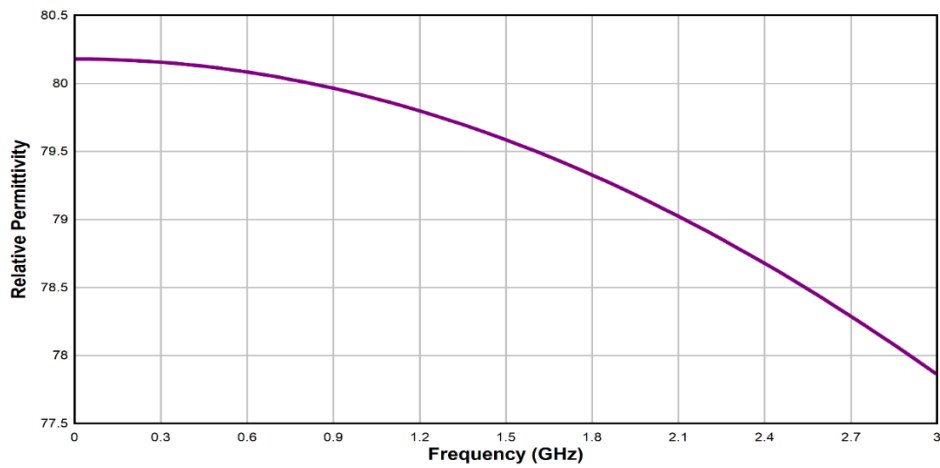
Table 3-1: Practical Properties of high relative permittivity dielectric substrate.

Dielectric Material	Relative Permittivity	Mass Density	Breakdown Voltage	Prices
BaTiO₃	>100	6.02 g/cm ³	0.18 Mv/cm	~ 30\$/kg
TiO₂	100	4.23 g/cm ³	2.7 Mv/cm	~ 10\$/kg
Distilled Water	~ 80	1 g/cm ³	16 Mv/cm	0.1 \$/liter

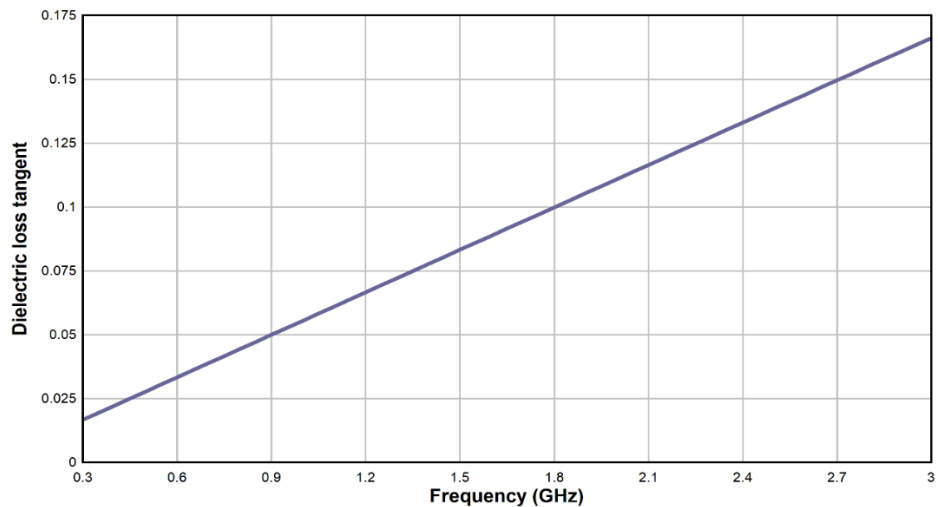
We found that the dielectric that has the lower cost and mass density with the higher breakdown voltage is the distilled water. It could be a good dielectric substrate looking toward its availability and its high relative permittivity with suitable dielectric loss tangent. Pure distilled water has a high dielectric constant due to strong bonds between hydrogen and oxygen as well as hydrogen bonding between water molecules.

View the targeted ultra-broadband of absorption, it is important to study the frequency dependence of the relative permittivity values and the dielectric loss tangent. For pure (distilled) water, a relatively simple model applicable to frequencies $f < 50$ GHz is offered by the Debye Model [8]. Their equations are cited in **Appendix 1** by a MATLAB code that was plotted in **Figure 3.1** as a function of our targeted band (0.3 GHz - 3 GHz).

By this model, we can view that in spite of the very broadband considered from [0.3-3 GHz] the relative permittivity is conserved in high values ranging from 77.75 to 80.2, with dielectric loss tangent ranged between 0.023 and 0.165. The relative permittivity is slightly varied but the variation of dielectric loss tangent is considerable.



(a)



(b)

Figure 3.1: Debye model of water properties: **(a)** Relative permittivity frequency dependence **(b)** Dielectric loss frequency dependence.

3.3.1 Insertion of Water Substrate

In simulation, the periodic boundary conditions are assigned along the x and y -directions. A wave port is launched along the z -direction with E field polarized along the y -direction. The copper is used as metallic material.

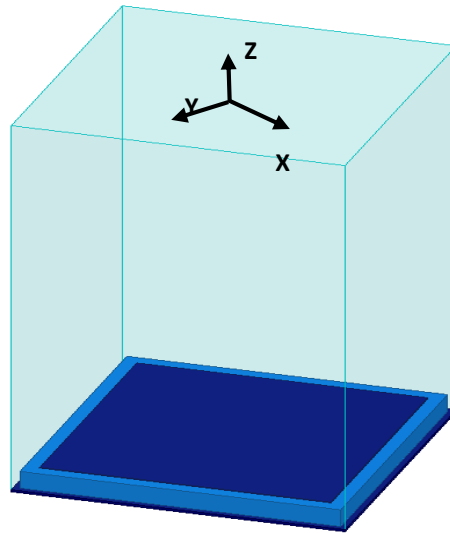


Figure 3.2: Patch design with water substrate.

As the first trial, the pure water substrate was ideally inserted as dielectric substrate in a simple patch design (see **Fig 3.2**) with Debye frequency dependence to test its efficiency in narrow band of absorption frequency. It gives as expected a low absorptive frequency (refer to **Fig 3.3**) with a unit cell dimension of (52.5 mm) in a substrate thickness of 6.25 mm.

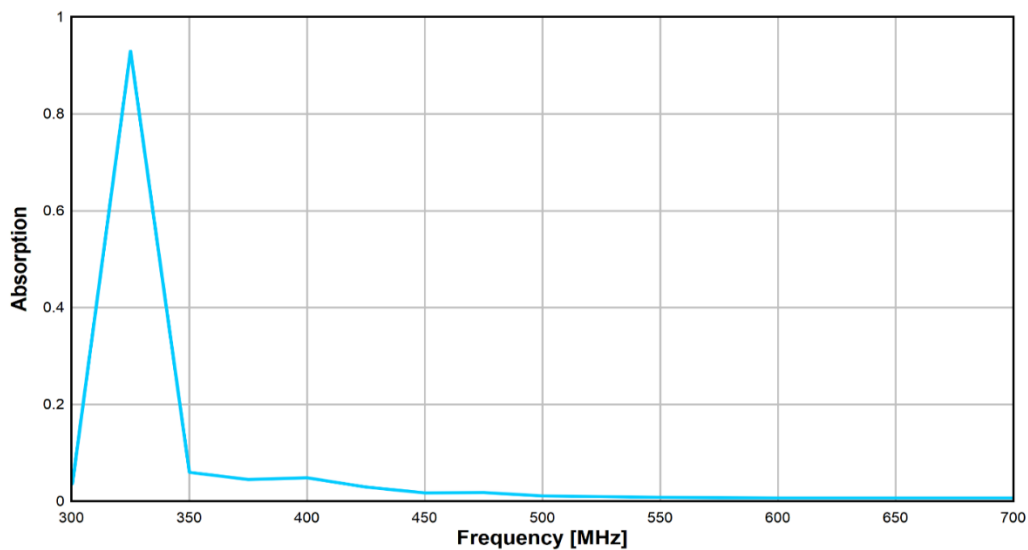


Figure 3.3: Absorption response of the patch design shown in **Fig. 3.2**.

3.3.2 Encapsulated Water in a FR4 Coating

In the previous section, the water dielectric seems impossible for realistic applications looking for its fluidity. In this section, we make our basic design closer to a realistic fabrication by inserting the water in an FR4 box as shown in **Fig. 3.4**. The obtained model looks like an encapsulated water in an FR4 box. In **Fig. 3.4**, the dimensions of the patch are optimized to be of a total thickness of 6.25 mm with an FR4 thickness of 0.3 mm and a unit cell length of 52.5 mm.

Theoretically, the addition of a dielectric material above a metamaterial substrate modifies the frequencies of the resonances. To define the frequency offset resulting from the stacking of FR4 layers, we have used a publication dealing with this subject for patches antennas [9]. The equivalent permittivity can be written as follows:

$$\varepsilon_{eq} = \left(\sum_{n=1}^N \frac{t_n}{\varepsilon_n} \right)^{-1} \quad (3.2)$$

With ε_n represent the permittivity of the dielectric layers and t_n represent the thickness of the dielectric layers.

In our case, from **Fig. 3.5** we can observe that there is a non-considerable shifting in resonant absorptive frequency. Based on **Equ. 3.2**, the slight modification is due to the very thin thickness FR4 with respect to the thickness of the water substrate beside the small value of relative permittivity of FR4 concerning the water value.

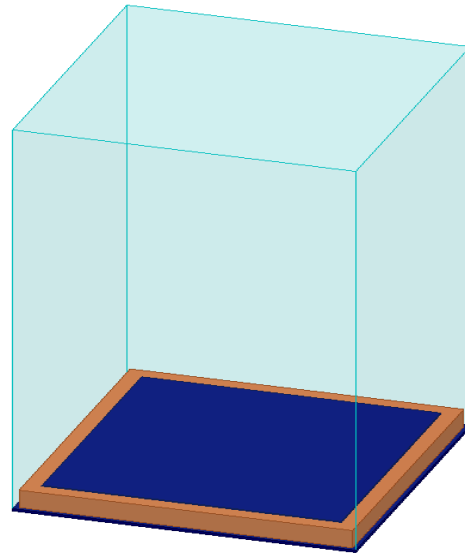


Figure 3.4: Patch design with water substrate encapsulated in FR4 box.

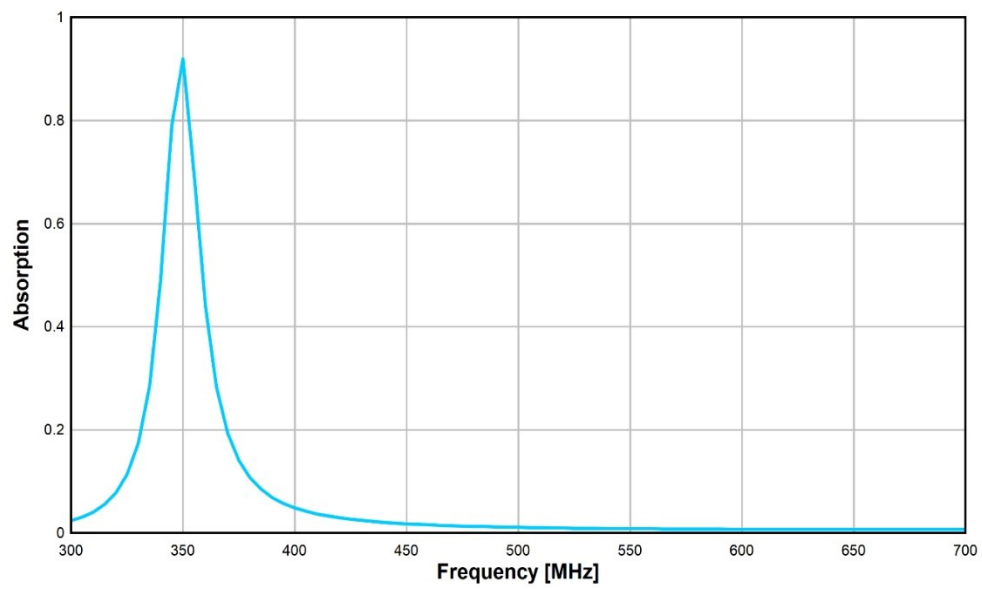


Figure 3.5: Absorption response of the patch design shown in Fig. 3.4.

3.3.3 Conclusion

We can conclude that by using high relative permittivity materials, we reach a low resonant frequency value with the dimension of $\lambda/16.3$ that is considered as a very good proportion.

Therefore, regarding the benefits of this idea with a comparison with presented absorbers like ferrite material, we are able to miniaturize the dimensions of the unit cell, but we are always suffering from the weight density of the high relative permittivity materials required. That puts a limitation on the contribution of metamaterials in low-frequency absorber. We can conclude that by metamaterial we miniaturize the enormous dimensions. However, we are always restricted by the mass density of necessary high relative permittivity material to low absorption frequency response. The advantage of metamaterial here is that it needs a thinner substrate which means that the overall mass is relatively reduced concerning the presented absorber as ferrite material.

In the next section, we try to make use of the geometrical advantage offered by the minimal surface design in miniaturizing absorber model.

3.5 Minimal Surface Geometry

Minimal surfaces are the surfaces of the smallest area spanned by a given boundary. Minimal surface theory is rapidly developed at recent time [10-11]. Many new examples are constructed and old altered. Minimal area property makes this surface suitable for application in architecture. The main reasons for application are the weight and amount of material reduced to minimum. In our work, we test its miniaturization efficiency in patch absorbers.

3.5.1 Rough Surface Effect

In this section, we test different patches of different roughness forms and levels. They are drawn using mathematical functions in MATLAB software. The MATLAB code was exported to Space Claim software to be sketched and then imported as a block design in HFSS where we study the absorption response by simulation. All MATLAB codes used are presented in Appendix 2.

3.5.1.1 Droplet Water Surface

Inspired by the roughness of the water ripple when dripping (see **Fig. 3.6**), the first patch was designed. In the simulated design shown in **Fig 3.7**, we apply these ripples to the copper layer on the top and the same ripples are applied in the substrate layer at the top face. Besides, in order to highlight the effect of the roughness applied, the same design properties were applied for a regular flat patch as shown in **Fig. 3**.



Figure 3.6: Droplet drops on the water surface creating the first roughness form modeled.

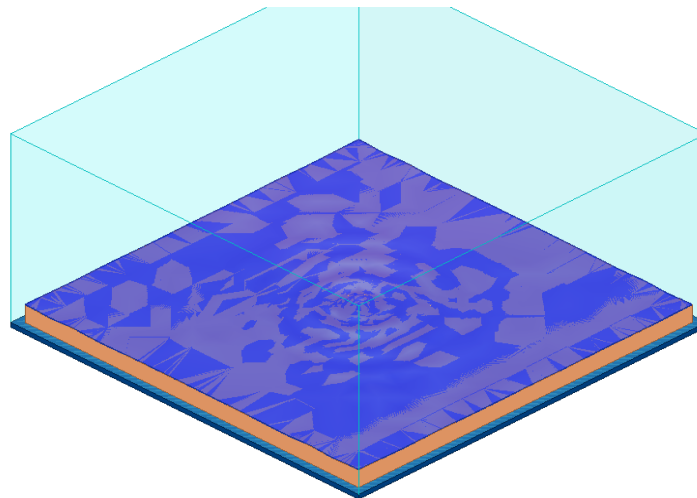


Figure 3.7: The first roughness form modeled in HFSS.

Just to remind, in these simulations, the periodic boundary conditions are assigned along the x and y-directions. A wave port is launched along the z-direction with E field polarized along the y-direction. The analysis mode is taken as a discrete sweep type with a high number of data

points to provide high accuracy for the obtained results. In these models, we assign the copper for the metallic part and high relative permittivity material ($\epsilon_r = 55$) as a substrate having dielectric loss tangent of 0.03.

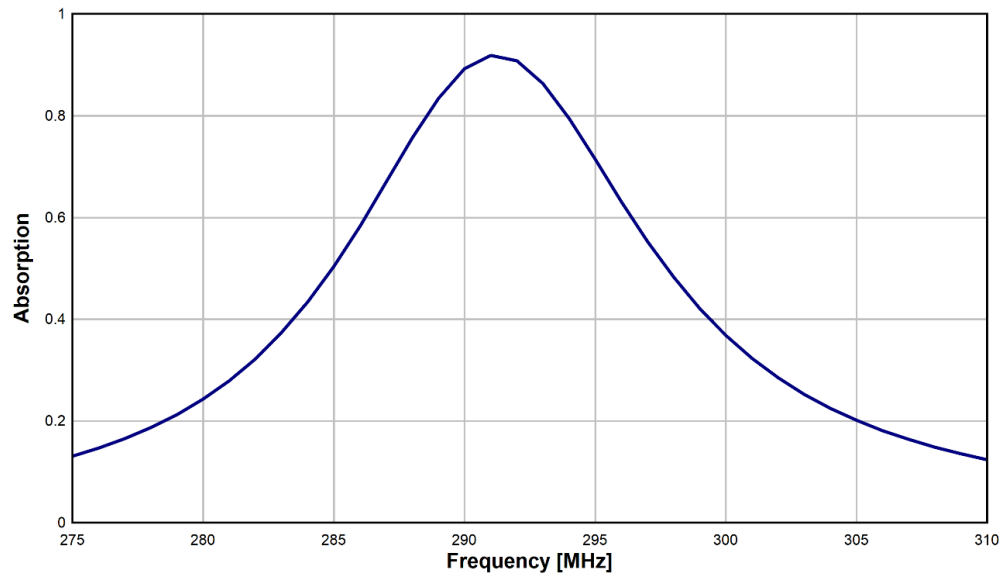


Figure 3.8: Absorption response of the Droplet Water surface.

After simulation, we obtain a narrow band of absorption at 292 MHz (see **Fig.3.8**). To show the effect of drawn roughness we design a regular flat patch (refer to **Fig 3.9**) with the same dimensions and material properties of the rough model in **Fig. 3.7**.

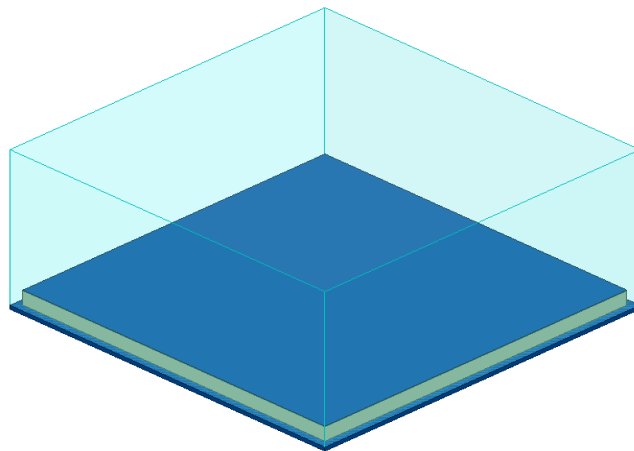


Figure 3.9: Regular patch with same dimension length of the model in **Fig. 3.7**.

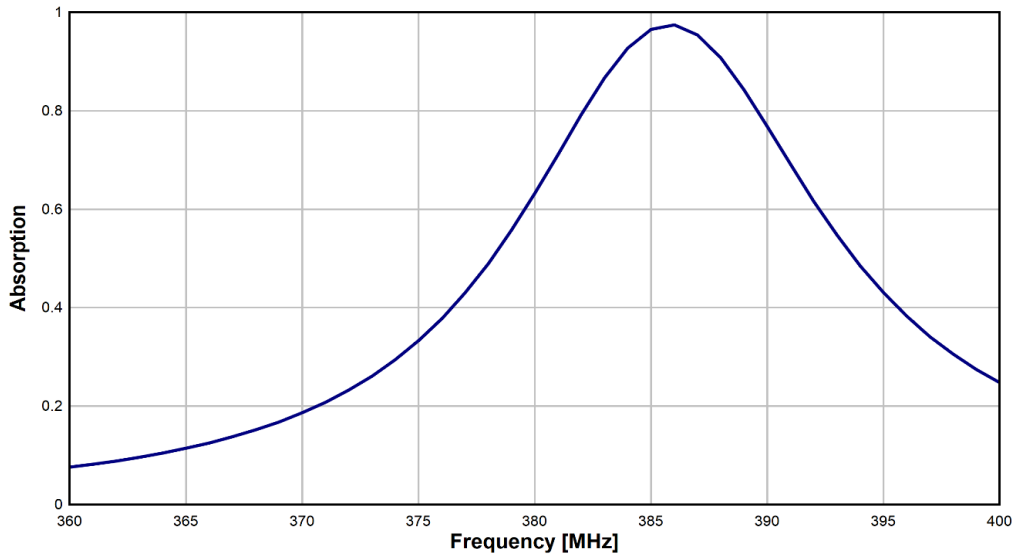


Figure 3.10: Absorption response of the regular patch.

From **Fig. 3.10**, we remark that the resonant absorptive frequency was shifted from 292 MHz in the rough surface model to 387 MHz in the plat patch. Such frequency shifting is considerable in low-frequency bands. Therefore, we can conclude that the only effect of the roughness is its help to shift the resonant frequency in lower value without the need to enlarge the dimensions. That result is due to the bigger surface exploited in the same actual space in the rough model.

From this conclusion, we go forward in designing other random rough surfaces with different Root Mean Square Height (RMS) height to identify more its enhancing effect and its limitations.

3.5.1.2 Random Rough Surface

In the following designs, we take the same material and design properties as the droplet drop surface. Therefore, following the same process of modeling, we obtain the results shown in **Fig. 3.11**.

The roughness of a surface is determined by its RMS Height and its correlation length. In our study to the effect of roughness, we take three different RMS Height values as a variable parameter with a fixed correlation length of 1 cm.

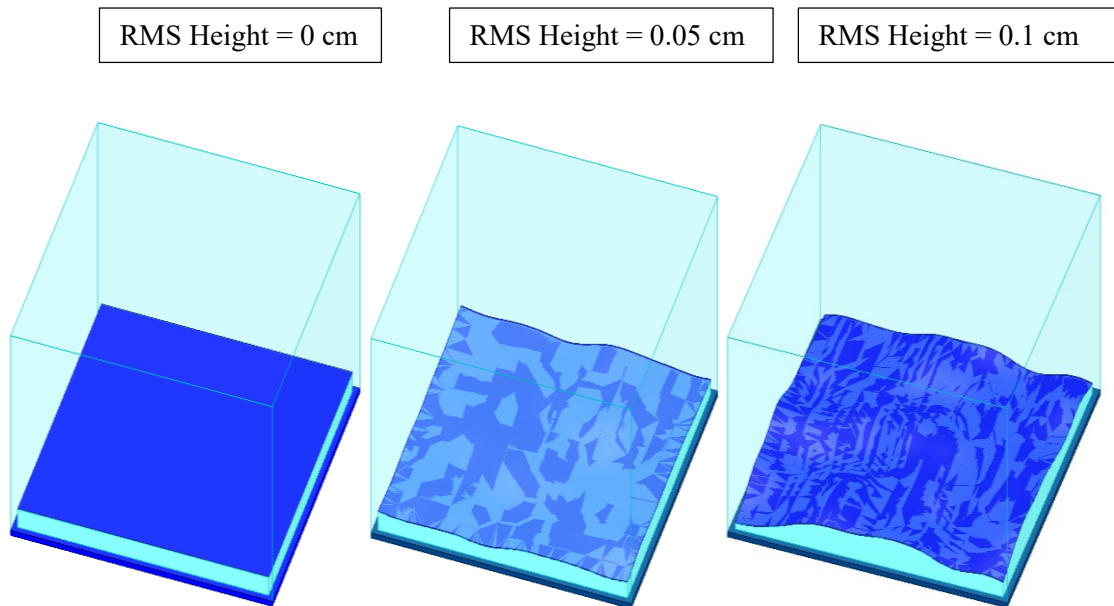


Figure 3.11: Three different RMS Height values applied to a random rough surface in a patch absorber.

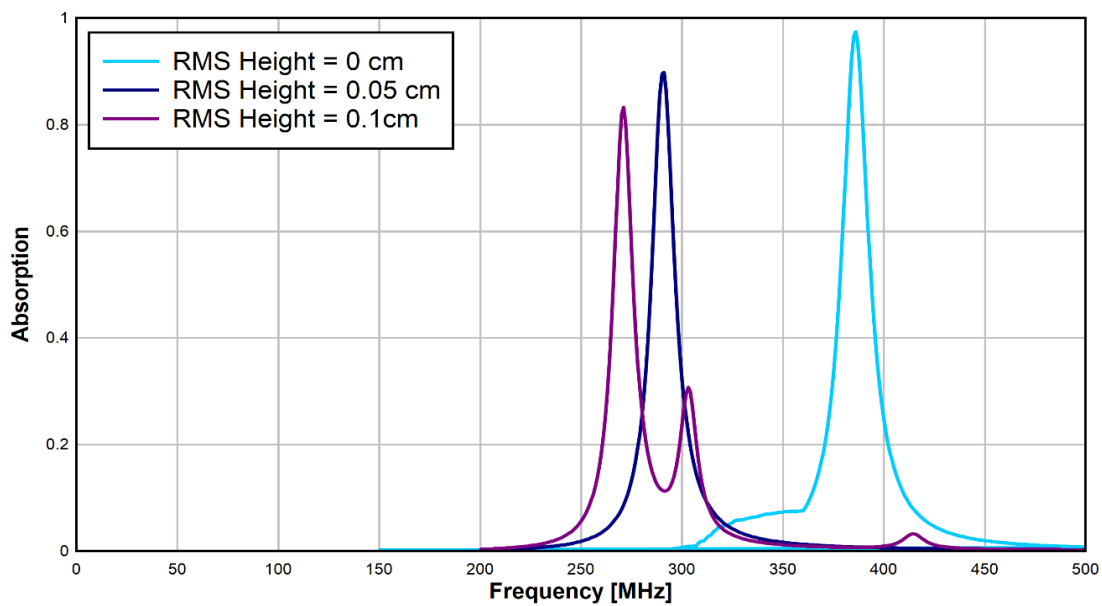


Figure 3.12: Absorption response of different roughness with different RMS Height.

Fig. 3.12 shows the effect of the roughness in shifting the absorptive frequency to lower values but with a degradation in the level of absorption. This degradation is caused by the changeable thickness due to the ripples.

By this result, we prove the effect of roughness in exploiting extra surfaces that result in shifting in the absorptive frequency. Nevertheless, by this idea, we are limited to a certain value of roughness because it causes thicker substrate in some regions of the rough surface due to the resulted ripples that change the optimized thickness.

In the last model, when we use high relative permittivity substrate material ($\epsilon_r = 55$) by applying a rough surface of RMS Height = 0.1 cm, we arrive to reach a resonant absorption at 270 MHz with an average thickness of 4 mm and unit cell dimension of 7.3 cm comparable to $\lambda / 15.2$ which is considered a great proportion.

3.5.1 Helicoid Model

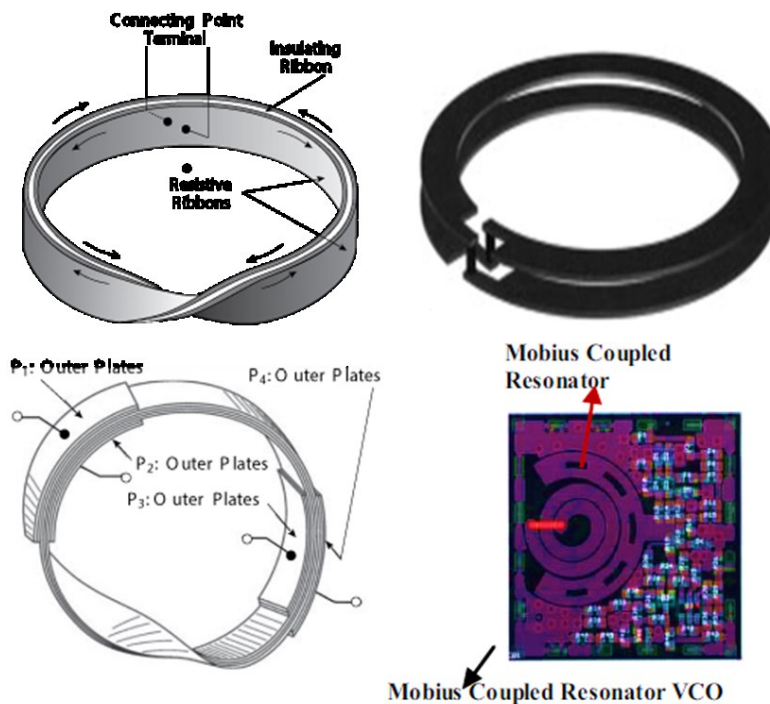


Figure 3.13: Different Mobius resonator shape for different applications [12-14].

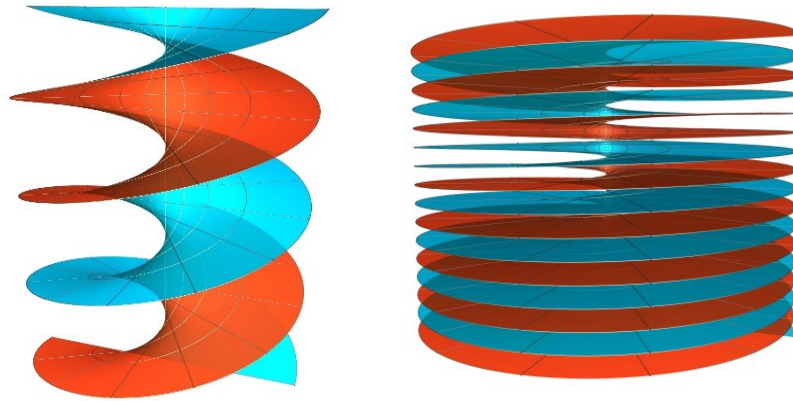


Figure 3.14: The helicoid surface shape.

Another Minimal Surface function is drawn for the same purpose using the equation surface in HFSS. The helicoid is shaped like Archimedes screw (**Fig 3.14**), but it extends infinitely in all directions.

This new model of absorber shape takes its inspiration from the contribution of different Mobius shapes (see **Fig. 3.13**) in miniaturization of resonators in different applications. In these references [12-14], the twister presented in Mobius designs leads to miniaturize the dimension until the half. For that, we aim to design a new patch resonator absorber using a similar twister idea. The latter is being applied to patch design through a helicoid function. It can be described by the following parametric equations in Cartesian coordinates:

$$\begin{aligned}
 X(u, v) &= v \times \cos(u) \\
 Y(u, v) &= v \times \sin(u) \\
 Z(u, v) &= u
 \end{aligned}
 \tag{3.3}$$

In our design, the helicoid is designed and assigned to be metallic nature of limited thickness. It is united with the ground plane and the top metallic layer. The FR4 substrate surrounds the helicoid in a cylindrical shape as shown in **Fig 3.15**. Three twisters were drawn between the ground plane and the top metallic layer to exploit the triple of the patch surface.

To show the effect of the helicoid in our patch, the same design is modeled without the helicoid by a circular patch with the same dimension and material properties as shown in **Fig. 3.16**.

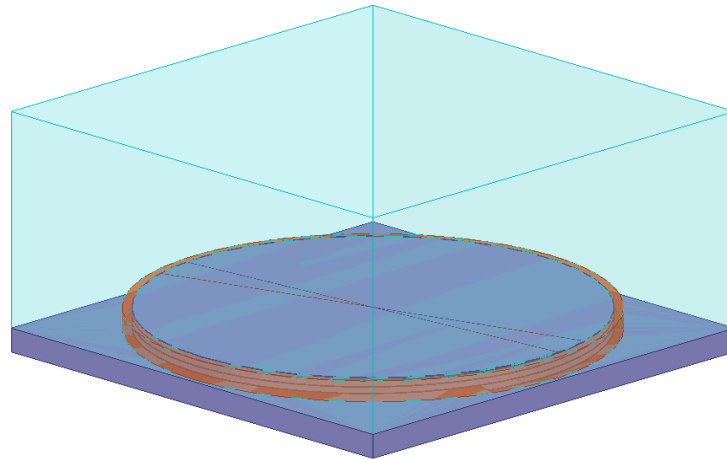


Figure 3.15: Resonator patch absorber with metallic Helicoid Model.

Fig. 3.17 shows resonance at 3.2 GHz while **Fig 3.18** shows the resonance at 2.9 GHz. The obtained 300 MHz shifting in this region is considered as slight shift showing the surface twisted three times in the helicoid region. We can conclude that the helicoid has insignificant effect in shifting the absorptive frequency to lower values because the surface is not exploited properly.

Missing always from the required characteristics, the Mobius design seems like a creative design that can give us a resonance response by minimized dimension but by simulation it proved that the expectation is contraindicated.

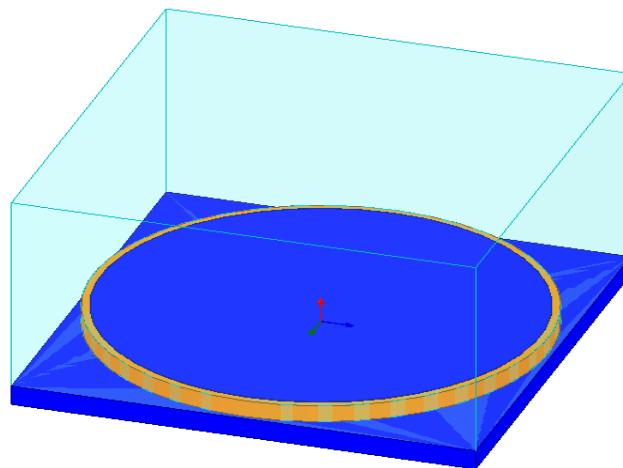


Figure 3.16: Circular Patch Design.

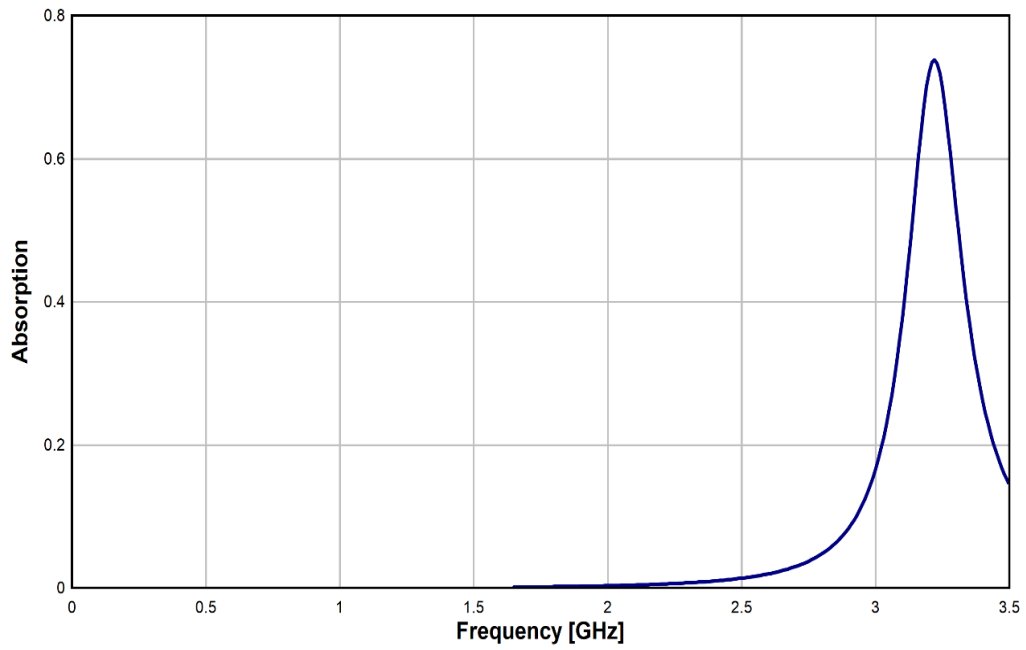


Figure 3.17: Absorption response of the circular patch design.

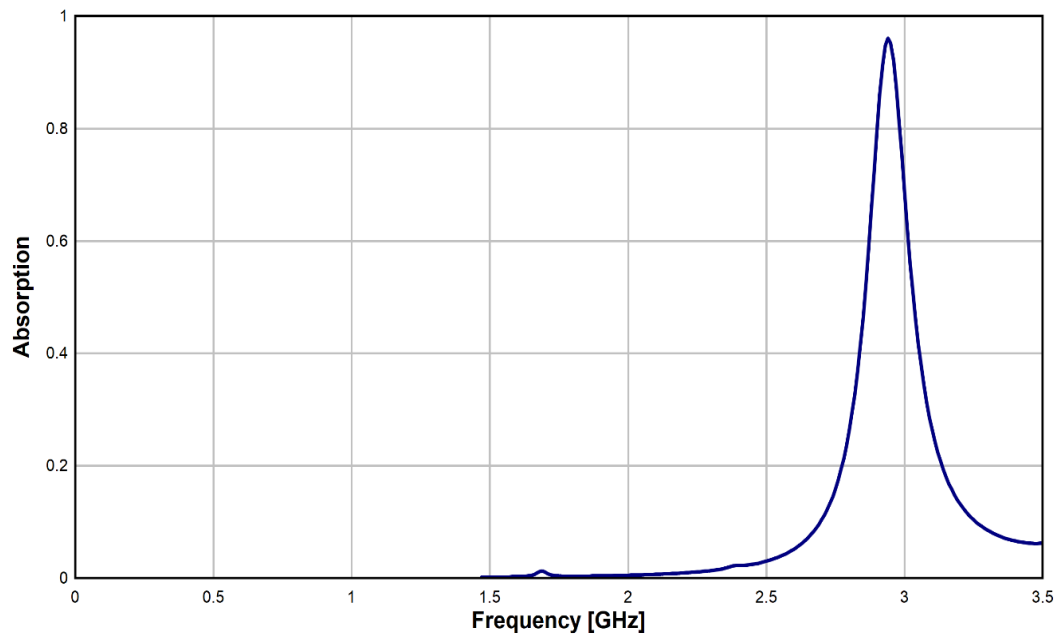


Figure 3.18: Absorption response of helicoid model.

3.6 Conclusion

In conclusion, to obtain a low-frequency absorption response with miniaturized dimensions, we tended to choose high relative permittivity substrate material with minimal surface design. Each way was discussed alone. As a first task, in the material properties study, different dielectric substrates with their practical properties were presented. Then after a comparison, distilled water proved to be the best dielectric suitable for low-frequency absorption. We made this idea more practical by inserting water in the FR4 box having almost the same absorptive response. Besides, for the aim of reducing patch dimensions, we designed different minimal surface designs as random rough surfaces. Such an idea shows a new miniaturization way to obtain an acceptable dimension with low frequency. Finally, in one design we combine these two ideas. As a result, we reached a low resonant frequency value with the dimension of $\lambda/15.2$ with a relatively thin substrate.

We can conclude that using metamaterial we can miniaturize well the enormous dimensions of unit cells. Nevertheless, the material of high relative permittivity imposes certain weight view its mass density but by the thin thickness of the metamaterial make such design relatively non-weighty. Besides, the roughness can miniaturize well the units, but we are limited by altitude to some level when the thickness is unsuitable for a good absorption level. It is worth mentioning that the breakdown voltage property is one of the standard competitive promoted by big actual institutions of anechoic chamber view the sensitivity to the pyramidal foam to power handling and fire (2000 W/m^2). The latter shows that metamaterial appears as a good candidate looking to the higher breakdown voltage of its substrate (distilled water has a power handling of $70 \times 10^6 \text{ W/m}^2$).

This chapter studied the ways of shifting absorption frequencies in lower band, but we are always concerned about the narrow band of absorption. In the next chapter, these ideas will be applied in new broadband structures based on pyramidal design that was studied in details in the previous sections.

3.7 Reference

- [1] Tuong, P. V., et al. "Polarization-insensitive and polarization-controlled dual-band absorption in metamaterials." *Applied Physics Letters* 102.8 (2013): 081122.
- [2] Bui, Son Tung, et al. "Small-size metamaterial perfect absorber operating at low frequency." *Advances in Natural Sciences: Nanoscience and Nanotechnology* 5.4 (2014): 045008.
- [3] Yoo, Y. J., et al. "Flexible and elastic metamaterial absorber for low frequency, based on small-size unit cell." *Applied physics letters* 105.4 (2014): 041902.
- [4] Huang, Li, et al. "Impact of resonator geometry and its coupling with ground plane on ultrathin metamaterial perfect absorbers." *Applied Physics Letters* 101.10 (2012): 101102.
- [5] Dayal, Govind, and S. Anantha Ramakrishna. "Broadband infrared metamaterial absorber with visible transparency using ITO as ground plane." *Optics Express* 22.12 (2014): 15104-15110.
- [6] Pitchappa, Prakash, et al. "Micro-electro-mechanically switchable near infrared complementary metamaterial absorber." *Applied Physics Letters* 104.20 (2014): 201114.
- [7] Landy, N. Iff, et al. "Perfect metamaterial absorber." *Physical review letters* 100.20 (2008): 207402.
- [8] Li, Lan, et al. "Early osteointegration evaluation of porous Ti6Al4V scaffolds designed based on triply periodic minimal surface models." *Journal of Orthopaedic Translation* (2019).
- [9] Park, Jun-Hyoung, and Jae-Chul Lee. "Peculiar elastic behavior of mechanical metamaterials with various minimal surfaces." *Scientific reports* 9.1 (2019): 2941.
- [10] Ulaby, Fawwaz Tayssir, et al. *Microwave radar and radiometric remote sensing*. Vol. 4. No. 5. Ann Arbor: University of Michigan Press, 2014.
- [11] Sellier, Alexandre. *Absorbants à métamatériaux: étude théorique et expérimentale*. Diss. Université Paris Sud-Paris XI, 2014.

- [12] Pond, Jeffrey M., Shaojun Liu, and Nathan Newman. "Bandpass filters using dual-mode and quad-mode mobius resonators." *IEEE transactions on microwave theory and techniques* 49.12 (2001): 2363-2368.
- [13] Chang, Chih-Wei, et al. "Optical Möbius symmetry in metamaterials." *Physical review letters* 105.23 (2010): 235501.
- [14] Poddar, Ajay K., Ulrich L. Rohde, and D. Sundararajan. "A novel Mobius-coupled printed resonator based signal sources." *2013 IEEE MTT-S International Microwave Symposium Digest (MTT)*. IEEE, 2013.

4. Chapter 4: Design of Metamaterial Broadband Absorber

4.1 Introduction

Landy [1] was the first to propose a type of perfect metamaterial absorber that separately couples with the electric and magnetic fields to absorb all incident radiation by independently manipulating the electrical and magnetic resonances. From then, metamaterial absorbers operating at microwave, terahertz, and infrared frequencies have been extensively investigated [2–13]. Following the study of Landy, Yang [2] also proposed a metamaterial absorber with a high absorptivity of 99.9%. However, its absorption bandwidth was quite narrow. Cumming [3], Lim [4], and Wen [5] prepared dual-band metamaterial absorbers with two distinct absorption peaks using dual electric resonators. Cui [7] designed a multi-band absorber that can operate at dual-band and triple-band absorptions. Nevertheless, each absorption bandwidth was still very narrow, limiting the potential application of these absorbers in the fields of cloaking and stealth technology among others.

Hence, developing broadband metamaterial absorbers [11–13] has become a challenging task. Genetic algorithms or multilayer structures are often used to devise a broadband metamaterial absorber [8, 9] such as pyramidal stacked layers but it is also limited until RAB of 65 % in best results [14-16].

In this chapter, we propose new structures of metamaterial absorber based on stacked elements that can overcome an ultra-large band of absorption respecting a miniaturized size in the UHF region.

All calculations were performed on an HPC of 24 cores with a system memory of 192 GB RAM. The discrete frequency analysis mode was adjusted with numerous data points to make simulation results with a very high level of precision. The finite element based electromagnetic solver HFSS by ANSYS was used for calculating the scattering parameters under normal and oblique incidences. In these designs, we use high relative permittivity material of ($\epsilon_r = 55$) as a dielectric substrate and copper as a metallic material.

4.2 By Adding Layers

Based on the operation of the pyramidal absorber discussed in Chapter 2 that refers to the absorption to the electromagnetic resonance occurred at each patch resonator, we can predict that the enlargement of the band can be done by adding supplementary patch until obtaining small patches at the top resulting in a pyramidal cone absorber. In the simulation of this idea, the periodic boundary conditions are assigned along the x and y -directions. A wave port is launched along the z -direction with E field polarized along the y -direction.

4.2.1 Simulation Setup

As cited in the previous chapter, when we use a high permittivity material of value 55 and adjusting the basic patch to be 72 mm, we were able to turn the operating frequency to be absorptive in the UHF band. The simulation setup of this pyramid is shown in **Fig. 4.1(a)**.

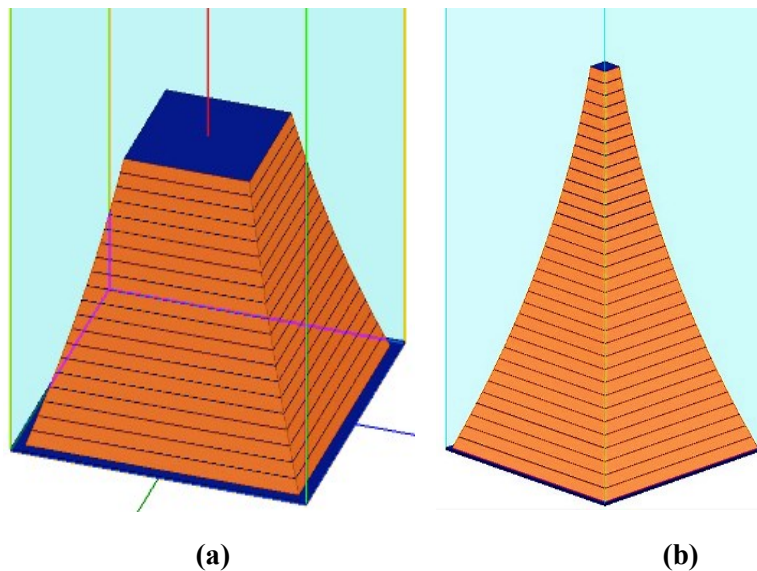


Figure 4.1: Enhanced Pyramid Design Absorbers. **(a)** Structure of the basic pyramid optimized in UHF Band. **(b)** Structure of the Pyramid Absorber after adding 15 layers, the basic layer is 72 mm of length and the smaller patch at the top is 11.7mm.

Inspired by the conic form of foam in an anechoic chamber and to enlarge the absorption band, we added 15 supplementary patches in the same stitching method to the pyramid scaled to the low frequency that is shown in **Fig. 4.1 (a)**. We obtained a new model of the structure formed of 35 stacked patches as shown in **Fig. 4.1(b)**. This design paves the way to have a sharpened peak in the top of the pyramid, an option that can decrease the interface between an electromagnetic wave and the design leading to a possibility for a decrease in its reflection. By *3 points arc* in HFSS, a curve was optimized in way to relate those 35 patches to combine well the successive resonance obtained by each dimension of patches. The curved altitude was applied in this design after proving its efficiency in a pyramidal design in Chapter 2.

4.2.2 Results and Discussion

First, we simulated the enhanced curved of the PA that is responsible to achieve a good reasonable absorption in the UHF band only. The absorption spectrum of the structure in **Fig. 4.1(a)** is shown in **Fig. 4.2** with absorptivity above 80% over the frequency band [300-625] MHz. Then, we added 15 successive layers as shown in **Fig. 4.1 (b)**. **Fig. 4.3** shows that this proposed design attained very ultra-broadband of absorption in the UHF/SHF frequency bands.

Normally, such a design must give 35 peaks of resonance in such a way that each patch resonates in one peak of frequency. Fortunately, the obtained results show an extra factor of absorption at higher frequencies. In the lower range of absorption [0.3 GHz - 1.92 GHz] (Phase I), we can say that the absorptive results to the successive resonant absorption modes occurred at multi-frequencies. To analyze the physics of the absorption occurred in this phase, the electric and magnetic field distributions at some frequencies are depicted in **Fig. 4.4**. It is evident that, at a certain frequency, the electromagnetic field is resonantly localized and then absorbed at some part of the pyramids. By referring to the design equation of a patch in (3), the electromagnetic field is localized at the bottom side of the pyramids (i.e. the largest patch) at a smaller frequency.

In a resonant mode, electric and magnetic resonance both exist in **Fig. 4.4**. They make the absorber impedance match well with the free space, and the incident wave is absorbed in the dielectric with low reflection.

In the second phase (1.92 GHz- 30 GHz), the ultra-broadband continues with a level greater than 90% (Fig.4.3 (b)). In this phase, we can relate the cause of absorption to the strong coupling observed between spaced patches where some absorbing modes were created as shown in Fig. 4.5. Besides, each of the following factors may have a role that can contribute significantly to achieving this response: the conical geometry with a peaked top that can decrease the reflection, and the high permittivity material where a high absorption occurred inside it. Such a result needs to be more investigated by experimental testing.

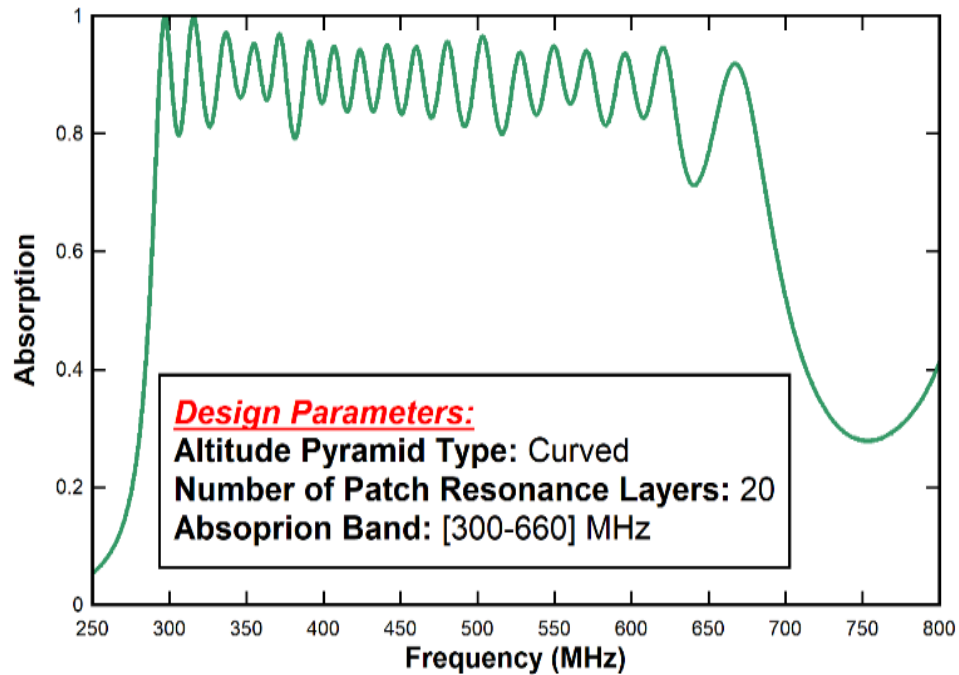
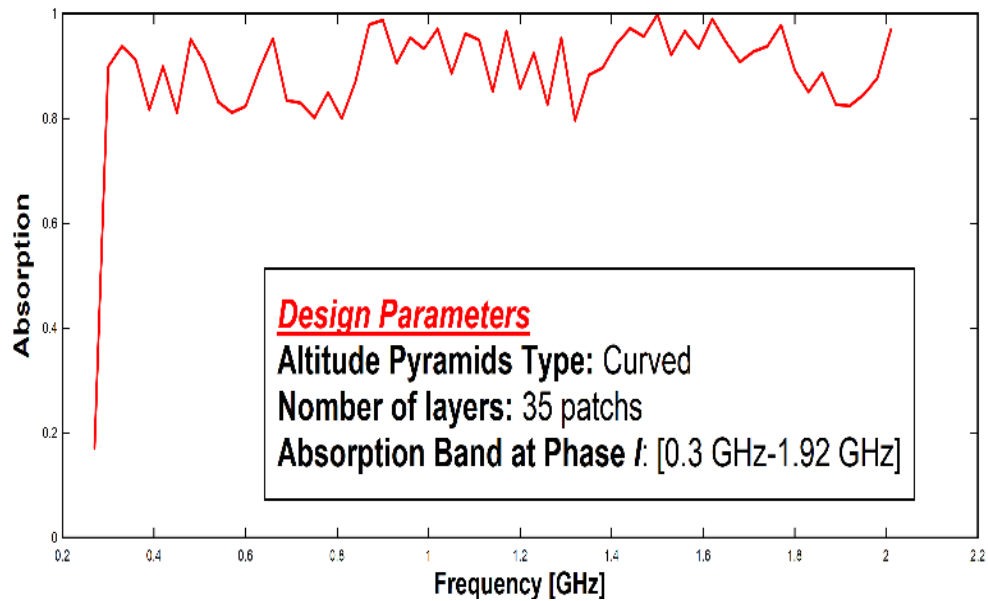
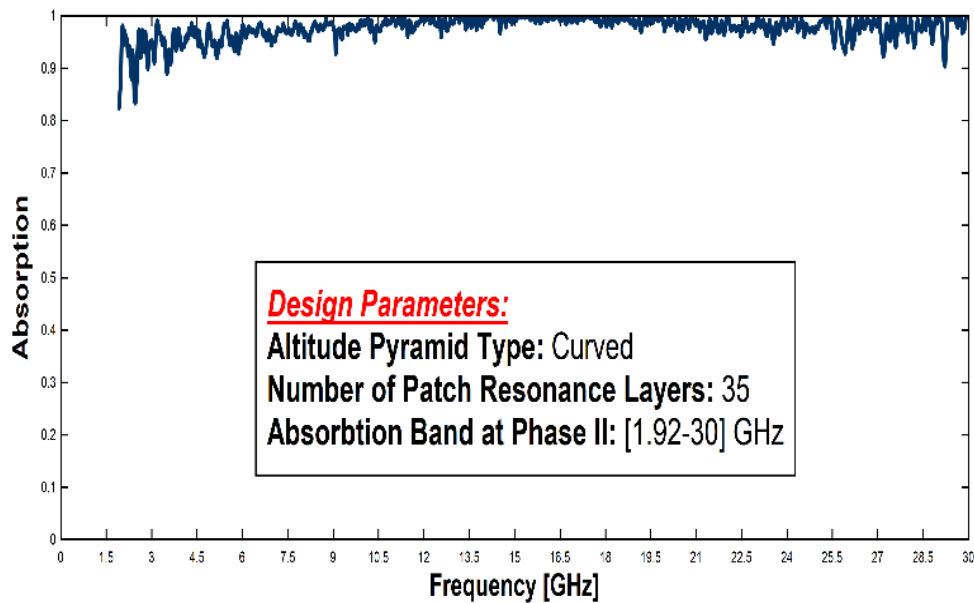


Figure 4.2: Absorption response of the enhanced pyramidal design of Fig. 4.3(a) in the UHF band.



(a)



(b)

Figure 4.3: Absorption response of the EP design of Fig. 4.3(b) in the UHF/SHF band after adding 15 layers. (a) Phase I of absorption. (b) Phase II of absorption.

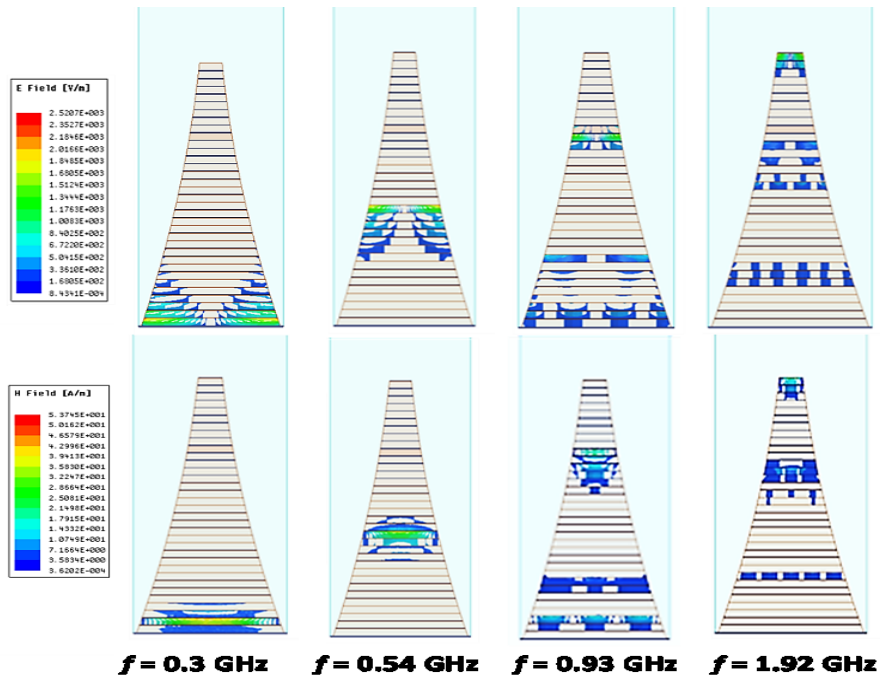


Figure 4.4: Simulated Electric and Magnetic magnitude distributions at some frequencies at phase I of absorption [0.3 -1.92 GHz].

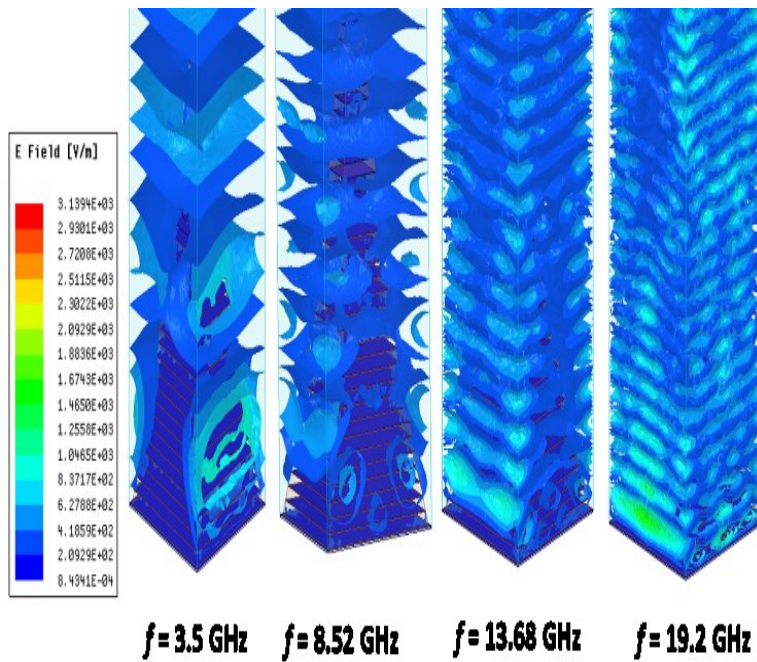


Figure 4.5: Simulated Electric magnitude distributions at some frequencies at Phase II of absorption [1.92 - 30 GHz].

To make sure of the precision of our obtained result, we looked forward in testing another periodic boundary conditions and another excitation type. In this context, we considered more data points to elevate the accuracy of the obtained results. As a result, after applying the master-slave boundary conditions to periodic boundary modulation and after exciting the structure by an incident plane wave, we obtained similar absorption results.

4.3 By Combining Complementary Pyramids

Generally, this broadband objective can be realized by increasing the number of resonators with size variation either in transverse or longitudinal directions as applied in the previous structure. In this section, we propose a bandwidth enhancement of MA through varying the transverse dimension of elementary pyramidal resonators.

This way shows its efficiency in some design in literature [17-18] for combining elementary narrow band absorber, but in this section we propose for the first time its efficiency by combining elementary broadband absorber in one unit cell structure.

4.3.1 Simulation Setup

For the aim of covering a broaden absorption frequency band, we apply a new idea. It consists of grouping two kinds of curved and optimized PA that operate on complementary frequency bands in a one-unit cell. This combined unit cell should also respect the geometrical symmetry that permits to make the model insensitive to the wave polarization as shown in **Fig. 4.6**.

For that, we adjust two PA with the same material properties to be absorptive in complementary bands (refer **Fig. 4.7**).

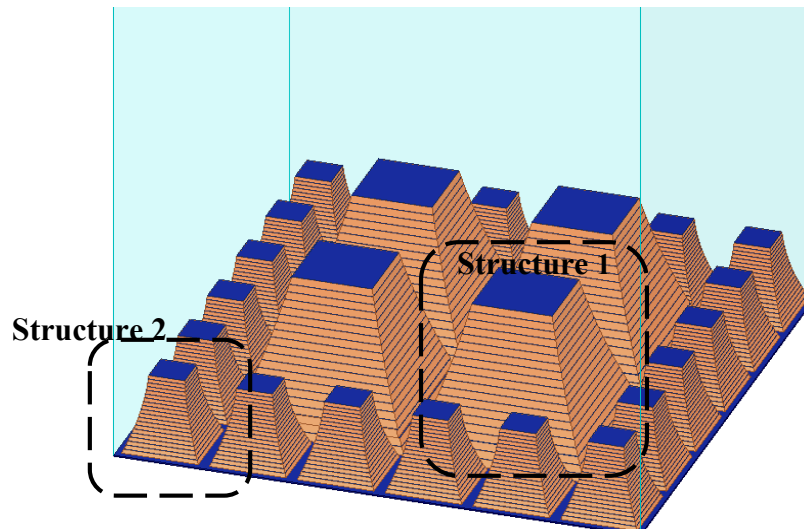


Figure 4.6: Structure of the combined structure operating in complementary bands.

As shown in **Fig. 4.7**, structure 1 operates in the lower band covering [0.29-0.68 GHz] and structure 2 operates in the complementary band covering [0.68-1.48 GHz]. These structures were optimized well in order to obtain an absorption level greater than 80%.

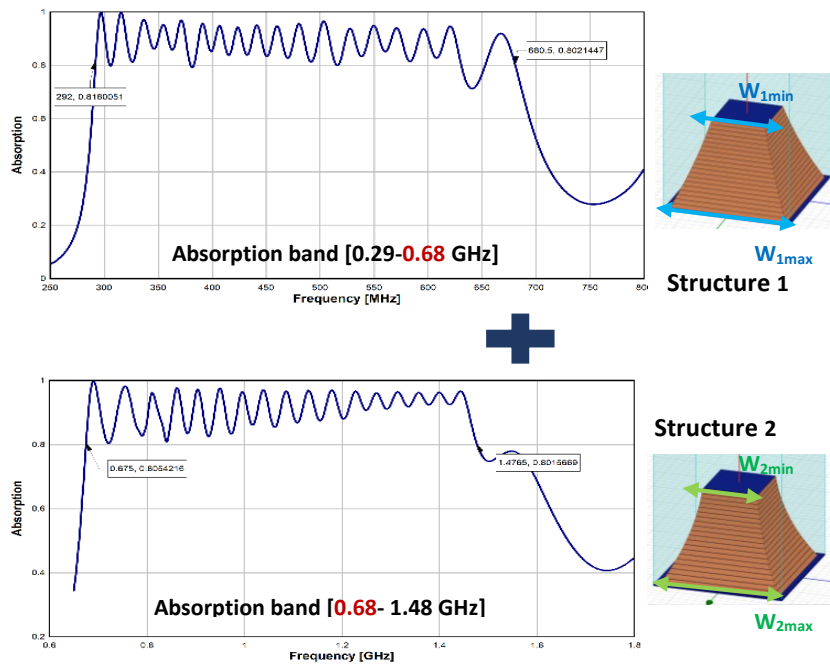


Figure 4.7: The operating absorption band of structures composing the unit cell with geometrical dimensions: $W_{1max}=72$ mm; $W_{1min}=33$ mm; $W_{2max}=31.5$ mm; $W_{2min}=14.7$ mm.

This design imposes a geometrical spacing between pyramids with the same dimensions that can degrade the grouping performance of complementary bands. For that, the periodicity between pyramids is taken to be as minimum as possible in such a way to get the pyramids close to each other preventing any additional spacing between the same pyramid's dimensions as shown in **Fig 4.6**.

It is worth to mention that this minimum spacing reduces also the space of ground planes causing reflection of waves. On the other side, this closeness of pyramids provides an increase in the risk of coupling between cells.

4.3.2 Results and Discussion

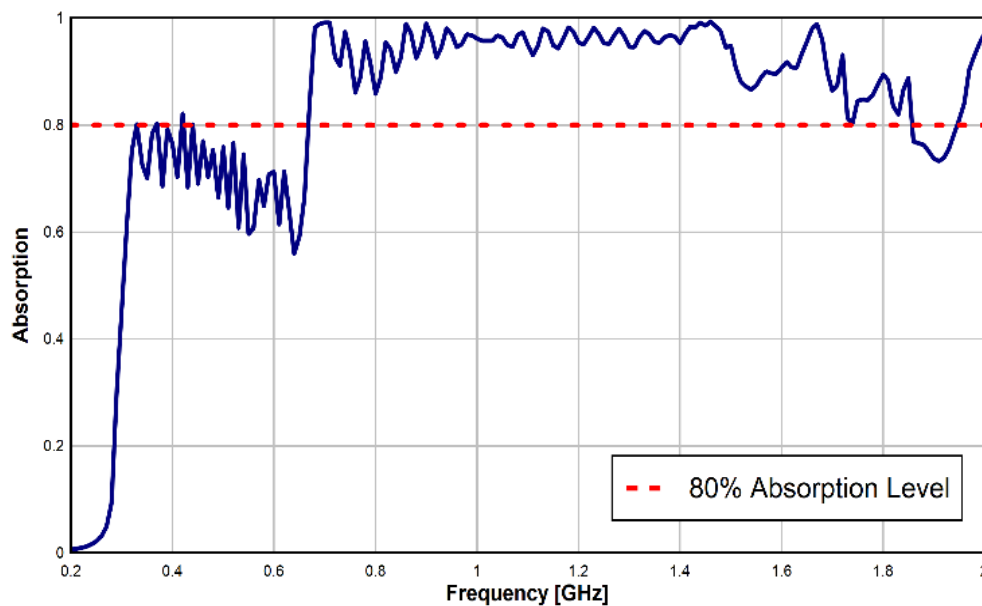


Figure 4.8: Absorption response of the first combined design presented in **Fig. 4.6**.

This result shows that the idea was admitting considerable results. The pyramids were combined as planned in the same mechanism of absorption in a pyramidal absorber (electrical and magnetic resonance at each patch dimension). Nevertheless, **Fig. 4.8** shows also that the bands are not combined properly by this idea. What is particularly striking is the loss of absorption in the lower frequency band. This loss of absorption can be explained by the considerable distance between patches of the same size and by the risky coupling

imposed by the necessary closeness of pyramids. As a conclusion, we must take those two factors as a limitation of this structure.

4.4 Enhanced Combined design

4.4.1 Simulation Setup

Trying to resolve the geometrical disadvantage imposed by this structure, we present this enhanced design. It consists of inserting a third pyramid as shown in **Fig. 4.9**. The latest pyramid is structured and optimized to operate in a medial band covering [0.42 GHz - 0.99 GHz]. This structure must decrease the spacing between similar patch dimensions by this third pyramid functioning as a “bridge”.

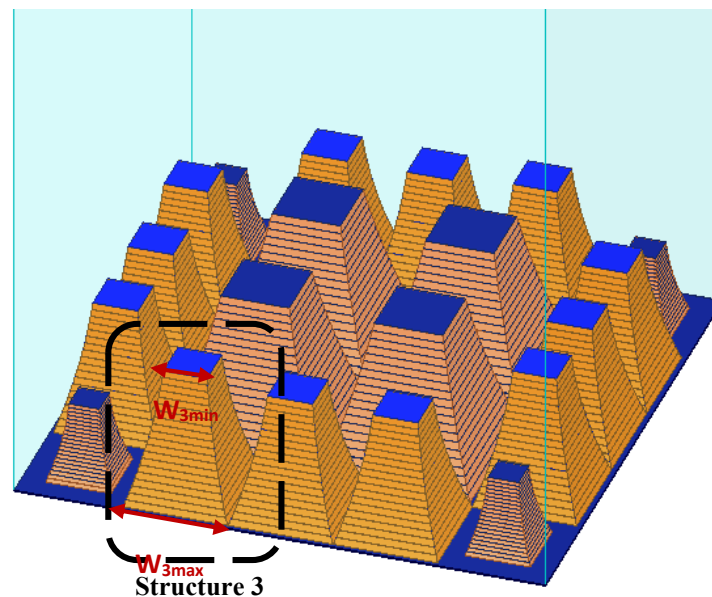


Figure 4.9: Enhanced Model of the combined structure, considering these geometrical dimensions for structure 3: $W_{3max} = 50.22$ mm; $W_{3min} = 21.06$ mm.

4.4.1 Results and discussions

Results show that the bands are now combined better but the part of the lower band is still below 80% of absorption (see **Fig 4.10**). By this result, we obtained an absorption band covering [0.41 GHz -1.89 GHz] with an absorption level greater than 80%. Such band refers to a RAB of **128.69 %** that is considered as a very ultra-large bandwidth.

We can remark that the lowest part of frequency is for the lowest absorption level. It is the part excluded from the absorption band of the “bridge” pyramid. At the same time, there is no problem with the higher level excluded from Bridge Pyramid. This phenomenon can be explained by the phenomenon that declares: “the biggest region of resonance induces the biggest noise coupling effects”. The four big pyramids are coupled with each other in basic patches that weaken their roles and results a lower level of absorption.

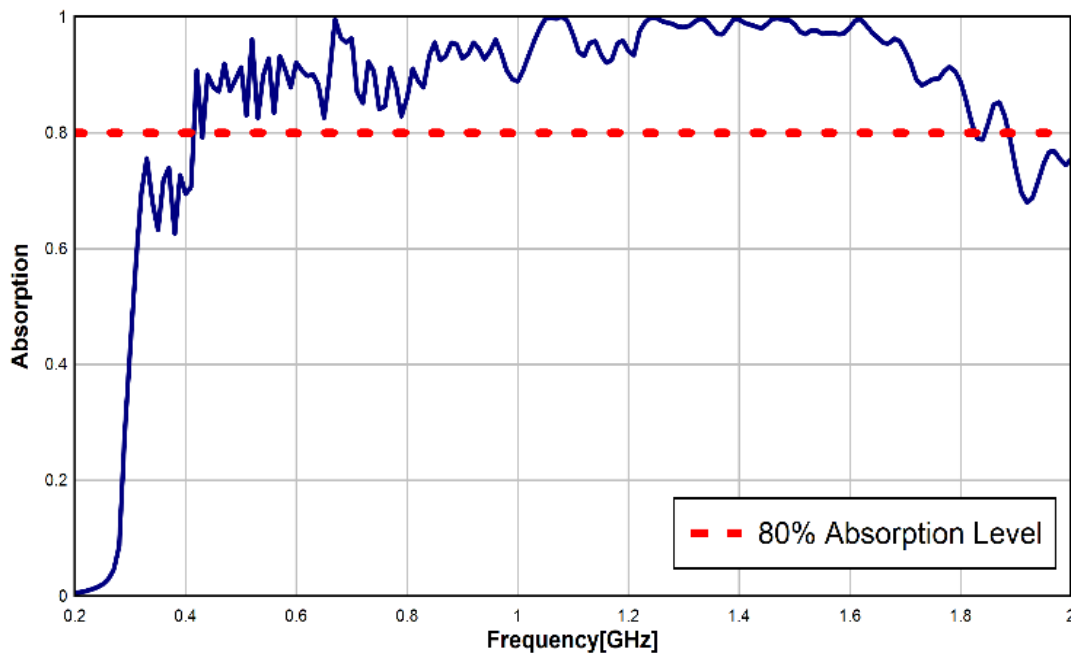


Figure 4.10: Absorption response of the enhanced combined design presented in **Fig. 4.6**.

4.5 “Heel and Heads” Structure

4.5.1 Simulation Setup

This structure is designed in such a way to prevent the additional size of the total unit cell thus reduces the spacing between pyramids with the same dimension. It consists to set longitudinally the pyramids of structure 1 and structure 3.

Based on our studies done on the pyramid operation (cited in Chapter 2), the mechanism of absorption is related to the electromagnetic resonance that occurred in each

stacked patch. That means that if we invert the pyramid, we must obtain the same absorption.

For that, we are free to combine two pyramidal structures with different dimensions operating in complementary bands inverting the biggest pyramidal dimension and putting the smallest pyramidal on the top to obtain what can be called “Heel and Heads Structure” (see **Fig 4.11**).

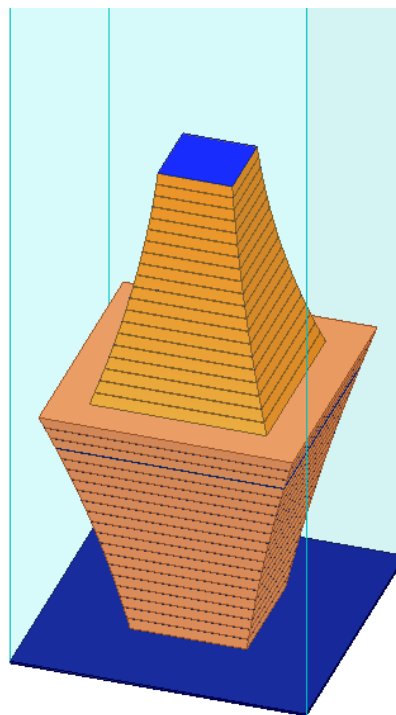


Figure 4-11: “Heal and Heads” structure.

4.5.2 Results and Discussion

Fig. 4.12 shows that the bands are combined properly, but we have a slight degradation in the level of absorption at the higher band. In order to understand well the causes of this degradation, we study the effect of the inverted pyramid alone (**Fig 4.13**). It shows that the inversion of pyramids affects its absorption response, which shows the effect of the peaked top in reducing the reflection. In conclusion, the Heal and Heads structure succeeds in combining bands but the inversion degrades its absorption response.

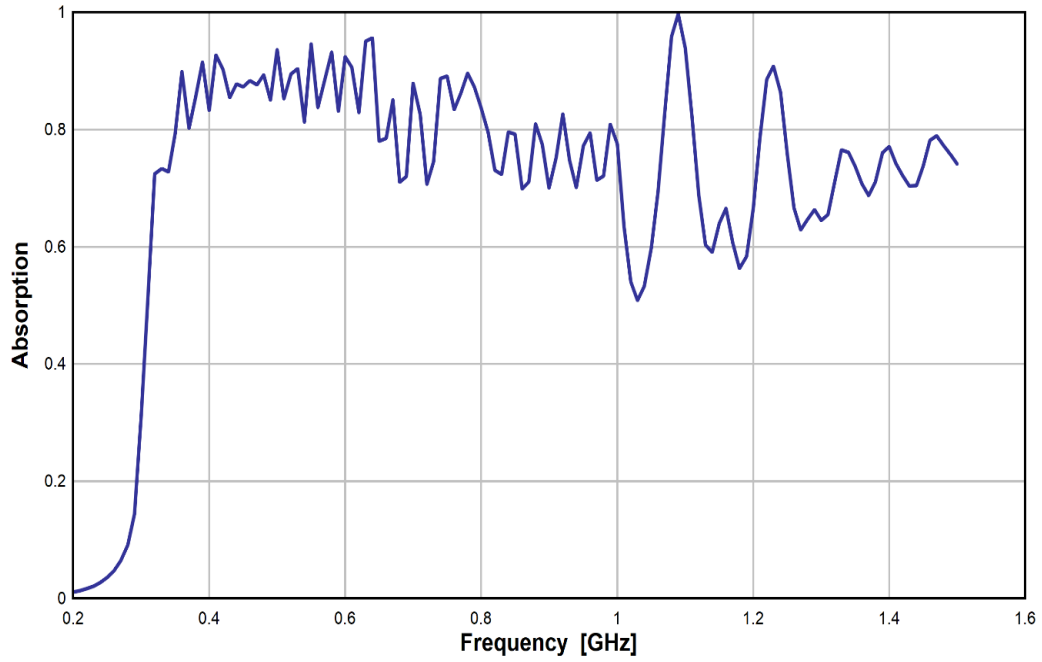


Figure 4.12: Absorption response of the simulated “Heel and Heads” structure of Fig 4.11.

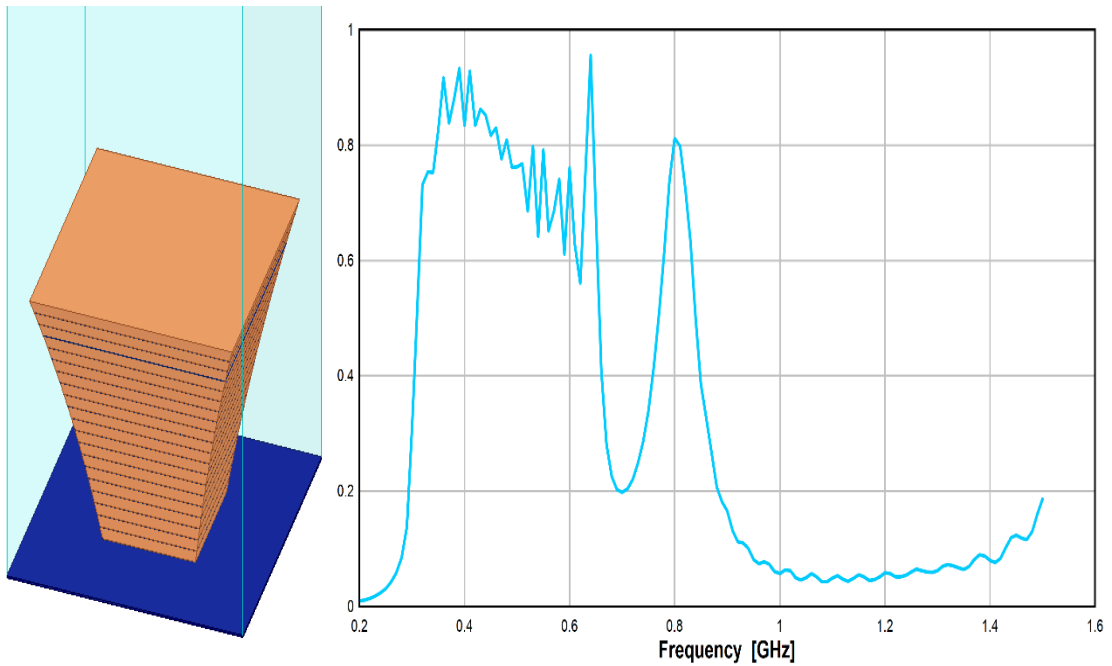


Figure 4.13: Absorption response of the inverted pyramid.

4.6 By Applying Helicoid Cone

This design adds an electromagnetic property to our designed absorber that is “chirality” [19]. The application of the chiral material was seen in the design of radar absorbing material with the start of the Second World War in order to reduce the radar cross-section for aero scope vehicles [20-21]. However, advanced studies showed that introducing of the chiral obstacles results in no enhancement in the reflection characteristics [22-23].

4.6.1 Simulation Setup

The helicoid equation surface was drawn and applied in Chapter 3 in order to test its miniaturization efficiency for a narrow band of absorption and it shows its inefficiency. Now, we test the broadband absorption response of a new-engineered helicoid in its conical form “screw” (Fig. 4.14). In this design, exceptionally we use FR4 epoxy as a dielectric substrate.

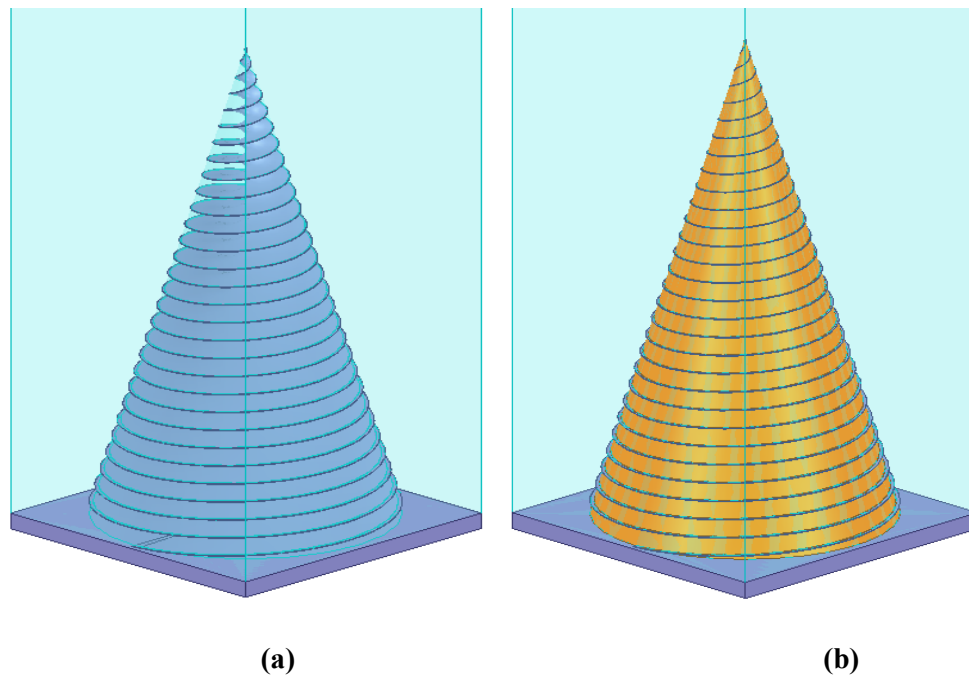


Figure 4.14: Helicoid cone design: (a) metallic helicoid cone (b) metallic helicoid cone covered by FR4 substrate (Altitude = 4.5 cm, Radius = 1.2 cm)

The designed structure is modeled in order to give as expected the same absorption mechanism of pyramidal design but with related patches in helicoid form instead of stacked patches as in a pyramid.

4.6.2 Results and Discussion

The obtained absorption band covers more than [3.8 GHz – 30 GHz] (see **Fig 4.15**) the absorption is still in continue but because it takes a giant space memory we stopped it in 30 GHz that concern the maximum of the SHF band. This band corresponds to a RAB of 162.5 %. The absorption band obtained is not a successive peak of resonances; therefore, the mechanism of absorption is not similar to the pyramidal one. Such results show an extra factor of absorption occurred in this structure.

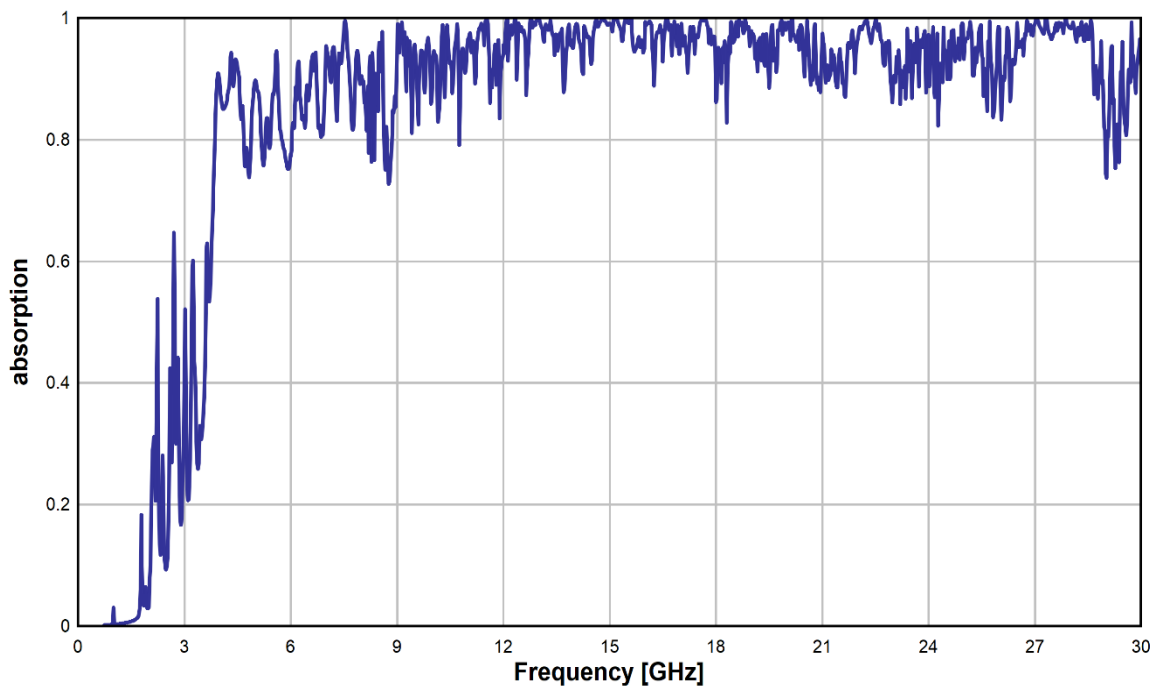


Figure 4.15: Absorption response of the helicoid cone structure.

To understand the mechanism of absorption in this model, we study the magnitude of electrical and magnetic field distribution on this structure in some frequency point when a maximum level of absorption is obtained (see **Fig 4.16**).

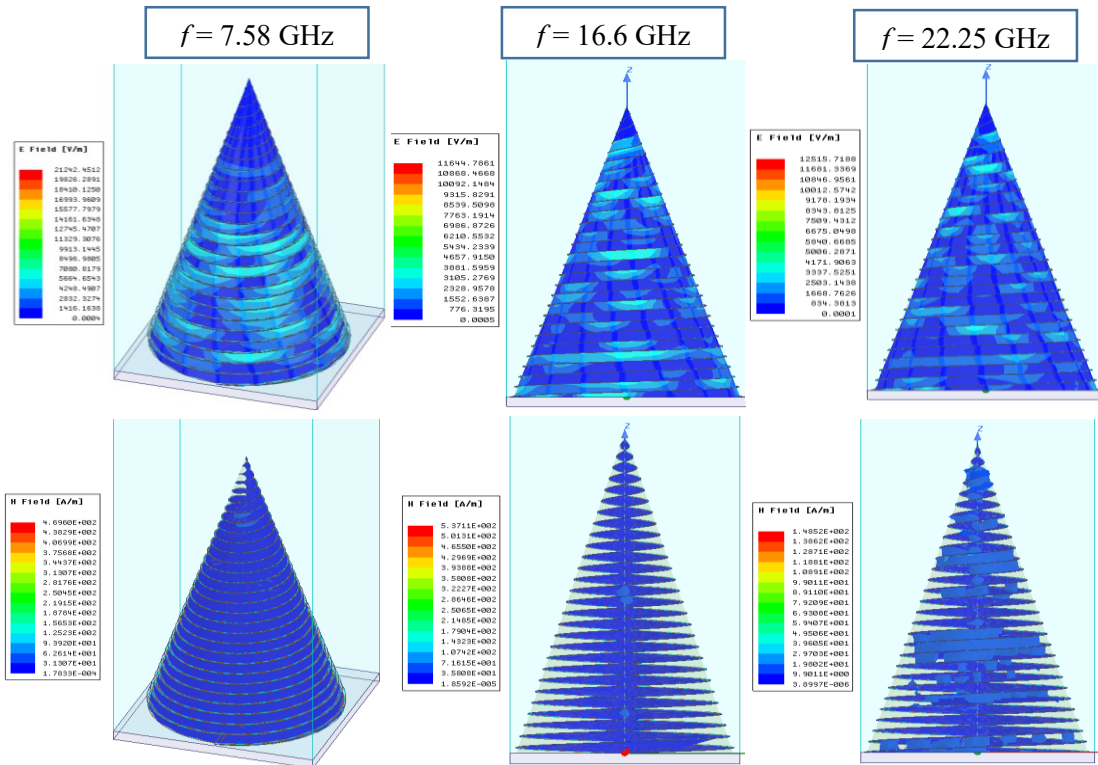


Figure 4-16: Magnitude of Electrical and Magnetic Field distribution on the helicoid structure for different frequencies.

Fig. 4.16 shows that at the frequencies when a perfect absorption has occurred there is only an electrical resonance. Besides, the electrical resonance is not concentrated in one disc dimension; it is distributed on all the structures at each absorption frequency. The interaction of the magnetic field slightly appeared. In this structure, the conical form of this structure with the peaked top was one of the factors that help reduce the reflection of electromagnetic waves because in Chapter 3 when the cylindrical shape was studied, this result did not appear with this broadening.

This structure needs more investigations, but it appears as an interesting structure that can give an ultra-broadband.

4.7 By Stacking Multi-Band Patches

Here we try to reduce the number of stacked patches by applying multi band patches at each layer in order to obtain an ultra-broadband response. By this structuring method, we unite the two broadband ways of absorption applied in the previous structure. The first way was the stitching patch layers longitudinally and the second way was combining transversally different dimensional patches.

4.7.1 Simulation Setup

Different articles designed the multi-band absorber by different forms and for different applications [24-26]. In this section, we benefit from some structures to test our structuring way for broadband absorption purposes. In [26], four different dimensions designed a quad-band absorber. The same design characterization was applied as a first step (refer to **Fig 4.6-a**). Then we adjust its dimension in such a way to have successive absorption peaks as shown in **Fig. 17-b**.

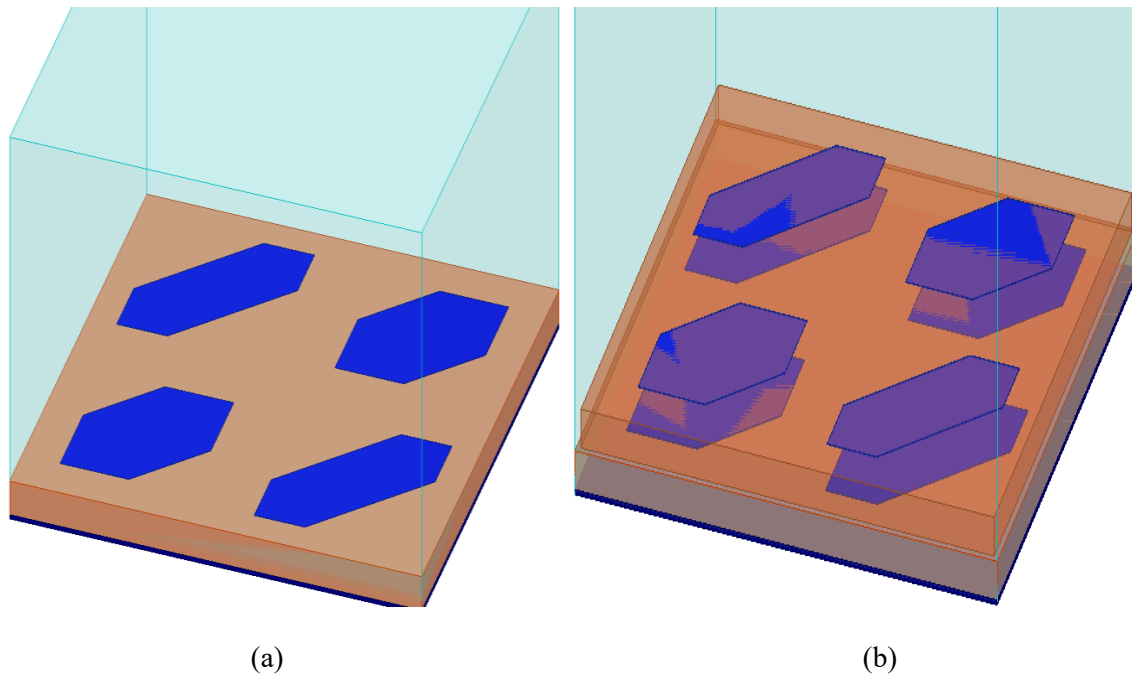


Figure 4.17: (a) Multi-band absorber design (b) stacked multi-band absorber design.

4.7.1 Results and Discussion

Fig. 4.18 shows the four absorptions frequencies that occurred by resonance. It is shown by the current density distribution on the structure. By stitching the adjusted quad-band, we remark that the four resonant frequencies undergo a distortion after stitching (**Figs. 4.19** and **4.20**).

Besides, there is no enhancement in the absorption band. This result can be explained by the coupling factor between the two layers when we stitch the additional layer. Multi-band structures suffer from their high sensitivity to any component added to their structure. As a conclusion, this way does not admit any enhancement in the absorption response.

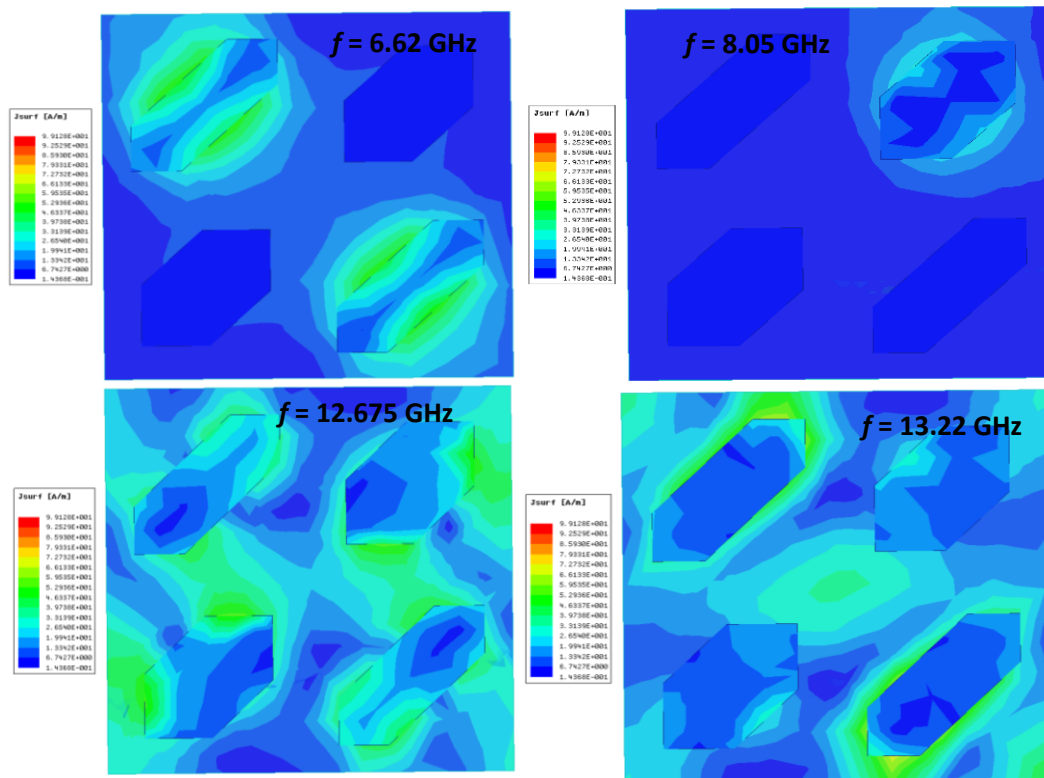


Figure 4.18: Current Density Distribution in the quad-band absorber at the four-absorber frequencies.

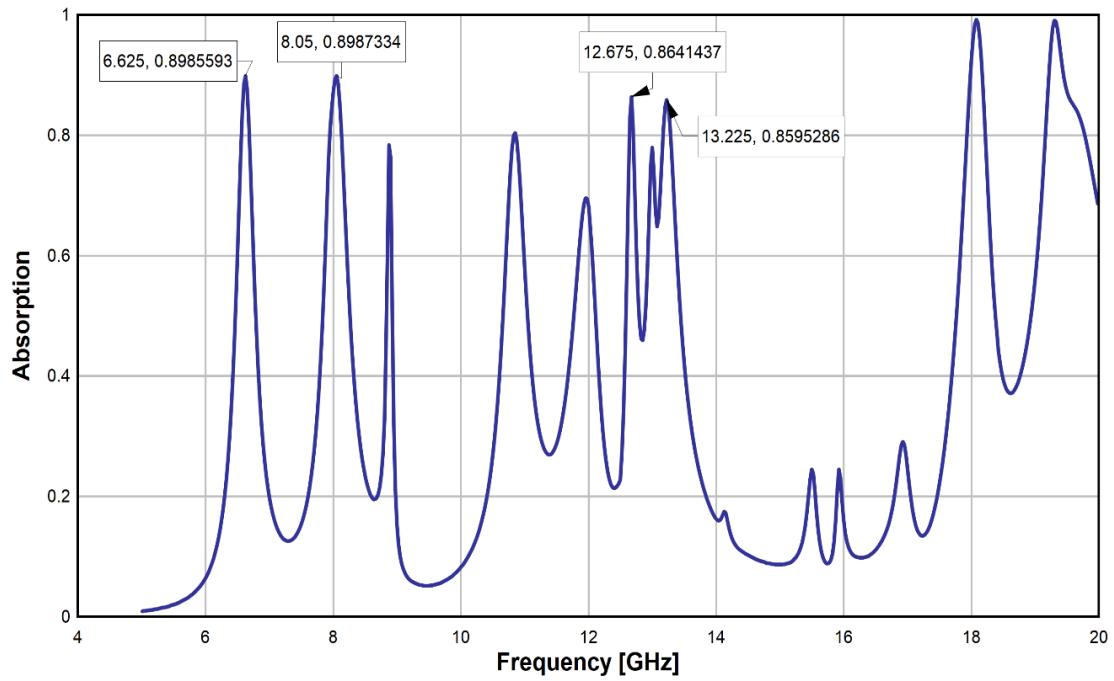


Figure 4.19: Absorption response of the quad-band absorber.

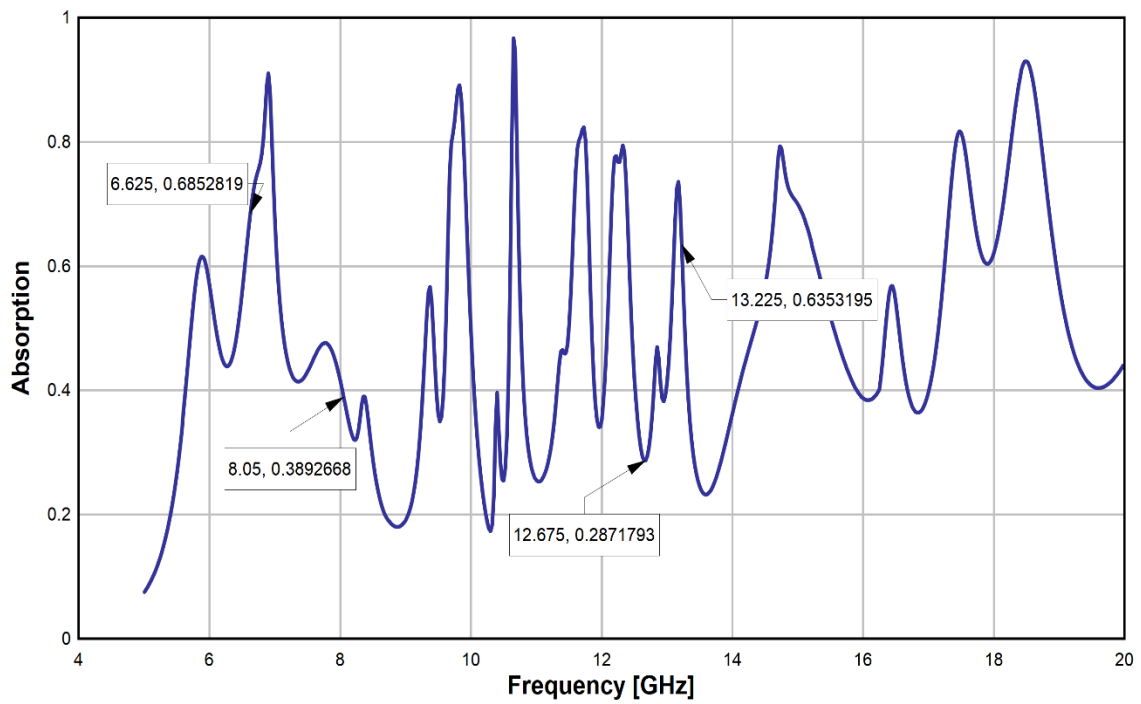


Figure 4.20: Absorption response of the stacked multi-band absorber.

4.7 Conclusion

Generally, the broadband objectives can be realized by increasing the number of simple resonators with size variation either in transverse or longitudinal directions. That is was applied in this chapter based on pyramidal units instead of simple patches where they were combined in-plane and in altitude. Each idea was proved its efficiency in broadening the band. We reached a RAB of **182.83 %** by applying the curved pyramid of 35 layers and **128.69 %** when applying the transverse combining method. The novelty in the ways of patches structuring applied in this chapter, admits to a RAB values unreachable in many broadband absorber essays in literature.

Other essays were tested as the “helicoid cone” and the “heal and heads” structures. As result, adding to the ultra-broadband obtained by the helicoid cone structure, a commune result was obtained from these structures that it is: the high necessity of the peaked top in reducing the reflection of an electromagnetic wave.

We can conclude that metamaterial has great importance in reducing the dimension of the absorber and can offer an ultra-broadband but with complex structure, as described in this chapter.

4.6 References

- [1] Landy, N. Ith, et al. "Perfect metamaterial absorber." *Physical review letters* 100.20 (2008): 207402.
- [2] Cheng, Yongzhi, and Helin Yang. "Retracted: Design, simulation, and measurement of metamaterial absorber." *Microwave and Optical Technology Letters* 52.4 (2010): 877-880.
- [3] Ma, Yong, et al. "A terahertz polarization insensitive dual band metamaterial absorber." *Optics letters* 36.6 (2011): 945-947.
- [4] Lee, J., and S. Lim. "Bandwidth-enhanced and polarisation-insensitive metamaterial absorber using double resonance." *Electronics Letters* 47.1 (2011): 8-9.
- [5] Wen, Qi-Ye, et al. "Dual band terahertz metamaterial absorber: Design, fabrication, and characterization." *Applied Physics Letters* 95.24 (2009): 241111.
- [6] Zhou, Xin, Yahong Liu, and Xiaopeng Zhao. "Low losses left-handed materials with optimized electric and magnetic resonance." *Applied Physics A* 98.3 (2010): 643-649.
- [7] Li, Hui, et al. "Ultrathin multiband gigahertz metamaterial absorbers." *Journal of Applied Physics* 110.1 (2011): 014909.
- [8] Bao, Shi, et al. "Broadband metamaterial absorber based on dendritic structure." (2010): 3187-3191.
- [9] Gu, S., et al. "A broadband low-reflection metamaterial absorber." *Journal of Applied Physics* 108.6 (2010): 064913.
- [10] Alici, Kamil Boratay, et al. "Experimental verification of metamaterial based subwavelength microwave absorbers." *Journal of Applied Physics* 108.8 (2010): 083113.
- [11] Zhu, Weiren, Xiaopeng Zhao, and Boyi Gong. "Left-handed metamaterials based on a leaf-shaped configuration." *Journal of Applied Physics* 109.9 (2011): 093504.
- [12] Wu, Chihhui, et al. "Large-area wide-angle spectrally selective plasmonic absorber." *Physical Review B* 84.7 (2011): 075102.
- [13] Wu, Chihhui, and Gennady Shvets. "Design of metamaterial surfaces with broadband absorbance." *Optics letters* 37.3 (2012): 308-310.

- [14] Ding, Fei, et al. "Ultra-broadband microwave metamaterial absorber." *Applied physics letters* 100.10 (2012): 103506.
- [15] Zhou, Jing, et al. "Experiment and theory of the broadband absorption by a tapered hyperbolic metamaterial array." *ACS photonics* 1.7 (2014): 618-624.
- [16] Ji, Dengxin, et al. "Broadband absorption engineering of hyperbolic metafilm patterns." *Scientific reports* 4 (2014): 4498.
- [17] Hao, Jianping. *Broad band electromagnetic perfect metamaterial absorbers*. Diss. Lille 1, 2016.
- [18] Sellier, Alexandre. *Absorbants à métamatériaux: étude théorique et expérimentale*. Diss. Université Paris Sud-Paris XI, 2014.
- [19] Ayad, Houssam. *Contrôle des performances des antennes par les métamatériaux*. Diss. 2012.
- [20] Brewitt-Taylor, C. R. "Modelling of helix-loaded chiral radar-absorbing layers." *Progress in Electromagnetics Research, PIER* 9 (1994): 288-310.
- [21] Cloete, Johannes H., Marianne Bingle, and David B. Davidson. "The role of chirality and resonance in synthetic microwave absorbers." *AEU-International Journal of Electronics and Communications* 55.4 (2001): 233-239.
- [22] Lu, ZeQin, et al. "Broadband polarization-insensitive absorbers in 0.3–2.5 μm using helical metamaterials." *JOSA B* 30.5 (2013): 1368-1372.
- [23] Reynet, O., and O. Acher. "Theoretical and Experimental Limitations of Chiral Microwave Absorbers." *Advances in electromagnetics of complex media and metamaterials*. Springer, Dordrecht, 2002. 461-470.
- [24] Li, Minhua, et al. "Perfect metamaterial absorber with dual bands." *Progress In Electromagnetics Research* 108 (2010): 37-49.
- [25] Pham, Van Tuong, et al. "Polarization-controlling dual-band absorption metamaterial." *Advances in Natural Sciences. Nanoscience and Nanotechnology (Online)* 4.3 (2013).
- [26] Ren, Yu-Hui, et al. "Design of a quad-band wide-angle microwave metamaterial absorber." *Journal of Electronic Materials* 46.1 (2017): 370-376.

5. Conclusion

In this thesis, we have taken the challenge to benefit from metamaterials to design a broadband absorber that can effectively operate in low frequencies trying to discover the potential of metamaterial replacing the present anechoic chamber.

Through the first chapter, we chose the pyramidal absorber to be the basis of our targeted design view; its broadband absorption, its insensitivity to incident wave angle and polarization of incident wave and its low cost in material. For that in the second chapter, we studied theoretically its mechanism as well as all its geometrical and material properties were analyzed to obtain the best-optimized absorption response. Our contribution in this part was in applying of curved altitude into the optimized pyramidal design that improved the RAB from 63.3 % to 73.6 %. Afterward, we studied the low-frequency metamaterial absorber requirements in the third chapter. These requirements are summarized by the need for a dimensional unit cell and for a high relative permittivity dielectric substrate. We reached a conclusion that using metamaterial we can obtain a miniaturized absorber compared with the enormous dimensions of conventional absorbers operating at this band. Nevertheless, a material of high relative permittivity imposes certain weight view its masse density but the thin thickness of metamaterial makes such design relatively non-weighty. Besides, our contribution here was to test of the efficiency of Minimal Surfaces in miniaturizing metamaterial unit cells that proved its validity through rough surfaces. In the last part of the thesis, the broadband objectives were realized through the pyramidal structure by increasing the number of resonators in transverse and longitudinal directions. Each idea proved its efficiency in broadening the band. We reached a RAB of 182.83 % by applying the curved pyramid of 35 layers and 128.69 % when applying the transverse combining method. The novelty in the ways of patch structuring applied in this chapter admits to a RAB values unreachable in many broadband absorber listed in literature. Those prototypes in spite of their complexities are possible to be fabricated, thanks to the services validated today by 3D printing technology.

As a general conclusion, targeting a broadband absorber, in one decade, over which an absorbance above 80 % is achieved, seems difficult to be satisfied with a single resonator array in a simple design. We noticed from our studies that we have to lose the simplicity of the design to reach a broadband absorption response.

6. Appendices

Appendix I

Debye Model of Pure Water for $f < 50$ GHz

```
clear all;
close all;
clc;
epsilon_inf=5.3;
epsilon_static=88.3;
relaxation_freq=8.84; %%8.84 GHz
relaxation_time=1/(2*pi*relaxation_freq);
%freq=10;
freq=[0:0.5:40];
w=(2*pi).*freq;
permittivity_complex=epsilon_inf+(epsilon_static-epsilon_inf)./(1-(w.*relaxation_time).*i);
Real=real(permittivity_complex);
Imag=imag(permittivity_complex);
figure(1)
plot(freq,real(permittivity_complex));
xlabel('frequency [Ghz]');
ylabel('Re(permittivity)');
figure(2)
plot(freq,imag(permittivity_complex));
xlabel('frequency [Ghz]');
ylabel('Imag(permittivity)');
freq_col=freq;
permittivity_colon=real(permittivity_complex);
loss=imag(permittivity_complex);
```

Appendix II

1. First Rough Surface “Droplet Water”

```
clc;
clear all;
close all;
N=200; %Number of surface points
rL=8/100; %Surface size in meters
h=0.05/100; %rms height
cl=1/100; %correlation length
x = linspace(-rL/2,rL/2,N);
y = linspace(-rL/2,rL/2,N);
[X,Y] = meshgrid(x,y);
%Z=randn(N,N);
%kx=2*pi*X./rL;
%ky=2*pi*Y./rL;
Z = h.*randn(N,N); % uncorrelated Gaussian random rough surface distribution
                % with mean 0 and standard deviation h
F = exp(-((X.^2+Y.^2)/(cl^2/2))); %Gaussian filter ACF
%Multiplication of the PSD and the random complex matrix in the Fourier
%domain is: fft2(Z).*fft2(F)
%f=ifft2(fft2(Z).*fft2(F));
% correlation of surface including convolution (faltung), inverse
% Fourier transform and normalizing prefactors
f = 2/sqrt(pi)*rL/N/cl*ifft2(fft2(Z).*fft2(F));
figure(1) %2D Plot
```

2. Random Rough Surface

```

clc;
clear all;
close all;
N=200; %Number of surface points
rL=8/100; %Surface size in meters
h=0.05/100; %rms height
cl=1/100; %correlation length

x = linspace(-rL/2,rL/2,N);
y = linspace(-rL/2,rL/2,N);

[X,Y] = meshgrid(x,y);
%Z=randn(N,N);
%kx=2*pi*X./rL;
%ky=2*pi*Y./rL;
Z = h.*randn(N,N); % uncorrelated Gaussian random rough surface      distribution
                    % with mean 0 and standard deviation h
F = exp(-((X.^2+Y.^2)/(cl^2/2))); %Gaussian filter ACF
%Multiplication of the PSD and the random complex matrix in the Fourier
%domain is: fft2(Z).*fft2(F)
%f=ifft2(fft2(Z).*fft2(F));
% correlation of surface including convolution (faltung), inverse
% Fourier transform and normalizing prefactors
f = 2/sqrt(pi)*rL/N/cl*ifft2(fft2(Z).*fft2(F));
figure(1) %2D Plot
surf(x,y,f,'edgecolor','none');
light;

stlwrite('z1.stl',X,Y,f);

```